Dissertation

Apolipoprotein Mimetic Peptide-based Nanodiscs in Targeting Granulocyte Effector Functions

submitted by

Alankrita RANI

for the academic degree of

Doctor of Philosophy

(PhD)

at the

Medical University of Graz

Otto Loewi Research Center

for Vascular Biology, Immunology, and Inflammation

Division of Pharmacology

under the supervision of

Assoc. Prof. Priv.-Doz. Mag. Dr.rer.nat. Gunther Marsche, PhD

2026

STATUTORY DECLARATION

"I hereby confirm that the present diploma thesis is the result of my own independent scholarly work. I also confirm that in all cases, where material from the work of others (in books, articles, essays, dissertations, and on the internet) is acknowledged, quotations and paraphrases are clearly indicated. No material other than that cited in the reference list has been used. I have read and understood the Medical University's regulations and procedures concerning plagiarism. Furthermore, I hereby declare that if artificial intelligence (AI) tools were used for the generation and/or correction of certain text passages in the creation of this work, such employment was conducted in compliance with ethical principles, academic integrity, and the regulations of my university. Additionally, it was ensured that this usage was transparently disclosed and appropriately attributed."

Graz, 26.01.2026

Alankrita Rani

DISCLOSURES

This dissertation is based on the following papers:

1. **Alankrita Rani** [a], Denys Balandin [b], Rohith Ravi [c], Julia Teppan [a], Ivan Vidakovic [b], Melanie Kienzl [a], Thomas Bärnthaler [a], Michael Holzer [a], Lamija Zijadic [a], Akos Heinemann [a], Katharina Jandl [a], Eva Böhm [a], Karin Kornmueller [b d], Mounir Tarek [c], Ruth Prassl [b], Gunther Marsche [a d] Peptide-based lipid nanodiscs suppress eosinophil recruitment and chemotaxis. J Controlled Release. 2025 Sep 10; 385:114060. https://doi.org/10.1016/j.jconrel.2025.114060

2. **Alankrita Rani** [a d], Gunther Marsche [a d]. A Current Update on the Role of HDL-Based Nanomedicine in Targeting Macrophages in Cardiovascular Disease. Pharmaceutics. 2023 May;15(5):1504. https://doi.org/10.3390/pharmaceutics15051504

[a] Division of Pharmacology, Otto Loewi Research Center, Medical University of Graz, Neue Stiftingtalstrasse 6, 8010 Graz, Austria. [b] Division of Medical Physics and Biophysics, Gottfried Schatz Research Center, Medical University of Graz, Neue Stiftingtalstrasse 6, 8010 Graz, Austria. [c] University of Lorraine, Laboratory of Theoretical Physics and Chemistry (LPCT), French National Centre for Scientific Research (CNRS), F-54000 Nancy, France. [d]BioTechMed-Graz, 8010 Graz, Austria

Copyright statement and compliance

Author contributions for the aforementioned manuscripts

Alankrita Rani: Writing – review & editing, Writing – original draft, Visualization, Validation, Methodology, Investigation, Formal analysis, Data curation, Conceptualization. **Denys Balandin:** Writing – review & editing, Methodology, Formal analysis. **Rohith Ravi:** Writing – review & editing, Visualization, Methodology, Investigation, Formal analysis. Dr. **Julia Teppan:** Writing – review & editing, Methodology, Investigation. **Ivan Vidakovic:** Writing – review & editing, Visualization, Methodology, Investigation. Dr. **Melanie Kienzl:** Writing – review & editing, Methodology. Dr. **Thomas Bärnthaler:** Writing – review & editing, Methodology. Dr. **Michael Holzer:** Writing – review & editing, Methodology. **Lamija Zijadic:** Writing – review & editing, Investigation. Dr. **Akos Heinemann:** Writing – review & editing, Resources. Dr. **Katharina Jandl:** Writing – review & editing, Funding acquisition. Dr. **Eva Böhm:** Writing – review & editing, Resources, Methodology. Dr. **Karin Kornmueller:** Writing – review & editing, Resources. Dr. **Mounir Tarek:** Writing – review & editing, Supervision, Resources, Funding acquisition. Dr. **Ruth Prassl:** Writing – review & editing, Supervision, Resources, Funding acquisition. Dr. **Gunther Marsche:** Writing – review & editing, Writing – original draft, Supervision, Resources, Project administration, Conceptualization.

Additionally, Dr. **Minzhi Yu** and Dr. **Antonela Rodriguez** helped with the optimization of methods related to LPC enriched sHDL nanodisc-characterization experiments, carried out under the supervision of Dr. **Anna Schwendeman**, during my stay abroad at the Biointerfaces Institute, University of Michigan, Ann Arbor, Michigan, USA.

During my PhD studies at the Medical University of Graz, I additionally contributed to the following publications:

1. Rodriguez A, Yu M, Gan J, Phoo MT, **Rani A**, Marsche G, Guo Y, Holinstat M, Schwendeman A, Phospholipase A_2 Products Influence the Antiplatelet Functions of Synthetic High-Density Lipoproteins, Journal of Lipid Research 2025 Dec 29:100972**;** *[Online ahead of print]*.

2. **Rani A**, Stadler JT, Marsche G. HDL-based therapeutics: a promising frontier in combating viral and bacterial infections. Pharmacology & Therapeutics. 2024 Aug; 260:108684.
3. **Rani A**, Stadler JT, Marsche G. HDL and SARS CoV-2: emerging theragnostic implications. Trends Mol Med. 2024 May 1;30(5):425–8.
4. Stadler JT, Bärnthaler T, Borenich A, Emrich IE, Habisch H, **Rani A**, et al. Low LCAT activity is linked to acute decompensated heart failure and mortality in patients with CKD. J Lipid Res. 2024 Sep 1;65(9):100624.
5. Annesley SJ, Kir S, Liu Y, **Rani A**. Science around the world. Trends Mol Med. 2024 May 1;30(5):417–9.
6. Stadler JT, Habisch H, Prüller F, Mangge H, Bärnthaler T, Kargl J, Pammer A, Holzer M, Meissl S, **Rani A**, Madl T, Marsche G. HDL-Related Parameters and COVID-19 Mortality: The Importance of HDL Function. Antioxidants (Basel). 2023 Nov 16;12(11):2009.
7. Holzer M, Ljubojevic-Holzer S, Souza Junior DR, Stadler JT, **Rani A**, Scharnagl H, Ronsein GE, Marsche G. HDL Isolated by Immunoaffinity, Ultracentrifugation, or Precipitation is Compositionally and Functionally Distinct. J Lipid Res. 2022 Dec;63(12):100307.
8. Stadler JT, Mangge H, **Rani A**, Curcic P, Herrmann M, Prüller F, et al. Low HDL Cholesterol Efflux Capacity Indicates a Fatal Course of COVID-19. Antioxidants. 2022 Oct;11(10):1858.
9. Stadler JT, Lackner S, Mörkl S, Meier-Allard N, Scharnagl H, **Rani A**, et al. Anorexia Nervosa Is Associated with a Shift to Pro-Atherogenic Low-Density Lipoprotein Subclasses. Biomedicines. 2022 Apr;10(4):895**.**

ACKNOWLEDGEMENTS

The research presented in this dissertation has been generously funded by the Austrian Science Fund (FWF) 10.55776/DOC129 (doc. funds RESPImmun), ApoA-I Mimetic Peptide Lipid Assemblies: I 5703-B, the French National Research Agency project ANR-21-CE11-0038 – AAMLA, The Marshall Plan Scholarship and The Marietta Blau Stipend from the Bundesministeriums für Frauen, Wissenschaft und Forschung (BMFWF) and Agentur für Bildung und Internationalisierung (OeAD).

I am deeply grateful to my mentor Prof. Gunther Marsche for guiding me throughout the academic process effectively. His mentorship has shaped me into a better researcher and a more confident individual. Working with him has been a privilege and a truly inspiring experience. I extend my gratitude to the members of my thesis committee Prof. Ruth Prassl, Prof. Mounir Tarek, Prof. Eva Böhm and Dr. Katharina Jandl for their insightful comments during my PhD. I am grateful to Prof. Akos Heinemann, Head of the Division of Pharmacology, for fostering effective collaborations within the department. Many thanks to all the administrative and technical staff at the Division of Pharmacology, specially – Claudia Krainer, Ilse Lanz, Iris Red, Juliana Schwanzer, Kathi Rohrer, Bernhard Sailer and Sabine Meissl- for or their excellent technical assistance. I acknowledge the valuable input from Dr. Michael Holzer, Dr. Senka Holzer, Dr. Melanie Kienzl, Dr. Eva Gruden, Dr. Minzhi Yu, Dr. Anna Schwendeman, Dr. Gayannée Kedia and Dr. Sudha Shashwati. Their positivity, wisdom and expert guidance filled my journey with a renewed scientific rigor, confidence and clarity. I thank Veronika Rechberger for her support with international student matters and for her uplifting company during my PhD.

Special thanks to my mother Dr. Kavita Rani Sharma and my brother Kushagra Anand for their patience around small and big hurdles of my life and for always believing in me. My dad, for being my support system as long as he could.

It warms my heart to thank my dearest souls: Yusuf Ceyhun Erdoğan for reminding me of my strengths every step of the way, enduring my struggles as his own, celebrating and co-regulating with me; Daniel de Jesus Platero Rochart for the resilience and hope he has inspired in me by being who he is; Dr. Nejra Cosic Mujkanovic and Dr. Snehlata Singh for showing me how beautiful and

empowering it can be to grow alongside open-minded, strong women full of love; Dušan Jeremić for his selfless care, support and belief in me; David Kaspret for the comfort and space he has so gracefully offered, expanding the potential of my mind; Sally Connolly for being the free spirited, kind hearted friend who always brings fresh perspectives; Dr. Aleksandra L. Ptaszek for her harmonious friendship and a wild belief in my potential.

I'm lucky to have had the support of Dr. Mark Vander Roest, Bill Vander Roest and Dr. Lorri Vander Roest. Their love, grace and selfless care nourished and sustained me through demanding times and I will always be grateful for having them in my life.

I extend my warm regards to Dr. Cyrus Alexander for the innumerable brainstorming sessions across several time zones; Raj Verma for consistently augmenting my willpower; Dušica Ristić and Simon Renner for always nudging me towards amazing outcomes; Bernhard Reiter for showing me the underrated power of effective venting; Harshit Singh for the random philosophical and poetic indulgences; Dr. Jamie Kraft for sharing her motivations with me; Dr. David Tandio for his clear judgement; Dr. Manu Kanti, Dr. Meenu Rohini Rajan, Dr. Jacob Kuruvilla and Dr. Matthias Mitteregger for their pragmatic advice, care and faith in me; Dr. Kassem Makki and Dr. Nassim Ghaffari Tabrizi – Wizsy for reigniting the artistic energy in me; Nemanja Radic for his encouragements and psychological discussions and Dr. Veer Vikram Singh for helping me navigate challenging times effectively.

The wonderful office girls- Lamija Zijadić, Karolina Herceg, Isabella Faimann, Sarah Felber, Sara Hirtler and Dr. Anja Pammer for being such empowering friends and lovely human beings I got to share my day-to-day life with.

I have a lasting appreciation in my heart for Dr. Antonela Rodriguez, Ali Rodriguez, Dr. Adaeze Aneli, Dr. Corrine Din, Luke Moriessette and May Phoo for filling my heart with joy and my mind with motivation during my stay in Michigan.

I appreciate Dr. Yogesh Mishra, D. Gulam Hussain Syed, Dr. Stephan Lange, Dr. Rohith Ravi, Dr. Mohd. Faraz Alam, Poornima Kokavalla, Subhashish Samantaray, Dr. Shamim Akhtar Sufi, Dr. Bharati Singh, Dr. Sima Kumari, Dr. Amit Kumar, Abhimanyu Prasad, Magnus Gustafsson, Saman Firdaus Chishti, Spela Mandl, Dr. Zdenko Kasáč, Satinee Xuying Loh, Juan Toledo-Marcos, Dr.

Oliver Kindler, Ana Santiso, Divya Guntur, Alicja Wawrzen, Wolfgang Platzer, Dr. Julia Stadler, Silvia Andaloro, Denisa Javor, Martin Vargek, Olida Reisoglu, Jan Haberfellner, Szymon Jakobczyk, Filip Kristić and Gabriela Wojcik for the innumerable ways in which they have instilled vitality in me.

I am grateful to my ex, Dr. Shubham Saurabh for always believing in my strengths and for celebrating all my little wins along the way.

Finally, I thank the city of Graz for being my home since late summer 2021. I am very fortunate to have lived here, through the beauty of this process. Every experiment ever performed is a success, if we can look behind the confines of human ego and I am grateful to every moment that has led to this mindset I will carry forward with me.

-Alankrita

TABLE OF CONTENTS

LIST OF ABBREVIATIONS

Abbreviation	Explanation
HDL	High-density lipoprotein
sHDL	Synthetic high-density lipoprotein
DMPC	1,2-Dimyristoyl-sn-glycero-3-phosphocholine
Apo	Apolipoprotein
22A	Apolipoprotein A-I mimetic peptide
4F-P-4F	Apolipoprotein A-I mimetic peptide (4F–Proline–4F)
ABCA1	ATP-binding cassette transporter A1
SR-BI	Scavenger receptor class B type I
TH2	T helper type 2
ERK	Extracellular signal-regulated kinases
STAT	Signal transducer and activator of transcription
JAK	Janus kinase
DLS	Dynamic light scattering
PDI	Polydispersity index
TEM	Transmission electron microscopy
IL	Interleukin
TNF	Tumor necrosis factor
IFN	Interferon
BAL	Bronchoalveolar lavage
MD	Molecular dynamics
CD	Cluster of differentiation
GPC	Gel permeation chromatography
FPLC	Fast protein liquid chromatography
FSC-A	Forward scatter area (flow cytometry)
SSC-A	Side scatter area (flow cytometry)
PI	Propidium iodide

ANOVA	Analysis of variance
SEM	Standard error of the mean
MFI	Mean fluorescence intensity
CCR	C-C chemokine receptor
CCL	C-C chemokine ligand
LPS	Lipopolysaccharide
LTA	Lipoteichoic acid
LCAT	Lecithin-Cholesterol Acyltransferase
fMLP	N-Formylmethionyl-leucyl-phenylalanine
PMA	Phorbol 12-Myristate 13-Acetate
LPC	Lysophosphatidylcholine
TLR	Toll-like receptors

ZUSAMMENFASSUNG

High-Density-Lipoproteine (HDL), die seit jeher für die Aufrechterhaltung der Gefäßgesundheit bekannt sind, indem sie überschüssiges Cholesterin aus peripheren Geweben entfernen und zur Leber transportieren, dienen auch als wichtige Regulatoren der angeborenen Immunantwort. Während synthetische HDL-Nanopartikel traditionell zur Behandlung von Herz-Kreislauf-Erkrankungen eingesetzt werden, ist ihr therapeutisches Potenzial für die Modulation von Granulozyten noch weitgehend unerschlossen. Diese Arbeit untersucht synthetische Lipoproteine hoher Dichte als vielseitige Plattform zur Regulierung von Entzündungen, die durch Eosinophile und Neutrophile ausgelöst werden.

Im ersten Teil dieser Studie wurden stabile, monodisperse synthetische HDL-Nanodiscs unter Verwendung des Apolipoprotein-A-I-Mimetikums 4F-P-4F in Kombination mit 1,2-Dimyristoyl-sn-glycero-3-phosphocholin (DMPC) hergestellt. Diese Partikel ordneten sich durch präzise molekulare Wechselwirkungen zwischen amphipathischen Helices und Phospholipiden zu einer konsistenten scheibenförmigen Morphologie an. Die resultierenden synthetischen Partikel hemmten in vitro wirksam die Eotaxin-induzierte Migration menschlicher Eosinophilen über Scavenger-Rezeptor-Klasse-B-Typ-1- und ATP-bindende Kassettentransporter-A1-abhängige Mechanismen. Diese hemmende Wirkung stand im Zusammenhang mit einem verstärkten Cholesterinausfluss und der Modulation des C-C-Chemokinrezeptors Typ 3, der extrazellulären signalregulierten Kinase 1/2 und der Signaltransduktions- und Transkriptionsaktivator-Signalwege. Darüber hinaus reduzierte das auf einem mimetischen Peptid basierende synthetische High-Density-Lipoprotein in einem Mausmodell der Interleukin-5-induzierten Eosinophilie die Rekrutierung von Eosinophilen in die Lunge signifikant. Im zweiten Teil der Studie wurde die Zusammensetzung des 22A-basierten synthetischen HDL durch teilweisen Ersatz von DMPC mit ausgewählten Lysophosphatidylcholin-Spezies optimiert. Die modifizierten Partikel blieben stabil, monodispers und zeigten keine Zytotoxizität in primären humanen polymorphkernigen Leukozyten. Während nicht angereicherte Partikel wirkungslos waren, reduzierte mit Lysophosphatidylcholin 18:0 angereichertes synthetisches HDL die IL-8-induzierte Formveränderung von Neutrophilen signifikant. Diese Ergebnisse belegen, dass gezieltes Peptid-

und Lipid-Engineering eine selektive Modulation der Granulozytenaktivität ermöglicht und das therapeutische Potenzial synthetischer HDL bei granulozytenvermittelten entzündlichen Lungenerkrankungen unterstützt.

ABSTRACT

Historically recognized for maintaining vascular health by removing excess cholesterol from peripheral tissues and transporting it to the liver, high-density lipoproteins (HDL) also serve as critical regulators of the innate immune response. While synthetic HDL (sHDL) nanoparticles are traditionally utilized to target cardiovascular disease, their therapeutic potential for the modulation of granulocytes remains largely untapped. This thesis investigates synthetic high-density lipoproteins as a versatile platform to regulate inflammation driven by eosinophils and neutrophils.

In the first part of this study, stable, monodisperse synthetic HDL nanodiscs were generated using the apolipoprotein A-I mimetic peptide 4F-P-4F combined with 1,2-dimyristoyl-sn-glycero-3-phosphocholine (DMPC). These particles self-assembled into a consistent discoidal morphology through precise molecular interactions between amphipathic helices and phospholipids. The resulting synthetic particles potently inhibited eotaxin-induced human eosinophil migration in vitro via Scavenger Receptor Class B Type I– and ATP-binding cassette transporter A1–dependent mechanisms. This inhibitory effect was associated with enhanced cholesterol efflux and the modulation of C-C chemokine receptor type 3, Extracellular Signal-Regulated Kinase 1/2, and Signal Transducer and Activator of Transcription signaling pathways. Furthermore, in a murine model of Interleukin-5-driven eosinophilia, the sHDL lipoprotein significantly reduced eosinophil recruitment to the lungs.

In the second part of the study, the composition of 22A peptide-based sHDL was tuned by partially substituting DMPC with specific lysophosphatidylcholine species. These enriched particles demonstrated monodispersity and remained stable, with no observed cytotoxicity in primary human polymorphonuclear leukocytes. Notably, while non-enriched particles showed no significant effect, lysophosphatidylcholine 18:0–enriched synthetic HDL significantly attenuated Interleukin-8–induced neutrophil shape change.

Overall, these findings show that apolipoprotein A-I mimetic peptide-based sHDL nanoparticles can regulate granulocyte activity and can be engineered to serve as therapeutic candidates for granulocyte-driven inflammatory lung diseases.

1. INTRODUCTION

1.1 Lipoproteins in heath and disease

Lipids are essential biomolecules that play a role in energy storage, membrane architecture and cellular signaling. As most lipids are poorly soluble in aqueous environments, such as blood plasma, efficient transport through the circulatory system requires them to be packaged into macromolecular assemblies. These assemblies known as lipoproteins, serve as the main carriers of cholesterol, triglycerides and other hydrophobic lipids between tissues (1,2). Each lipoprotein particle consists of a hydrophobic core, primarily composed of triglycerides and cholesteryl esters, which is surrounded by an amphipathic surface monolayer of proteins, phospholipids and free cholesterol (1,3). This architecture stabilizes the particle in circulation and facilitates interactions with enzymes, receptors and proteins involved in lipid metabolism.

Lipoproteins are traditionally classified according to their density, size, and lipid-to-protein ratio. These parameters reflect their composition and metabolic function. The major classes include chylomicrons, very-low-density lipoproteins (VLDL), intermediate-density lipoproteins (IDL), low-density lipoproteins (LDL) and high-density lipoproteins (HDL) (1,3). As density increases from chylomicrons to HDL, particle size decreases and relative protein content increases. These classes participate in coordinated lipid transport pathways. HDL has been recognized as a multifunctional particle whose diverse biological activities arise from its heterogeneous protein, and lipid composition (1,2). They are the smallest and most protein-rich class of lipoproteins and play a central role in reverse cholesterol transport, whereby cholesterol is collected from peripheral tissues and delivered to the liver for excretion or recycling (1,4). Interest in HDL as a determinant of cardiovascular health emerged in the mid-20th century, when circulating lipoprotein cholesterol levels were first identified as predictors of cardiovascular disease risk (5).

1.1.1 High Density Lipoproteins are multifunctional immunomodulators

Native HDL particles exert multiple protective effects, largely attributed to their ability to promote cholesterol efflux, attenuate oxidative stress and inflammation in monocytes, macrophages and endothelial cells (6,7). In particular, the enhancement of macrophage cholesterol efflux has been

shown to facilitate atherosclerotic plaque regression and anti-inflammatory effects in cardiovascular disease (7). Given its central role in cholesterol homeostasis and its association with cardiovascular protection, HDL has become a major focus of both basic and translational research. HDL has long been associated with cardiovascular protection and its roles within the immune system are clinically relevant (8). Beyond their classically described role in lipid transport, lipoproteins, particularly HDL, are now recognized as immunoregulatory entities with functions extending to modulation of inflammation, oxidative stress, endothelial function, and immune responses (9,10). HDL particles are evolutionarily conserved and play important roles in host defense such as wound healing and bacterial lipopolysaccharide (LPS) binding (11). These pleiotropic effects are influenced by HDL-particle size, apolipoprotein content and lipid content, which exists in a dynamic state (7,9). Recent studies show that HDL also carries other bioactive molecules, such as microRNAs, opening new avenues for understanding its functional roles (12,13). A detailed understanding of native HDL structure and metabolism therefore provides the essential foundation for the rational design of synthetic HDL systems aimed at enhancing the beneficial properties of endogenous HDL.

1.1.2 Composition of HDL

Apolipoproteins are the major protein components of HDL responsible for its structural stability and bioactivity (1,2). They stabilize particle architecture, act as ligands for cellular receptors, and serve as essential cofactors for enzymes involved in lipid metabolism (1,4). The specific apolipoprotein composition of a lipoprotein particle largely determines its metabolic fate, receptor interactions, and biological activity. Apolipoprotein A-I (ApoA-I) is the dominant protein in HDL, accounting for roughly 70% of its protein content, followed by Apolipoprotein A-II (ApoA-II) and smaller contributions from proteins such as ApoC-II, ApoC-III, ApoE, ApoM paraoxonase-1 (PON1), which provides antioxidant capacity (4). In 45 published reports, almost 1000 individual proteins have been detected in preparations of HDL. Of these, 251 have been identified in at least three different laboratories (14). The lipid matrix of HDL is composed predominantly of glycerophospholipids, sphingolipids, cholesterol, and cholesteryl esters, providing a flexible structural configuration that supports cholesterol transport and facilitates receptor engagement (4,15). Advances in lipidomic technologies have been crucial in uncovering this complexity,

revealing that variations in HDL lipid composition may underlie differences in HDL functionality (15). Together, these core proteins and lipids establish the physical framework and functional potential of the HDL particle, shaping its interactions with structural cells and immune cells and its role in cholesterol trafficking. HDL particle formation begins when lipid-poor apolipoprotein ApoA-I acquires phospholipids and free cholesterol via interaction with the ATP-binding cassette transporter A1 (ABCA1), and this initial lipidation event marks the start of HDL biogenesis (16). The reverse cholesterol transport process is a cycle of particle remodeling. Small, discoidal pre-β HDL (nascent particles) serve as the primary acceptors for cellular cholesterol efflux via the ABCA1 transporter. As these particles acquire cholesteryl esters through the action of Lecithin-Cholesterol Acyltransferase (LCAT), they mature into larger HDL3 and eventually HDL2 spheres, which is reflected by several HDL subclasses ApoA-I is a key mediator of HDL functionality and is well established as the principal regulator of macrophage cholesterol efflux via ATP-binding cassette transporters (ABCA1 and ABCG1) (7). Apolipoprotein A-I also serves as a principal ligand for the scavenger receptor class B type I (SR-BI), and its interaction with SR-BI on cells mediates selective uptake of HDL cholesteryl esters and influences HDL's anti-inflammatory and lipid-homeostatic roles (17,18). Apart from forming the primary structural foundation of HDL, ApoA-I modulates intracellular cholesterol accumulation in macrophages, limits foam cell formation and attenuates atherogenesis (7). In addition to its role in reverse cholesterol transport, ApoA-I stabilizes and enhances the lipoprotein's antioxidant and anti-inflammatory properties, including the attenuation of endothelial activation and the neutralization of oxidized lipid species (19,20). The ability of ApoA-I to preserve endothelial function, reduce vascular inflammation and maintain lipid homeostasis establishes it as a primary component in HDL-mediated cardiovascular protection (21). Moreover, reduced ApoA-I levels have been associated with unfavorable outcomes in a plethora of inflammatory diseases namely, atherosclerosis (22,23) sepsis (24,25), viral infections (24,26) and pulmonary arterial hypertension (27).

1.1.3 Inflammation alters HDL composition and function

Extensive clinical and biochemical research confirms that both acute (e.g., sepsis, trauma, or influenza) and chronic (e.g., rheumatoid arthritis, diabetes, or obesity) inflammatory states trigger a process known as HDL remodeling, where HDL structure and function are altered. This

transformation shifts HDL from a vasoprotective particle into a dysfunctional or even pro-inflammatory one. In acute systemic inflammation such as sepsis, circulating HDL levels decline rapidly, accompanied by extensive remodeling of HDL particles driven by the acute-phase response (26). Protective apolipoproteins, particularly ApoA-I, are partially displaced by acute-phase proteins such as serum amyloid A, while oxidative enzymes and phospholipases modify HDL lipids and proteins (26). These changes impair cholesterol efflux capacity, antioxidant activity, and the ability of HDL to neutralize pathogen-associated molecules, thereby amplifying systemic inflammation and organ dysfunction (26,28). Viral infections induce similar disturbances in HDL structure and function through inflammation-associated dyslipidemia and oxidative stress. During severe viral disease pathogenesis, HDL particles display altered lipid and protein cargo, leading to diminished anti-inflammatory and endothelial-protective activities (26). The loss of functional ApoA-I and enrichment of pro-inflammatory components compromise HDL-mediated immune regulation and contribute to endothelial dysfunction and vascular injury (29–31). Persistent oxidative and inflammatory stress promotes post-translational modification of ApoA-I, reducing cholesterol efflux efficiency and impairing anti-oxidative and anti-inflammatory functions. These dysfunctional HDL particles fail to suppress endothelial activation and foam cell formation, thereby accelerating atherosclerotic progression (7). Collectively, these observations demonstrate that both acute and chronic inflammation compromise HDL quality and function, reinforcing the concept that HDL functionality, rather than circulating HDL levels alone, is central to its protective role in disease. Disturbances in HDL quantity and function further contributes to a wide range of inflammatory and metabolic disorders which has been discussed at length by us and others (28,32,33). Collectively, these molecular features highlight HDL as a highly specialized and multifunctional nanoparticle rather than a passive lipid transport vehicle (11,12). Given the strong evidence connecting HDL structure and function to disease outcomes, strategies aimed at improving HDL quality have emerged as an attractive therapeutic approach.

1.2 Native HDL as a Template for Drug Development

Native HDL is an endogenous nanoparticle that forms through the lipidation of ApoA-I, resulting in nanoscale particles with exceptional cholesterol efflux capacity. This fundamental aspect of

HDL biosynthesis has directly inspired a broad class of drug development strategies collectively referred to as HDL mimetics.

In this context, the term HDL mimetics encompasses formulations composed of purified ApoA-I or ApoA-I mimetic peptides assembled with phospholipids, as well as nanoparticle systems engineered to reproduce the size, composition, and functional behavior of native HDL. These constructs typically consist of phospholipids combined with amphipathic α-helical proteins which are most commonly ApoA-I (7,34). HDL mimetics generated using full-length ApoA-I are generally referred to as reconstituted HDL (rHDL; e.g., CSL112), whereas formulations based on ApoA-I mimetic peptides are classified as synthetic HDL (sHDL; e.g., ETC-642) (7).

Through interactions with endothelial and immune cells, ApoA-I supports vascular homeostasis and facilitates cholesterol efflux, forming the mechanistic basis for its use in HDL mimetic nanotherapeutics. Structurally, ApoA-I is a 28.3 kDa protein composed predominantly of class A amphipathic α-helices, which enable stable association with phospholipids while maintaining aqueous solubility. These structural features allow ApoA-I to interact with lipid transporters such as ABCA1, initiating cholesterol efflux and promoting the formation of discoidal HDL particles (35,36).In reconstituted HDL (rHDL) formulations, ApoA-I is sourced either from human plasma or produced recombinantly (34). While full-length ApoA-I closely reproduces native HDL structure and function, its large size, production cost, and purification requirements limit its practicality for widespread therapeutic application (7,34). Consequently, considerable effort has been directed toward the development of ApoA-I mimetic peptides as alternative protein components.

ApoA-I mimetic peptides are short, chemically synthesized sequences designed to replicate the amphipathic α-helical architecture of the full-length protein (35,36). Despite limited primary sequence homology to ApoA-I, these peptides retain key functional properties, including phospholipid binding, cholesterol efflux promotion, and anti-inflammatory activity (7). Their reduced length enables cost-effective synthesis, high purity, and improved scalability, while also minimizing the risk of immunogenicity associated with host-derived contaminants (34). Variations in peptide hydrophobicity, helicity, and amino acid composition allow fine-tuning of lipid affinity and biological activity (35,37). Early prototypes such as the 18A peptide and its derivatives validated the amphipathic helix hypothesis and demonstrated the feasibility of assembling stable

nanodiscs capable of cholesterol efflux and inflammation modulation (38). Subsequent generations of mimetic peptides, including 4F, 5A, and 22A, were optimized to enhance lipid interactions, transporter specificity, and safety profiles (37,39). Notably, asymmetric and bihelical designs have improved cholesterol efflux efficiency while reducing cytotoxicity (40). More recent mimetics such as proline linked dimeric 4F, have further expanded the functional scope of HDL nanoparticles, demonstrating efficacy in preclinical models of atherosclerosis, metabolic disease, and inflammation (41). For effective therapeutic and drug delivery applications HDL mimetics must exhibit comparable particle size, density and biochemical characteristics to ensure stability in circulation, alongside favourable biocompatibility, low immunogenicity, and minimal toxicity (42–44). Lipidation is essential not only for the nanodisc assembly to resemble native HDL, but also increasing the circulation time of the mimetic peptides (43). Both full-length ApoA-I and ApoA-I mimetic peptides provide viable protein scaffolds for HDL mimetic nanoparticles. While full-length ApoA-I offers close structural fidelity to native HDL, mimetic peptides provide greater flexibility, scalability, and tunability, making them particularly attractive for the development of next-generation HDL-based nanotherapeutics.

The majority of sHDL formulations employ commercially available phospholipids capable of forming stable bilayers. Commonly used lipid components include dipalmitoyl phosphatidylcholine (DPPC), dimyristoyl phosphatidylcholine (DMPC), palmitoyl-oleoyl phosphatidylcholine (POPC), sphingomyelin (SM), and other phosphatidylcholine derivatives (45,46). These phospholipids differ in their acyl chain saturation, phase transition temperatures, and biophysical properties, all of which influence sHDL performance (39,45,46). Figure 1 highlights the structures of commonly used peptide scaffolds and phospholipids in the design of sHDL nanodiscs. Despite their central role, systematic optimization of phospholipid composition in sHDL formulations remains limited. Comparative studies have demonstrated that lipid selection can markedly influence biological outcomes. For example, sHDL nanodiscs formulated with sphingomyelin rather than POPC exhibited enhanced anti-inflammatory and anti-atherogenic effects in both in vitro and in vivo models when combined with the 5A peptide (45). These formulations also differed in their ability to remodel endogenous HDL and in their cholesterol efflux pathways, with sphingomyelin-containing nanodiscs favouring scavenger receptor class B type I (SR-BI)-mediated efflux without significantly altering ABCA1-dependent transport (45).

Stronger lipid-peptide interactions in sphingomyelin-based systems resulted in more uniform nanoparticles and extended circulation times (39). Phospholipid composition critically influences the pharmacokinetic and pharmacodynamic behaviour of sHDL nanoparticles. Studies using 22A-based nanodiscs have shown that altering phospholipid saturation and transition temperature significantly affects cholesterol mobilization, LCAT activation, particle remodeling, and peptide stability (47). In these systems, sHDL formulated with higher–transition temperature phospholipids exhibited prolonged plasma half-lives and substantially increased cholesterol exposure compared with POPC-based formulations (47). These findings highlight the dominant role of lipid composition in determining in vivo cholesterol mobilization and therapeutic performance. Beyond phosphatidylcholine species, incorporation of anti-inflammatory lipids can further modulate biological activity. The addition of phosphatidylserine to POPC-based sHDL has been shown to enhance anti-inflammatory effects through mechanisms largely independent of ABCA1 and ABCG1, while significantly augmenting SR-BI-mediated responses (48,49). Collectively, these observations underscore the importance of tailoring phospholipid composition to disease context and therapeutic objectives, emphasizing that lipid selection is a critical design parameter for next-generation HDL mimetic nanoparticles.

Over time, multiple HDL mimetics have progressed into clinical evaluation for atherosclerosis-related conditions, with a particular focus on targeting mononuclear phagocytes that differentiate into lipid-laden foam cells and drive the progression of coronary artery disease (7). Table 1 summarizes the HDL mimetics evaluated in clinical trials to date. Owing to their nanoscale size, inherent targeting capabilities, prolonged circulation time, and in vivo stability, sHDL nanoparticles represent an effective platform for drug delivery while mimicking some endogenous protective functions of HDL, like cholesterol efflux and receptor engagement (7). Beyond these advantages, a key benefit of synthetic HDL systems is their favorable biocompatibility profile, which minimizes the need for extensive safety and tolerability assessments (34). This stands in contrast to many non-lipoprotein nanoparticle platforms, where issues related to immune compatibility and rapid or unpredictable clearance remain major challenges (34).

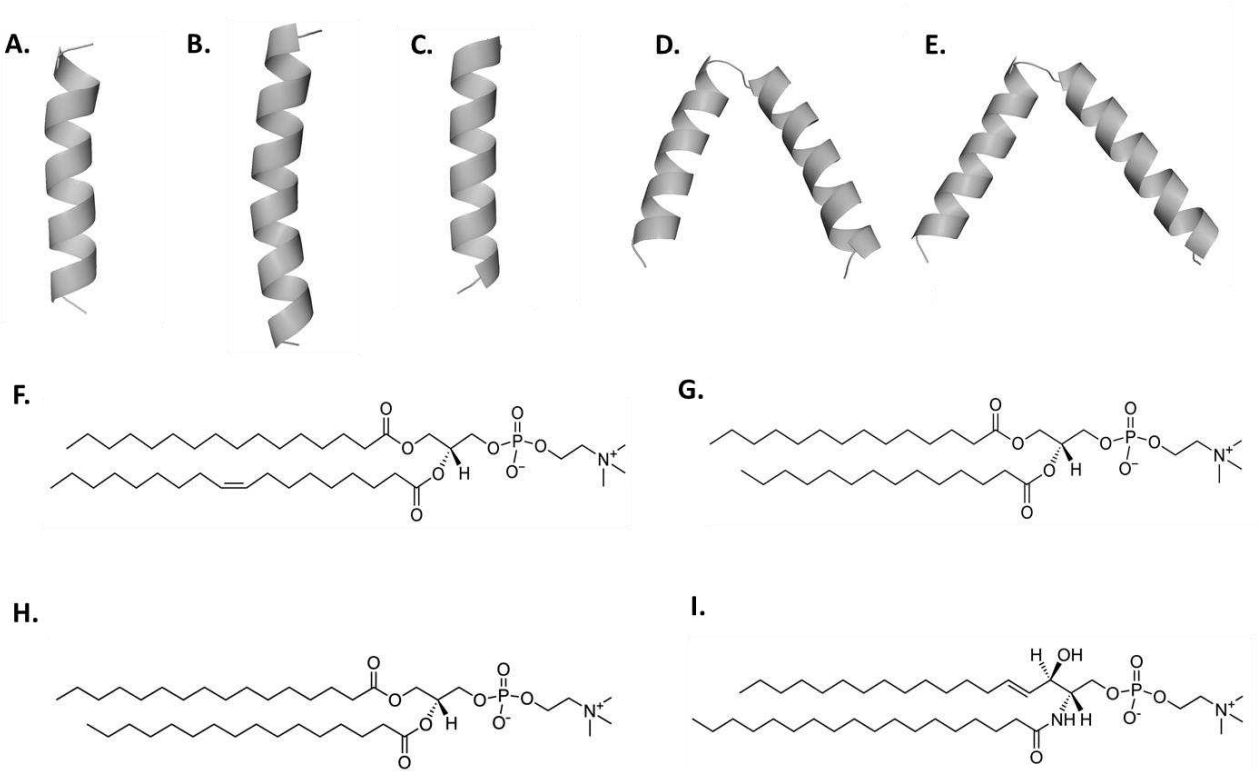

Figure 1. Structures of widely used peptide scaffolds and phospholipids employed in sHDL nanodisc design. A. 22A peptide, **B.** 18A peptide, **C**. 4F peptide, **D**. Dimeric 4F (proline linked dimer of the monomeric 4F peptide) **E**. 5A peptide. **F**. palmitoyl-2-oleoyl-sn-glycero-3-phosphocholine (POPC) **G**. 1,2-dimyristoyl-sn-glycero-3-phosphocholine (DMPC) **H**. dipalmitoyl phosphatidylcholine (DPPC) **I**. sphingomyelin (SM); A-E peptide structure- prediction performed using AlphaFold 3 and visualized using PyMOL 3.1. Phospholipids F-I generated with Biorender.com.

Table 1 HDL mimetics evaluated in clinical trials, adapted from (7) under the terms and conditions of the Creative Commons Attribution (CC BY) license (https://creativecommons.org/licenses/by/4.0/) which permits unrestricted use, distribution, and reproduction in any medium, provided the original authors and the source are credited.

HDL Mimetic	Protein (P)	Phospholipid (L)	Nanoparticle Size	Ratio (P/L)	Clinical Trial	Major Findings
ETC-216	ApoA-I Milano	DPPC	7–30 nm	1:2.7 (w/w)	Milano, Phase II	Significant reduction in atheroma volume
MDCO-206	ApoA-I Milano	POPC	7–30 nm	1:1.1 (w/w)	MILANO-PILOT Phase III NCT02678923	80.4% increase in cholesterol efflux, no plaque regression
CER-001	ApoA-I native	SM, DPPG	7–13 nm	1:2.7 (w/w)	CHI-SQUARE / CARAT Phase II	No significant coronary atherosclerosis regression
CSL111	ApoA-I native	Soy PC	7–30 nm	1:150 molar	ERASE Phase II NCT00225719	Plaque index improvement; liver enzyme elevation
CSL112	ApoA-I native	Soy PC	7–13 nm	1:55 molar	AEGIS-I Phase II NCT02108262	Safe; no renal/hepatic toxicity

CSL112	ApoA-I native	Soy PC	7–13 nm	1:55 molar	AEGIS-II Phase III NCT03473223	Primary CV endpoint not met at 90 days; improved efflux capacity
ETC-642	22-aa single helix	DPPC, SM	7–13 nm	1:1.1 molar	Phase I	Safe; increased LCAT activation
D-4F	18-aa bihelical	Non-lipidated	–	–	Phase I NCT00907998	Anti-inflammatory; blocks oxidized lipid absorption
L-4F	L-amino acid 4F	Non-lipidated	–	–	Phase I NCT00568594	Short half-life vs D-4F
5A	37-aa bihelical	SM	7–13 nm	1:8 (primate study)	Phase I NCT04216342	ABCA1-specific efflux

Abbreviations: dipalmitoyl phosphatidylcholine (DPPC), 1,2-dimyristoyl-sn-glycero-3-phosphocholine (DMPC), dipalmitoyl phosphatidylglycerol (DPPG), palmitoyl-2-oleoyl-sn-glycero-3-phosphocholine (POPC), 1-palmitoyl-2-linoleoyl phosphatidylcholine (PLPC), phosphatidylcholine (PC), sphingomyelin (SM), amino acids (aa).

1.3 Granulocytes in Host Defense and Inflammatory Response

Inflammation is an essential physiological process that enables host defense against infection and tissue injury, yet its persistence or dysregulation underlies a wide range of pathological conditions. Among innate immune cells, neutrophils and eosinophils represent two major granulocyte populations with distinct but overlapping roles in inflammatory responses. Granulocytes are the largest fraction of leucocytes (50) often described as the 'first responders' of the immune system. The distinguishing characteristic of these cells is their pre-loaded arsenal of granules, which enables them to respond to threats within minutes, whereas other immune cells take longer for an active response. Traditionally viewed as short-lived effector cells involved primarily in acute inflammation, both neutrophils and eosinophils are recognized as dynamic participants in inflammatory disease. Their functions extend beyond microbial defense to include immune regulation, tissue remodeling, and interactions with adaptive immune mechanisms (51). Understanding the context-dependent activities of these granulocytes is therefore critical for elucidating the mechanisms driving both acute and chronic inflammation.

Eosinophils are a distinct subset of granulocytic leukocytes that contribute to both host defense and immune regulation, accounting for up to 5% of the total leucocyte population (50). Traditionally recognized for combating parasitic infections, eosinophils also participate in tissue homeostasis, wound repair, and modulation of immune responses through cytokine secretion and crosstalk between immune and structural cells (52,53). In homeostatic conditions, they reside at low levels in blood and select tissues such as the gastrointestinal tract, where they support epithelial barrier integrity and immune surveillance (52,53). Dysregulation of eosinophil function underlies a range of inflammatory and allergic diseases, including asthma (54), eosinophilic esophagitis (55), chronic rhinosinusitis (56) and chronic obstructive pulmonary disease (57). In these contexts, increase in circulating eosinophil numbers, excessive eosinophil activation and tissue accumulation contribute to tissue damage via release of cytotoxic granule proteins, lipid mediators, and pro-inflammatory cytokines, making them central players in disease pathogenesis and potential therapeutic targets (52,53). A defining feature of eosinophil biology is their preferential recruitment from the bloodstream into tissues during inflammation (52,53). This process is orchestrated by chemokine gradients and adhesion interactions that direct eosinophils to specific sites. The CC chemokine receptor 3 (CCR3) is the principal receptor mediating eosinophil chemotaxis (58–60). It is

constitutively expressed at high levels on eosinophils, far more so than on most other leukocyte subsets, and serves as the major receptor for the eotaxin family (notably CCL11, CCL24, and CCL26) (61,62). Elevated expression of CCR3 ligands in disease states amplifies recruitment, correlating with disease severity in conditions such as asthma (62,63) and eosinophilic gastrointestinal disorders (64). Binding of these chemokines to CCR3 initiates intracellular signaling cascades that trigger directed migration, integrin activation, and cytoskeletal rearrangement, enabling eosinophil movement toward inflammatory foci (62,65,66). CCR3 engagement activates G-protein-coupled signaling pathways that converge on downstream effectors such as PI3K/AKT, which regulate cell survival, motility, and degranulation (62,65,66). Genetic or pharmacologic disruption of CCR3 signaling significantly impairs eosinophil migration and reduces tissue infiltration in experimental models of allergic inflammation, indicating CCR3's essential role in pathophysiology (67,68). In addition to chemotaxis, CCR3 influences eosinophil trafficking from bone marrow into circulation and ultimately into inflamed tissues, synergizing with cytokines like IL-5 that promote eosinophil proliferation and survival (62). In allergic diseases and chronic inflammatory syndromes, eosinophil accumulation mediated by CCR3 pathways contributes to tissue injury and symptom persistence. In Eosinophilic esophagitis, disease progression involves marked eosinophil infiltration driven by Th2 cytokines and eotaxin-CCR3 signaling, leading to mucosal dysfunction and fibrosis (55). Asthma severity often parallels levels of CCR3 ligands and eosinophilic inflammation, highlighting the therapeutic relevance of this axis (69). Targeting CCR3 or its ligands has emerged as a rational strategy to attenuate eosinophil migration and mitigate disease, with antagonists showing reduced eosinophil accumulation and inflammation in preclinical models (70).

Neutrophils are highly dynamic innate immune cells that serve as a first line of defense against invading pathogens and play a central role in cellular immunosurveillance (71,72). They constitute about 40-60% of the total leucocyte population in human blood (50). In the resting stage, neutrophils maintain a rounded, quiescent morphology, but upon exposure to inflammatory stimuli they undergo profound cytoskeletal reorganization that enables functional activation (71,73). Much like in eosinophils, such cellular responses in neutrophils are mediated by chemokines. Interleukin-8 (IL-8/CXCL8) is one of the most potent chemoattractants and activators of human neutrophils via CXCR1 and CXCR2 (74). Beyond acute inflammation, IL-8 also promotes

angiogenesis and has been implicated in tumor progression, making the IL-8–CXCR1/2 axis an important therapeutic target in inflammatory and neoplastic diseases (74). Complement protein 5a (C5a), N-formyl-methionyl-leucyl-phenylalanine (fMLP), and phorbol 12-myristate 13-acetate (PMA) are canonical neutrophil agonists that activate distinct signaling pathways. C5a and fMLP stimulate neutrophils through their respective G-protein–coupled receptors (C5aR1 and FPR1), inducing calcium flux, actin reorganization, chemotaxis, degranulation, and oxidative burst (75,76). In contrast, PMA directly activates protein kinase C downstream of surface receptors, eliciting strong respiratory burst and degranulation without chemotactic signaling (77).

Neutrophil activation is generally characterized by alterations in cell shape, surface receptor expression such as CD11b/CD18 activation followed by inflammatory signaling pathway-activation that collectively enhance their effector capacity (71,73). These morphological changes are closely linked to functional responses such as chemotaxis, degranulation, production of reactive oxygen species, and phagocytosis, aimed at pathogen clearance (71,73).

While these responses are essential for host defense, excessive or prolonged neutrophil activation contributes to tissue injury and chronic inflammation. Neutrophils normally cycle through distinct activation states that allow them to eliminate pathogens but persistent or excessive activation can lead to a prolonged, unresolved inflammatory response. Dysregulated neutrophil activation and aberrant morphological changes are increasingly recognized as key drivers of pathology in sepsis (78), cardiovascular disease (79), and autoimmune disorders (80), underscoring the need for regulating neutrophil activation states to preserve immune homeostasis. In sepsis, for example, neutrophils exhibit impaired migration, altered deformability, excessive adhesion, and exaggerated formation of neutrophil extracellular traps, which contribute to endothelial injury, microvascular occlusion, and multiple organ dysfunction (78). In cardiovascular disease, hyperactivated and mechanically stiff neutrophils infiltrate ischemic tissues and atherosclerotic plaques, where they release reactive oxygen species, proteolytic enzymes, and extracellular traps that promote vascular inflammation, plaque destabilization, and tissue damage (79,81). In systemic autoimmune diseases such as rheumatoid arthritis and systemic lupus erythematosus, aberrant neutrophil activation and dysregulated extracellular trap formation expose autoantigens and amplify inflammatory cascades, thereby perpetuating chronic tissue injury (80). Collectively, these observations highlight that

precise regulation of neutrophil activation is critical for maintaining immune homeostasis and preventing immunopathology.

1.4 Interplay Between Native HDL and Granulocytes in Inflammation

Beyond lipid transport, endogenous HDL particles exert broad immunomodulatory and anti-inflammatory actions that influence multiple facets of the immune response. Majority of immunomodulatory effects of native HDL have been documented on mononuclear phagocytes (7), endothelial cells (6), with emerging interest in lymphocytes and granulocytes (9,82). This intersection of lipid metabolism and innate immunity has important implications for both health and inflammatory diseases.

1.4.1 Native HDL and Eosinophil Function

Emerging evidence indicates an inverse relationship between HDL levels and eosinophil counts in inflammatory contexts. Higher serum HDL-cholesterol is statistically associated with lower circulating eosinophil counts in asthmatic individuals, suggesting that HDL may influence eosinophil homeostasis or activation states. This correlation persists after adjusting for demographic, lifestyle, and comorbidity factors, implying that HDL composition or function itself may modulate eosinophilic inflammation (83).

Endogenous HDL and its associated components exert direct regulatory effects on eosinophil activation, survival, and tissue recruitment, as demonstrated in both human and animal studies. In human eosinophils, HDL isolated from patients with allergic rhinitis inhibits eosinophil shape change and chemotaxis, indicating that HDL-associated factors actively restrain eosinophil migratory responses under inflammatory conditions (84). In contrast, eosinophils from patients with atopic dermatitis show a reduced sensitivity to these inhibitory effects, suggesting that disease-associated alterations in HDL composition or eosinophil responsiveness may compromise this regulatory axis (85). Studies in allergic individuals further demonstrate that HDL and its apolipoproteins, including ApoA-I and ApoA-IV, suppress eosinophil chemotaxis and promote apoptosis, supporting a role for HDL in limiting both eosinophil accumulation and persistence at sites of inflammation (86). HDL-associated lipids are also critical modulators of eosinophil

function, as exemplified by LPC and its analogs such as miltefosine, which potently inhibit eosinophil shape change, adhesion molecule expression, calcium flux, degranulation, and directed migration in human eosinophils (87,88). These findings are mirrored in animal models of allergic inflammation, where administration of ApoA-I, ApoA-IV, or specific LPC species reduces eosinophil infiltration into the airways, lowers bronchoalveolar lavage eosinophil counts, and improves lung function (86–88). Collectively, these findings indicate that native HDL and its components regulate eosinophilic effector functions in allergic disease.

1.4.2 Native HDL and Neutrophil Function

Epidemiological and mechanistic studies consistently support an inverse relationship between HDL and neutrophil burden in inflammatory settings. HDL-cholesterol is inversely associated with circulating neutrophil count in men during acute inflammation (e.g., post-vaccination), suggesting HDL modulates neutrophil numbers in inflammatory states (89). Importantly, this relationship extends beyond HDL quantity to HDL function, as cholesterol efflux capacity inversely correlates with the neutrophil–lymphocyte ratio in healthy individuals, linking superior HDL functionality to lower relative neutrophil dominance (90). Clinically, these interactions are reflected in the prognostic value of the neutrophil-to-HDL-cholesterol ratio, which has emerged as a robust marker of disease severity and mortality in sepsis and cardiovascular disorders, reinforcing the concept that reduced HDL is tightly linked to heightened neutrophil-driven inflammation (91–93).

The anti-inflammatory functions of HDL are mediated in part by its apolipoproteins and associated lipids. HDL can bind and neutralize bacterial LPS and lipoteichoic acid (LTA), thereby reducing innate immune cell activation triggered by microbial stimuli (94,95). LPS and LTA are agonists for neutrophil activation during infection (96,97), hence the toxin neutralizing activity reduces the overall inflammatory burden on neutrophils.

HDL has been shown to modulate N-formyl-methionyl-leucyl-phenylalanine induced CD11b expression in human neutrophils (98). HDL associated sphingosine-1-phosphate (S1P) inhibits neutrophil recruitment a mouse model of myocardial ischemia-reperfusion, suggesting cardioprotective roles modulated via neutrophils (99). ApoA-I, has been shown to modulate neutrophil activation in whole blood against LPS and PMA induced inflammation in an ABCA1

and SR-BI dependent manner (100). This reduction in activation also correlates with the lipid raft abundance on neutrophils suggesting membrane lipid modulation by ApoA-I (100). Beyond its protein components, the HDL lipidome plays a considerable role in regulating its anti-inflammatory activities. Modification of HDL by secretory phospholipase A_2 has been shown to suppress neutrophil activation underscoring the importance of lysophosphatidylcholine (LPC) content in endogenous HDL as a key immunomodulatory factor (101). LPC treatment has also been shown to modulate neutrophilic inflammation and ameliorate LPS-induced lung injury (102). Hence, endogenous HDL and its components modulate neutrophil activation by scavenging pathogenic molecules as well as directly interacting with the neutrophils to exert immunomodulatory activities.

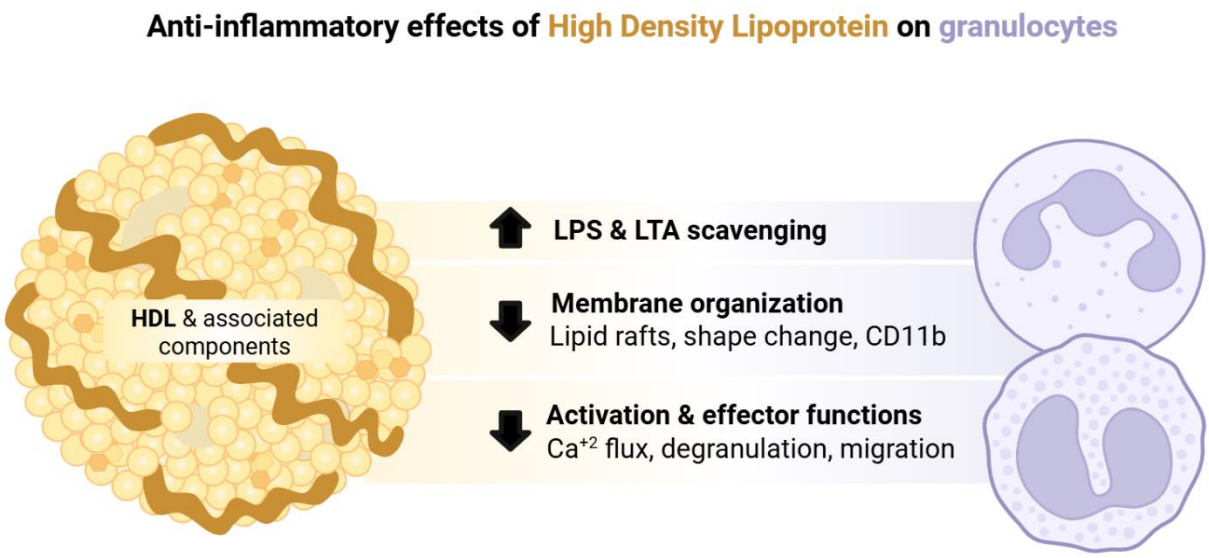

Figure 2. **Summary of anti-inflammatory effects of endogenous HDL and its components on neutrophils and eosinophils highlighting its immunomodulatory potential** (9). Abbreviations: LPS-lipopolysaccharide, LTA- lipoteichoic acid, CD- cluster of differentiation figure generated with Biorender.com

1.5 Targeting Granulocyte Activation with Synthetic HDL nanodiscs

Unlike endogenous HDL, sHDL particles can be engineered for consistent composition, payload delivery, and targeted interactions with immune cells, making it an attractive candidate to modulate granulocyte-driven inflammation (34). Opportunities for targeting granulocytes with sHDL hinge on several strategic advantages. First, based on the outcomes of clinical trials, ApoA-I mimetic peptides can be selected to maximize cholesterol modulating functions while minimizing immunogenicity (7). Second, the nanoparticle format allows co-delivery of small molecules that favor interaction with granulocyte subsets or inflamed endothelium (34,103–105). Third, the composition can be tuned to ensure targeted delivery of sHDL in inflamed microenvironments and to retain functional cargo under oxidative stress (34,49,104,106,107). HDL mimetics also exert indirect anti-inflammatory effects on granulocytes by modulating the activation state of endothelial cells (104) and epithelial cells (108), thereby regulating their adhesion and transmigration to the inflamed tissues.

Emerging work indicates that the ApoA-I mimetic peptides limit eosinophil recruitment and chemotactic responses in chronic Th-2 inflammatory diseases such as asthma (109,110). ApoA-I mimetic peptides such as 5A and 4F have been shown in allergic inflammation models to reduce eosinophil recruitment to the lungs and lower eosinophil counts in bronchoalveolar lavage fluid (111,112). ApoA-I mimetic peptides also reduce the overall oxidative stress burden in the lung thereby reducing pathogenic remodeling of the lung tissue (107,112). Despite several studies reporting the protective effects of ApoA-I mimetic peptides in eosinophilic inflammation, the underlying mechanisms that alter eosinophil functions are not well understood. Furthermore, lipidated sHDL nanodiscs, which have been described in the context of infectious diseases (26), have not yet been investigated in relation to allergic inflammation.

Preclinical and clinical studies provide proof-of-principle that HDL mimetics reduce granulocyte-mediated pathology (22). In models of bacterial sepsis and endotoxemia, administration of sHDL reduces inflammatory cytokine levels (25), limits neutrophil overactivation and adhesion to endothelial wall (113) preserves organ function and improves survival (107,114,115). These protective effects are largely attributed to LPS neutralization and suppression of toll-like receptor (TLR) -driven signaling as key contributors (25,46,114).

These findings indicate that HDL mimetics can blunt both neutrophilic and eosinophilic arms of inflammation through distinct molecular mechanisms. sHDL exerts these immunoregulatory effects that are relevant to granulocytes through two major pathways. First, sHDL can bind and sequester LPS (25,115), reducing ligand availability for pattern-recognition receptors and potentially blunting downstream activation of granulocytes. Second, sHDL and ApoA-I mimetics alter membrane cholesterol content through cholesterol efflux (7,25,26), which alters TLR clustering and signal transduction required for granulocyte activation.

2. HYPOTHESIS

2.1 We hypothesize that sHDL nanodiscs composed of the ApoA-I mimetic peptide 4F-P-4F and DMPC exert potent anti-inflammatory effects on eosinophils by attenuating eosinophil activation, effector functions, and inflammatory signaling pathways. In disease-relevant inflammatory settings, we expect these nanodiscs to reduce the eosinophil driven inflammation involving specific mechanisms.

2.2 We propose that LPC incorporation alters nanodisc physicochemical properties and bioactivity when formulated using 22A ApoA-I mimetic peptide as an example, thereby allowing isolation of lipid-driven effects on granulocytes.

3. RATIONALE & AIMS

3.1 4F-P-4F DMPC nanodiscs synthesis and characterization

The first objective of this research was to synthesize and rigorously validate a sHDL nanodisc platform based on the ApoA-I mimetic peptide 4F-P-4F and the phospholipid DMPC, characterize particle assembly and check if our preparation systems yield homogeneous nanodiscs. Concurrently, molecular dynamics simulations and circular dichroism spectroscopy were utilized to study peptide secondary structure and peptide–lipid interactions, with the objective of ascertaining whether lipid incorporation preserves the intrinsic α-helical conformation of 4F-P-4F and promotes an amphipathic, belt-like arrangement that is essential for nanodisc stabilization. We

also characterized the specific molecular interactions governing nanodisc integrity and to establish a robust, structurally validated HDL-mimetic nanodisc system as a foundation for subsequent functional investigations.

3.2 Anti-inflammatory effects of 4F-P-4F DMPC sHDL nanodiscs on eosinophils

Tissue-specific granulocyte recruitment is a hallmark of inflammation and a major contributor of disease severity (54,55,116,117). Through this dissertation work we aim to dive deeper into the effects of sHDL nanodiscs on granulocyte effector functions. sHDL nanodiscs provide a controlled platform to investigate HDL-mediated anti-inflammatory mechanisms independent of endogenous HDL heterogeneity.

In this study, sHDL nanodiscs composed of the apolipoprotein mimetic peptide 4F-P-4F and the phospholipid DMPC are used to assess their effects on eosinophil activation and inflammatory responses. 4F-P-4F is a tandem ApoA-I mimetic peptide designed to enhance lipid affinity, structural stability, and biological activity compared to single-helix mimetics. The 4F sequence mimics the amphipathic α-helices of ApoA-I and has been shown exhibit protective effects in cardiometabolic disease settings (41). The dimeric 4F-P-4F configuration further improves lipid binding due to the presence of a proline linker and this ensures lower polydispersity in the resulting formulations (35,37,41,44), making it particularly suited for evaluating anti-inflammatory functions. DMPC (1,2-dimyristoyl-sn-glycero-3-phosphocholine) is a phospholipid routinely employed in sHDL formulations due to its well-defined phase behavior, high biocompatibility (118), and strong ability to form stable discoidal particles with ApoA-I mimetic peptides (34). Its saturated acyl chains promote reproducible nanodisc size and structural integrity, making DMPC an ideal lipid matrix for mechanistic studies of peptide-mediated anti-inflammatory effects. Apart from structural advantages, DMPC also functions as a bioactive phospholipid with significantly superior anti-inflammatory effects compared to other phospholipid candidates for sHDL synthesis (45,46,119,120). To assess the anti-inflammatory efficacy of the characterized nanoformulations, their effects were evaluated using primary human eosinophils isolated from peripheral blood as well as an interleukin-5 (IL-5) transgenic mouse model of eosinophilic inflammation.

3.3 Improving Anti-inflammatory Effects of 22A DMPC sHDL nanodiscs by LPC-enrichment

The 22A peptide is a well-characterized ApoA-I mimetic peptide, with several studies reporting its stability during the process of enrichment with bioactive cargo (105,46,49). 22A is frequently used as a benchmark peptide in HDL structure–function studies (44). Using 22A allows a clear dissection of how lipid composition alone changes affect nanodisc physicochemical properties and biological behavior. To further explore how lipid composition influences sHDL structure and function, this aim examines the impact of LPC incorporation into sHDL nanodiscs. LPCs is are known to modulate granulocyte effector functions (88,102) and is also an active metabolic product of sHDL treatment in vitro and in vivo . Hence, enriching the sHDL with LPCs may offer significant anti-inflammatory advantages. For the enrichment studies we chose the 22A peptide as the peptide scaffold along with DMPC as the phospholipid component and evaluated its immunomodulatory effects on polymorphonuclear leucocytes. These experiments were performed under the supervision of Dr. Anna Schwendeman at the University of Michigan, Ann Arbor, USA.

4. MATERIALS AND METHODS

4.1 4F-P-4F DMPC sHDL nanodisc synthesis

The synthesis and quality control characterization were performed in cooperation with the lab of Prof. Ruth Prassl following a similar protocol as published before (41). The 4F-P-4F peptide, with the amino acid sequence DWFKAFYDKVAEKFKEAFPDWFKAFYDKVAEKFKEAF (L-form stereoisomers), was chemically synthesized by GenScript Biotech (Rijswijk, Netherlands). The N- and C-terminal modifications were acetylation and amidation, respectively (Ac4F-P-4FNH_2). Formation of sHDL nanodiscs was achieved using a microfluidic strategy combining the peptide and DMPC (Avanti Polar Lipids, Alabama, USA). The microfluidic assembly consisted of a herringbone-structured (Little Things Factory GmbH, Elsoff, Germany) attached to two programmable NE-1002× syringe pumps (NewEra Pump Systems, Inc., Farmingdale, USA). Prior to experimental use, the microfluidic device was sequentially flushed with ethanol and ultrapure

water. All reagent solutions were freshly prepared and combined immediately before being introduced into the syringe pump system. A borosilicate microfluidic chip comprising three channels, two inlet ports, and a single outlet port was used for the mixing process. The peptide solution in double distilled water was delivered into the system at a flow rate of 5 mL/min, while the DMPC solution in ethanol was simultaneously infused at a flow rate of 1 mL/min.

Following nanodisc formation, the suspension was subjected to concentration using ultracentrifugal filters with a molecular weight cutoff of 10 kDa (Sigma, Vienna, Austria) in order to eliminate unincorporated peptides and ethanol. This concentration and washing process was executed three consecutive times and the resulting sample was subsequently resuspended in phosphate-buffered saline (PBS), pH 7.4 without calcium and magnesium. The phospholipid concentration was quantified using the Phospholipids FS assay kit (DiaSys Diagnostic Systems GmbH, Holzheim, Germany) in accordance with the manufacturer's instructions. Protein concentration was determined by ultraviolet absorbance at 280 nm using a NanoPhotometer P-330 (Implen, Munich, Germany).

4.2 Dynamic Light Scattering

Determining the the size (hydrodynamic radius) of the nanodiscs and the homogeneity of the formulations with Dynamic Light Scattering (DLS) is crucial before proceeding to the in vitro and vivo experimentation. We used Litesizer 300 instrument (Anton Paar GmbH, Graz, Austria), equipped with a 40 mW laser source operating at an emission wavelength of 658 nm. Prior to measurement, sHDL samples were diluted to achieve a final protein concentration of 0.2 mg/mL and transferred into disposable semi-micro cuvettes (Eppendorf, Hamburg, Germany). DLS measurements were conducted at a fixed scattering angle of 90°, with each sample analyzed in three independent runs. The resulting data were processed using Kalliope software (Anton Paar GmbH, Graz, Austria). Particle size results are reported as mean values, and sample homogeneity was assessed with the polydispersity index.

4.3 Transmission Electron Microscopy of 4F-P-4F DMPC sHDL nanodiscs

Transmission Electron Microscopy (TEM) was performed to examine the morphology of the resulting formulations and to determine whether discrete nanodiscs were formed. The procedure

involves negative staining to improve contrast. Carbon-coated CF400-Cu-50 grids with a 400-mesh copper support were pretreated by glow discharge using a Pelco easiGlow system (Ted Pella, USA) to ensure uniform spreading of the sample across the grid surface. An aliquot of 5 µL of the sample was deposited onto the prepared grid and left to adsorb for 1 min. Excess liquid was then carefully wicked away using filter paper. For contrast enhancement, 5 µL of a 1% uranyl acetate solution (that had been centrifuged prior to use) was added to the grid and allowed to incubate for 1 min before removal. This staining procedure was performed twice, after which the grids were left to air-dry. Imaging was carried out using a Zeiss EM900 transmission electron microscope (Carl Zeiss AG, Jena, Germany) operated at an accelerating voltage of 80 kV. Acquired digital micrographs were processed and analyzed using Image SP software (Version 1.2.7.96, SysProg TRS).

4.2 Size exclusion chromatography with 4F-P-4F DMPC sHDL nanodiscs

Size Exclusion Chromatography (SEC) was performed as previously reported for native HDL (121). To assess size distribution of nanodiscs and we used NGC QUEST FPLC system (Bio-Rad, Vienna, Austria) fitted with a Superdex 200 Increase 10/300 column (GE Healthcare Europe GmbH, Munich, Germany) with PBS at pH 7.4 as the running buffer, a constant flow rate of 0.5 mL/min and absorbance detection at 280 nm. The sHDL nanodiscs were analyzed for size distribution and to rule out the presence of any unbound peptide following preparation.

4.5 Molecular dynamics simulations of the 4F-P-4F DMPC sHDL nanodiscs

All atom Molecular Dynamics (MD) simulations (performed by Prof. Mounir Tarek's lab) were used to visualize how the peptide and lipids interact over time and to assess the stability of the assembled sHDL nanodiscs. 4F-P-4F peptide structures were generated using the PEP-FOLD server (122) (Supplementary Fig. 1). The N- and C-termini of the resulting peptide models were subsequently modified through acetylation and amidation, respectively, using the CHARMM-GUI interface (123). Guided by prior Nuclear Magnetic Resonance (NMR) investigations of ApoA-I mimetic peptides (36,124–126) the 4F-P-4F peptides were assembled into anti-parallel dimers, with the majority of charged amino acid residues oriented toward the exterior, thereby generating an amphipathic structural arrangement (Supplementary Fig. 2). Depending on the dimensions of

the nanodiscs (Supplementary Table 1), the appropriate number of peptide dimers was arranged into a circular configuration with an inter-dimer spacing of 0.5 nm. These dimers were positioned around a pre-equilibrated DMPC lipid bilayer patch with disk-like geometry, such that the hydrophobic surfaces of the peptides were oriented toward the hydrophobic core of the lipid assembly. The resulting peptide–lipid complexes were subsequently immersed in a solvent box containing 0.15 M NaCl. All simulations were performed using the CHARMM36m force field (127) in combination with the GROMACS simulation package (128). Following standard energy minimization steps, short constant-volume, constant-temperature simulations were carried out. During this phase, positional restraints applied to the peptide backbone atoms and lipid head groups were progressively released. Production MD simulations for each system were then executed using a 4 fs integration timestep enabled by Hydrogen Mass Repartitioning (129), under conditions of constant temperature (303 K) and constant pressure (1 atm). Pressure regulation was achieved using the Parrinello–Rahman barostat (130), while temperature control was maintained with a Nosé–Hoover thermostat (131).

Long-range electrostatic interactions were treated using the Particle Mesh Ewald method (132) under three-dimensional periodic boundary conditions, in accordance with current best practices in MD simulation. An identical simulation workflow was applied to peptide-only systems solvated in water. Detailed descriptions of the structural composition of each nanodisc system are provided in Supplementary Table 1.

4.6 Circular Dichroism of 4F-P-4F DMPC sHDL nanodiscs and the peptide

Circular dichroism (CD) was used to confirm the peptide's secondary structure and how it changes upon lipid binding. CD measurements were carried out using a Jasco J-1500 spectropolarimeter (Jasco Inc., Easton, USA). Spectral acquisition was performed over a wavelength range of 190–260 nm using a scan rate of 50 nm/min, with a digital integration time of 2 s and a spectral bandwidth of 2 nm. All samples were adjusted to a final concentration of 0.2 mg/mL prior to analysis. Measurements were conducted in a quartz cuvette with a 1 mm optical path length (Hellma GmbH & Co. KG, Müllheim, Germany) maintained at 37 °C. For each condition, ten successive scans were recorded to ensure spectral reliability. To enable direct comparison between experimental CD data and secondary structure predictions derived from MD simulations, far-UV

CD spectra were calculated from simulated trajectories. For nanodisc-containing systems, peptide conformations in proximity to the lipid bilayer were extracted as structural snapshots at 10 ns intervals from the final 100 ns segment of the simulations. In simulations containing peptides alone, structural frames were collected at 5 ns intervals from the final 100 ns of the trajectories. All extracted structures were converted into PDB format and submitted to the PDBMD2CD web server (133), which applies an empirically based algorithm to generate predicted CD spectra from atomic-level structural information. Spectral deconvolution was carried out using the CDSSTR algorithm implemented within the DichroWeb platform (134,135) in combination with the SP175 reference dataset, enabling quantitative determination of secondary structure composition. The resulting average values were expressed in delta epsilon units. Furthermore, mean residue ellipticity values (MRE [θ], expressed in $deg \cdot cm^2 \cdot dmol^{-1} \cdot residue^{-1}$) at 222 nm were extracted from the CD spectra. These values were subsequently used to calculate and compare fractional helicity according to the specified equation (136).

4.7 Isolation of Human HDL

Native human HDL was isolated from plasma collected from healthy donors by means of density gradient ultracentrifugation, in accordance with a previously reported method (121). All procedures were reviewed and approved by the Ethics Committee of the Medical University of Graz (approval number 17–291 ex 05/06). Prior to centrifugation, the density of the plasma samples was increased to 1.24 g/mL with the addition of potassium bromide. For gradient formation, a two-layer system was prepared in centrifuge tubes with dimensions of 16 × 76 mm (Beckman, California, USA). The density-adjusted plasma (1.24 g/mL) was carefully placed beneath a sodium chloride solution adjusted to a density of 1.063 g/mL. Following gradient preparation, the tubes were sealed and subjected to ultracentrifugation at 90,000 rpm for 4h using a 90Ti fixed-angle rotor (Beckman Instruments, Krefeld, Germany). After centrifugation, the HDL-containing fraction was isolated and subsequently desalted using PD10 desalting columns (GE Healthcare, Vienna, Austria).

4.8 Eosinophil isolation from human blood

Polymorphonuclear leukocytes (PMNLs), including neutrophils and eosinophils, were obtained from peripheral blood collected from healthy human volunteers. Blood sampling was performed in

accordance with a protocol approved by the Ethics Committee of the Medical University of Graz (approval number EK17–291 ex 05/06), and written informed consent was obtained from all participants prior to donation. Whole blood was anticoagulated using 3.8% sodium citrate and centrifuged to remove platelet-rich plasma. Red blood cells were subsequently allowed to sediment by incubation with 6% dextran for 30 min at room temperature. The leukocyte-enriched supernatant was carefully layered onto a Histopaque density gradient (Sigma-Aldrich, Darmstadt, Germany) and centrifuged at 400 ×g for 20 min. Following centrifugation, peripheral blood mononuclear cells (PBMCs), saline, and Histopaque were removed. The remaining PMNL fraction was washed with calcium- and magnesium-free phosphate-buffered saline (PBS) supplemented with 0.1% bovine serum albumin, 10 mM HEPES, and 10 mM glucose (pH 7.4). Residual erythrocytes were eliminated by hypotonic lysis using 0.2% saline. Eosinophils were isolated from the PMNL population using a commercially available human eosinophil isolation kit (Miltenyi Biotec, Gladbach, Germany) based on negative magnetic selection. Cell purity was verified by morphological evaluation using Kimura staining and consistently exceeded 95%. Assay buffer consisting of PBS containing Ca^{2+} and Mg^{2+}, supplemented with 0.1% bovine serum albumin, 10 mM HEPES, and 10 mM glucose (pH 7.4), was used for eosinophil experiments unless otherwise specified.

4.9 Eosinophil Viability Assay

Eosinophil viability was evaluated using an apoptosis–necrosis assay based on Annexin V and propidium iodide (PI) staining. For each experimental condition, approximately 50,000 eosinophils were incubated in assay buffer with either vehicle, a positive control consisting of 20% DMSO, or the specified concentrations of sHDL nanodiscs. Incubations were carried out for 4 h at 37 °C in a humidified atmosphere containing 5% CO_2.

Following incubation, cells were labeled with an anti-Annexin V-APC antibody (BioLegend, San Diego, USA) and PI (Sigma, Vienna, Austria). The Annexin V antibody was diluted 1:50, while PI was used at a dilution of 1:20. Annexin V staining was performed for 30 min at 4 °C, and PI staining was conducted for 1 min at room temperature. Cells were analyzed without prior fixation.

The gating strategy used for data analysis defined early apoptotic cells as Annexin V^+/PI^-, late apoptotic cells as Annexin V^+/PI^+, necrotic cells as Annexin V^-/PI^+, and viable cells as Annexin V^-/PI^-. Data were processed using FlowJo software version 10.8.1 and cells negative for both Annexin V and PI fluorescence were selected as viable.

4.10 Eosinophil Shape Change Assay

Shape-change assays are used to capture early granulocyte activation, since cytoskeletal remodeling rapidly alters forward scatter profiles (137,138). This morphological change reflects cytoskeletal reorganization, which is essential for neutrophil adhesion, migration, and interaction with the endothelium and other immune cells (137,138). Eosinophils were placed in assay buffer and incubated with sHDL nanodiscs for 30 minutes, then exposed to eotaxin-1 for 4 minutes at 37°C. The cells were subsequently fixed on ice using a mixture of distilled water, FACS sheath fluid, and CellFix (BD Biosciences, Vienna, Austria) and kept at 4°C until acquired for assessment on a BD FACS Canto II. Morphological activation was quantified by forward-scatter area (FSC-A) increase, expressed as the geometric mean and analyzed in FlowJo 10.8.1.

4.11 Eosinophil Chemotaxis Assay

Chemotaxis assay was performed to measure eosinophil migration toward defined chemoattractants and to assess how the formulations modulate this aspect of eosinophil effector function. Isolated human eosinophils were incubated with either vehicle, the 4F-P-4F peptide, or synthetic high-density lipoprotein at the indicated concentrations for 30 min at 37 °C in assay buffer. Some experiments were also performed in RPMI medium supplemented with 10% fetal bovine serum (FBS; Thermo Fisher Scientific, Waltham, USA). Following pre-treatment, eosinophil migration was assessed toward 3 nM eotaxin-1 (ImmunoTools, Friesoythe, Germany) using an HTS Transwell 96-well migration system equipped with a polycarbonate membrane featuring 5-µm pores (Corning, Berlin, Germany). A total of 70,000 cells were seeded per well and allowed to migrate for 1 h at 37 °C under an atmosphere containing 5% CO_2. For receptor-blocking experiments, eosinophils were pre-incubated with anti-SR-BI and anti-ABCA1 antibodies (Novusbio NB400-101 and NB400-105 respectively, Bio-Techne, Oxon, England), and the chemotaxis assay was subsequently conducted in the continued presence of these antibodies

following a 30-min pre-incubation period without additional washing steps, as described previously (86). After completion of the migration period, cells from the lower chamber were collected in their entirety, fixed using 100 µL of fixative solution, and analyzed by flow cytometry using a BD FACS Canto II system. Quantification of migrated cells was performed using FlowJo software version 10.8.1.

4.12 Eosinophil CCR3 expression

Human eosinophils were isolated and incubated at 37 °C for 30 minutes in assay buffer containing either vehicle or sHDL (25 µg/mL). Cells were then exposed to eotaxin-1 (10 nM) for an additional 30 minutes. Additionally, for some experiments, eosinophils were treated with phenylarsine oxide (PAO; 8 µM), a known blocker of CCR3 internalization (88,139), 4F-P-4F (25 µg/mL), or purified human HDL (25 µg protein/mL).

Following treatment, cells were washed with PBS, and stained for surface CCR3 using a PE-conjugated anti-CCR3 antibody in PBS containing 2% FBS for 30 minutes at 4 °C in the dark. Unstained sample was used as a gating control. After a final wash, cells were fixed with CellFix (BD Biosciences, Vienna, Austria) at 4 °C and analyzed by flow cytometry. CCR3 surface expression was quantified as the geometric mean fluorescence intensity in the PE (B585–42 A) channel using a BD FACS Canto II, and data were analyzed with FlowJo version 10.8.1.

4.13 Western Blot for SR-BI Detection in Human Eosinophils

1-2 million human eosinophils were processed in radioimmunoprecipitation assay lysis buffer. Lysates prepared in sample buffer were electrophoresed for 1.5 hours at 120 V using the NuPage, Bis-Tris gel (Invitrogen, Waltham, MA, USA). Proteins were transferred to a membrane with iBlot™ Transfer Stacks and iBlot™ Dry Transfer system (Invitrogen, Waltham, MA, USA). Polyvinylidene fluoride membranes after transfer were blocked for 1 h with TBST (1× TBS + 0.1% Tween) containing 5% skim milk. The membranes were incubated at 4 °C overnight with the primary anti-SR-BI antibody (Novusbio NB400-101, Bio-Techne, Oxon, England, diluted 1:1000), washed and incubated with secondary HRP-conjugated goat anti-rabbit antibody (diluted 1:5000) for 2 hours at room temperature under shaking conditions. Blots were washed and developed using

Clarity ECL western blot reagents (Bio-Rad, Vienna, Austria) and imaged using a Bio-Rad ChemiDoc™ MP Imaging System (Bio-Rad, Vienna, Austria).

4.14 Cholesterol Efflux from Human Eosinophils

The cholesterol efflux assay was used to confirm that the sHDL nanodiscs actively remove cholesterol from eosinophils, a key function expected from HDL-mimetic particles (7). Demonstrating this activity verifies that the nanodiscs interact effectively with cellular lipid pools. This mechanistic link helps explain how altering membrane cholesterol content might contribute to the understanding of their functions. For each experimental condition, approximately 5×10^5 eosinophils were radiolabeled with [^{3}H]-cholesterol at a concentration of 0.5 µCi/mL for 3 h at 37 °C in a humidified incubator under 5% CO_2. Radiolabeling was performed in RPMI medium supplemented with 1% penicillin/streptomycin and 2 µg/mL of an acyl-CoA cholesterol acyltransferase (ACAT) inhibitor (Sigma, Darmstadt, Germany). Following labeling, cells were washed three times with assay buffer consisting of PBS containing Ca^{2+} and Mg^{2+}, 10 mM HEPES, 10 mM glucose, and 0.1% bovine serum albumin (pH 7.4). Each wash was performed by centrifugation at 500 ×g for 5 min.

After washing, eosinophils were treated with HDL, sHDL, or 4F-P-4F for 1 h at 37 °C in a 5% CO_2 atmosphere. The efflux incubation was carried out in RPMI medium supplemented with 1% penicillin/streptomycin and 2 µg/mL ACAT inhibitor. Upon completion of the efflux phase, cells were pelleted by centrifugation and the supernatants were collected. The cell pellets were lysed using 0.1% SDS in 0.3 N NaOH to determine the amount of intracellular [^{3}H]-cholesterol. For receptor inhibition studies, eosinophils were pre-treated with anti-SR-BI and anti-ABCA1 antibodies (Novusbio NB400-101 and NB400-105 respectively, Bio-Techne, Oxon, England), after which the efflux assay was conducted in the continued presence of these blocking antibodies, following a 30 min pre-incubation without additional washing steps, as previously described (86). All experimental conditions were performed in triplicates, and each individual sample was analyzed in duplicate. PBS-treated cells were included as vehicle controls. Cholesterol efflux was calculated as the proportion of radioactive signal detected in the supernatant relative to the total radioactivity recovered from both the supernatant and corresponding cell lysate. To obtain specific

efflux values, background efflux measured in the vehicle control (typically <1%) was subtracted from all experimental conditions.

4.15 Phosphokinase Array with human eosinophils

The impact of sHDL treatment on the phosphorylation profiles of multiple kinases in eosinophils was analyzed using the Human Proteome Profiler Array Kit (R&D Systems, Minneapolis, USA). Purified human eosinophils obtained from three independent donors were pooled prior to experimentation. Cells were incubated in assay buffer containing either vehicle or sHDL nanodiscs and subsequently stimulated with eotaxin-1 at a concentration of 10 nM for 5 min at 37 °C.

All subsequent processing steps were conducted strictly according to the manufacturer's protocol. Array membranes were incubated with the cell lysates overnight at 4 °C. Following completion of the assay procedure, membranes were developed and imaged using a Bio-Rad ChemiDoc™ MP Imaging System. Quantification of signal intensities from duplicate array spots was carried out using ImageLab software version 5.2.

4.16 In vivo Migration Assay

Eosinophil migration in vivo was triggered by the intranasal administration of 4 µg recombinant human eotaxin-2 (R&D Systems, Bio-Techne, Dublin, Ireland) to male and female interleukin-5 transgenic (IL-5 Tg) mice on a BALB/c background aged 7–10 weeks. This experimental model, which has been previously established and validated (88,140,141) is specifically designed to investigate eosinophil function in severe asthma characterized by pronounced pulmonary eosinophilia following eotaxin stimulation (88,141). Thirty minutes prior to the eotaxin challenge, mice received an intravenous injection of either vehicle or sHDL nanodiscs at a dose of 75 mg/kg.

Bronchoalveolar lavage fluid was collected 4 h after the initiation of the experiment and subsequently processed for immune cell composition analysis. Flow cytometric gating strategies were applied to identify lymphocytes ($CD11c^{-}/CD11b^{-}$), eosinophils (Siglec $F^{+}/CD11b^{+}/CD11c^{-}$), alveolar macrophages (Siglec $F^{+}/CD11c^{+}$), and neutrophils (Siglec $F^{-}/CD11b^{+}/Ly6G^{+}$), as previously reported (140). All animal experiments were approved by the Austrian Federal Ministry of Science, Research, and Economy (protocol numbers: 2023–0.402.980 and BMWFW-66.010-

0041WF/II/3b/14). The study was conducted in compliance with the European Community's Council Directive (2022–0.626.093).

4.17 Synthesis of lysophosphatidylcholine enriched sHDL nanodiscs

Both DMPC and the ApoA-I mimetic peptide 22A were dissolved in acetic acid in weight ratios 1:2, separately and combined into one glass vial (keeping volume less than 3mL). The mixture was flash frozen in liquid nitrogen and freeze dried overnight (co-lyophilization). 1xPBS (without Ca and Mg) was used to re-constitute the formulation, using 3x heat-cool cycles of 37°C and 4°C. The pH was adjusted to 7.4 after the first cycle and the formulation was checked for clear appearance (49). To evaluate the possibility of improving the anti-inflammatory potential of sHDL, differential lipidation of sHDL nanodiscs was carried out. For this we chose the lysophosphatidylcholine (LPCs). Based on our previous findings (88,119), we chose LPC 14:0, LPC 16:0, LPC 18:0, to test the structural feasibility and enhancement in anti-inflammatory properties of sHDL. For this, we used the freeze-drying method and combined the LPCs with DMPC and ApoA-I mimetic peptide 22A. Different types of enrichment were carried out by removing DMPC and adding equivalent % of LPC. We used molar ratios and the % of enrichment is the % of enrichment over DMPC.

4.18 DLS with lysophosphatidylcholine enriched sHDL nanodiscs

Particle size and stability studies of the LPC enriched sHDL formulations was performed on a Malvern Zetasizer Nano ZSP (Malvern Panalytical, MA, USA) at 25°C. Samples were prepared by diluting the sHDL formulations in PBS to 1mg/ml. The instrument settings were optimized according to manufacturer recommendations, and each sample was measured in triplicate to ensure reproducibility. Data acquisition and analysis were conducted using Zetasizer software version 7.13. The reported values correspond to the volume intensity average hydrodynamic diameter, which provides an estimate of the effective particle size distribution weighted by particle volume.

4.19 Gel Permeation Chromatography with lysophosphatidylcholine enriched sHDL nanodiscs

To further characterize the size distribution of the sHDL nanoparticles, gel permeation chromatography (GPC) was employed. Samples of enriched sHDL and blank sHDL particles were injected onto the GPC system, which was operated at a controlled flow rate of 0.75 mL/min. As

particles traverse the column, larger particles are excluded from entering the smaller pores of the gel matrix and thus elute earlier, while smaller particles penetrate more deeply and elute later. This separation is quantified as retention time, which correlates inversely with particle size. Chromatograms were recorded and analyzed according to established protocols (49).

4.20 Liquid Chromatography- Mass Spectrometry

Nanodiscs were subjected to 7 kDa size-exclusion cleanup using Zeba Spin Desalting Columns prior to lipid extraction. Under these conditions, freely soluble lipids (<7 kDa) are retained in the resin, while nanodisc-associated lipids elute in the excluded fraction. Presence of LPCs in cleaned-up samples was quantified using Waters® ACQUITY UPLC H-Class system equipped with a QDa detector (Waters, Milford, MA). Chromatographic separation was performed on a Waters® ACQUITY UPLC® BEH C18 (1.7 µm, 2.1 x 50 mm) column, at a constant column temperature of 50°C. Mobile phase A consisted of 20:80 methanol: water, while mobile phase B was 76:19:5 methanol: acetonitrile: isopropanol, both containing 5 mM ammonium acetate. Separation was carried out at a flow rate of 0.5 mL/min with a 10-min gradient: initial (30% B), 0-2 min (70% B), 2-4 min (80% B), 4-7 min (99% B), 7-8 min (hold 99% B), 8-8.1 min (30% B), 8.1-10 min (hold 30% B). Prepared sHDL particles were divided in two and one of the fractions was passed through 7K molecular weight cut-off columns (Zeba™ Spin, Thermo Fisher Scientific, USA). Samples and standards were injected at a volume of 2 µL. Selected ion recording was used to detect lipid species of interest at a cone voltage of 15V. Positive mode was used for LPC 14:0 (m/z 468.3) and DMPC (m/z 678.5), as well as standards LPC 13:0 (m/z 454.3) and PC-d54 14:0 (m/z 732.8).

4.21 Neutrophil viability assay

Annexin V-APC / Propidium Iodide (PI) Staining for Apoptosis and Necrosis was performed on human neutrophils as described previously for eosinophils in chapter 4.9. PMNLs were treated for 30 min at 37°C with indicated concentrations of nanoformulations and the staining was performed as described earlier in chapter 4.9

4.22 Neutrophil shape change assay

Neutrophil shape change, an early and sensitive indicator of activation, was assessed using flow cytometry as previously described in chapter 3.1.9. Isolated PMNLs were resuspended in assay

buffer (approximately 3-5 × 10^5 cells per sample) and preincubated with sHDL formulations in indicated concentrations for 15min. Cells were then stimulated at 37 °C for 5min with 10nM IL-8. All stimulations were carried out in a final volume of 100 µL. To halt cellular activation and preserve morphological changes, samples were transferred to ice, and 150 µL of ice-cold fixative solution containing 4% paraformaldehyde in phosphate-buffered saline (PBS) was added. Samples were analyzed using a BD FACS Canto™ II flow cytometer (BD Biosciences). Neutrophils and eosinophils were distinguished based on their granularity (side scatter) and autofluorescence profiles using the B530 and V450 channels. Shape change of the neutrophils (V450 low, more abundant in number) was quantified as an increase in forward scatter area (FSC-A), relative to vehicle-treated controls, using FlowJo10.1.

4.23 Statistical analysis

All experimental data are presented as mean values with the associated standard error of the mean (SEM). Independent experiments were repeated using cells derived from different human donors and with separate groups of mice, as specified for each experimental setup. Statistical evaluations were performed using GraphPad Prism software version 10. Group comparisons were conducted using the statistical tests indicated individually for each experiment. Statistical significance was defined as $p < 0.05$, with exact p-values reported for the respective experiments

5. RESULTS

5.1 4F-P-4F DMPC nanodisc studies

5.1.1 4F-P-4F DMPC nanodiscs synthesis and characterization

Synthetic HDL (sHDL) nanodiscs were produced using a microfluidic synthesis platform enabling precise control over formulation parameters and particle assembly. Dynamic Light Scattering measurements demonstrated that the resulting sHDL particles possessed a mean hydrodynamic diameter of 13.2 nm (Fig. 3A). The corresponding polydispersity index was recorded as 0.216, indicating a narrow size distribution and a relatively homogeneous nanoparticle population.

To assess the secondary structure of the 4F-P-4F peptide and its lipid-associated form within sHDL nanodiscs, both MD simulations and experimental CD spectroscopy were performed. The simulated and experimental CD spectra were analyzed using the DichroWeb platform to determine secondary structure content (134). Fractional helicity (fH) values were calculated according to the method described in Section 2.5 and Supplementary Table 2. and compared with DichroWeb-derived estimates. Across all simulated spectra, characteristic α-helical features were evident, with pronounced minima at 208 nm and 222 nm, confirming the dominance of α-helical secondary structure (Fig. 3B). While the overall helical signatures were conserved, minor variations between the simulated and experimental spectra were observed and are detailed in Supplementary Table 2.

Deconvolution of the experimental CD spectra using DichroWeb indicated that the free 4F-P-4F peptide retained a predominantly α-helical conformation, with approximately 70% helical content. Importantly, this helical structure was preserved upon incorporation into the sHDL nanodiscs, demonstrating that lipid association did not disrupt the intrinsic secondary structure of the peptide (Fig. 3B, Supplementary Fig. 1A, Supplementary Table 1A–D). These results indicate that the nanodisc environment supports structural stability of the peptide backbone.

Guided by previous reports emphasizing the importance of peptide-mediated stabilization in pre-β HDL–like particles, peptide–lipid complexes composed of 4F-P-4F and DMPC were constructed (142). Due to the absence of solid-state NMR data specifically describing the orientation of 4F-P-4F, model construction was informed by existing solid-state NMR studies of structurally related

apolipoprotein mimetic peptides (124,143). Following equilibration, MD simulations yielded stable nanodisc assemblies with average diameters of 11.7 nm, 18.0 nm, and 25.6 nm, respectively. Throughout the simulation trajectories, these nanodisc models remained structurally stable. This stability was primarily mediated by electrostatic salt-bridge interactions between polar residues of the peptide and the lipid headgroups. Quantitative analysis revealed that lysine–phosphate interactions were more prevalent than choline–glutamic acid interactions across all simulated systems (Fig 3C, Supplementary Table 3, Supplementary Fig. 1B, C). The hydrophobic faces of the 4F-P-4F dimers consistently aligned toward the hydrophobic acyl chains of DMPC, while the hydrophilic surfaces remained exposed to the aqueous environment. This amphipathic orientation resulted in a belt-like arrangement of peptides encircling the lipid bilayer along the membrane normal, effectively stabilizing the discoidal nanodisc architecture (Supplementary Fig. 1D, E). MD simulations further highlighted the critical role of polar amino acids positioned at the interface between hydrophobic peptide residues and lipid headgroups. These residues facilitated sustained peptide–lipid interactions, enabling efficient shielding of the lipid hydrophobic core and preserving bilayer integrity across nanodiscs of different sizes. These optimized systems provided a realistic framework aimed at probing stabilizing interactions that are not readily accessible through experimental techniques alone.

To further validate the morphological characteristics of the sHDL formulation, FPLC measurements were performed. The resulting histogram displayed a single, well-defined peak, indicating a high probability of a uniform particle population and the presence of a single predominant particle type (Fig. 3D).

The transmission electron microscopy images illustrate the characteristic discoidal morphology of 4F-P-4F–DMPC sHDL nanodiscs observed at two distinct magnifications. Individual particles are clearly resolved, revealing both face-on (top-view) orientations and edge-on arrangements. In several regions, nanodiscs appear stacked, consistent with their flat, disc-like geometry. The coexistence of stacked and top-view confirms the discoidal structure of the nanoparticles and overall image the sample also depicts a uniformity in the particle size (Fig. 4).

Collectively, the integration of atomistic MD simulations with high-resolution experimental characterization as presented in figures 3 and 4, we demonstrate that sHDL formulations exhibit

consistent structural stability, uniform morphology, and robust peptide–lipid organization, supporting their functional potential as HDL-mimetic nanodiscs. These findings are consistent with well-assembled nanodisc systems (7,25,34) and suggest effective control of particle formation using microfluidics.

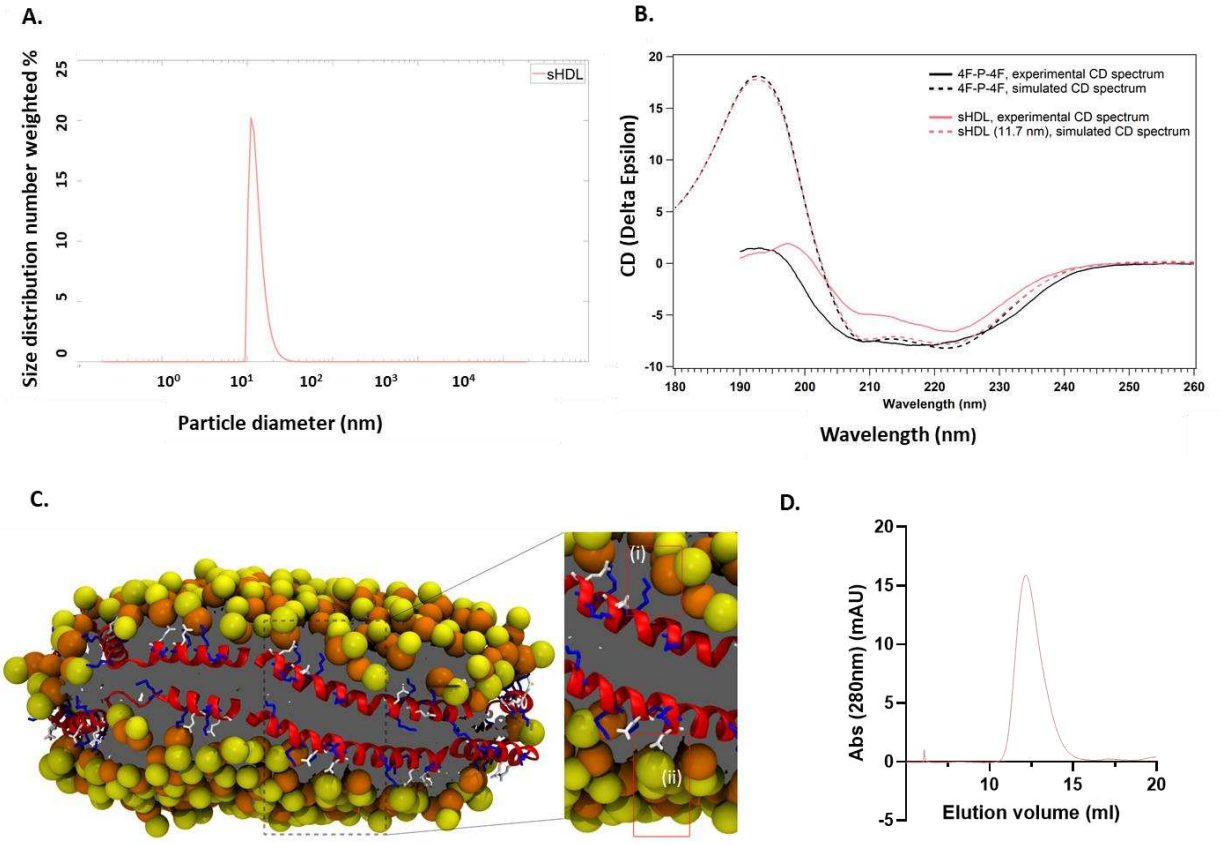

Figure 3 Synthesis and Characterization of 4F-P-4F DMPC sHDL nanodiscs. (A) Number based particle size distribution of the sHDL formulation, determined by dynamic light scattering (DLS). (B) Circular Dichroism (CD) spectra were analyzed to compare the structural characteristics of the sHDL formulation and the non-lipidated 4F-P-4F peptide. This analysis incorporated both experimental values and data from Molecular Dynamics (MD) simulations, utilizing the DichroWeb platform for interpretation. (C) Molecular Dynamics Simulation of sHDL Nanodiscs. Representation of a configuration of the 11.7 nm diameter 4F-P-4F DMPC nanodisc sampled during the MD simulation highlighting the salt bridge interactions between the peptides

and the lipid head groups. (i) showcases a lysine–phosphate salt bridge manifested by interactions between the nitrogen of the lysine amino group (blue) and the phosphorus of the lipid phosphate group (orange) and (ii) showcases a glutamic acid–choline salt bridge, manifested by an interaction between the carbon of the glutamate carboxyl group (white) and the nitrogen of the lipid choline group (yellow). (D) FPLC histogram depicting the elution time and size distribution of the sHDL nanodiscs with a protein detector with the peak maxima at the absorbance of 280nm with a Superdex 200 column. Panels A, B and C adapted from (144) under the terms and conditions of the Creative Commons Attribution (CC BY) license (https://creativecommons.org/licenses/by/4.0/) which permits unrestricted use, distribution, and reproduction in any medium, provided the original authors and the source are credited.

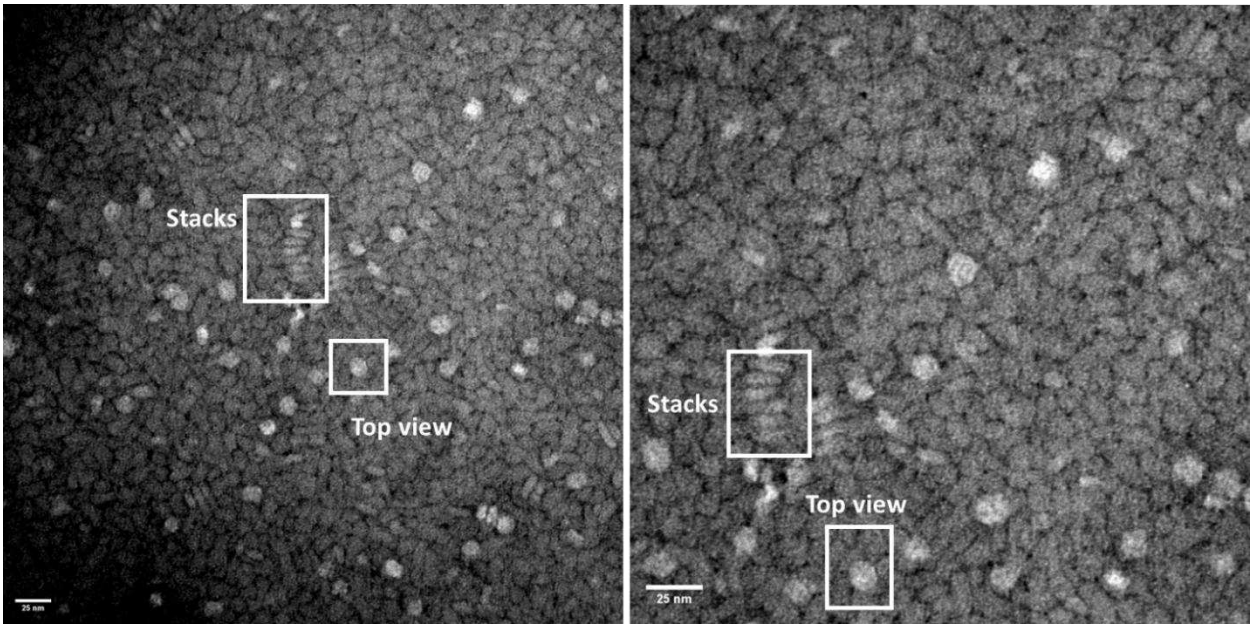

Figure 4. Representative transmission electron microscopy (TEM) image depicting the discoidal morphology of 4F-P-4F DMPC sHDL nanodiscs. Images shown at two different magnifications in the same field, showing the stacked form of the discs as well as the flat, top view, confirming the discoidal morphology, adapted from (144) under the terms and conditions of the Creative Commons Attribution (CC BY) license (https://creativecommons.org/licenses/by/4.0/)

which permits unrestricted use, distribution, and reproduction in any medium, provided the original authors and the source are credited.

5.1.2 4F-P-4F DMPC nanodiscs inhibit eosinophil chemotaxis in vitro

Eosinophil recruitment and retention within inflamed tissues is a key contributor to the propagation of inflammatory responses and is largely orchestrated by chemoattractant mediators such as eotaxin-1 (66). To evaluate whether the 4F-P-4F peptide or its lipidated sHDL nanodisc formulation could modulate this process, we examined eosinophil migratory responses triggered by eotaxin-1 (3 nM). All the treatments are based on protein concentrations throughout this dissertation work. Exposure to sHDL nanodiscs resulted in a clear, concentration-dependent suppression of eosinophil migration toward both chemoattractants. This inhibitory effect was consistently observed for eotaxin-1–driven chemotaxis (Fig. 5A) as well as prostaglandin D_2 induced migration (Supplementary Fig. 2). In contrast, treatment with the non-lipidated 4F-P-4F peptide failed to alter eosinophil migratory behavior under identical conditions (Fig. 5A).

We also investigated the possible effect lipidation-extent on this eosinophil chemotaxis by preincubating eosinophils with sHDL formulations with varying lipidation ranges. Among the formulations tested, sHDL nanodiscs assembled at a peptide-to-lipid ratio of 1:20 exhibited the strongest inhibitory effect on eosinophil migration, identifying this composition as the most effective configuration for suppressing chemotactic responses (Fig. 5B). These findings underscore the functional importance of lipidation in the nanodisc design, in mediating the observed anti-migratory effects.

To confirm the activity of sHDL nanodiscs a more physiological setting, we performed the chemotaxis assay in RPMI+10% FBS as shown in Fig 6A. The sHDL nanodiscs retain their activity in the presence of serum and the peptide alone remained ineffective in regulating eosinophil chemotaxis (Fig 6A). Notably, native human HDL isolated from healthy donors, did not exert a measurable effect on eosinophil migration (Fig 6B). Importantly, eosinophil shape change, a commonly used indicator of cellular activation (87) , was not altered by sHDL treatment or receptor blockade (Fig 6C), suggesting that the observed effects were specific to migratory behavior rather

than reflecting generalized activation. Using the Annexin V and PI staining, we also studied the viability of eosinophils in the presence of sHDL formulation at increased conc. and time compared to the chemotaxis assay. We did not see any significant changes in the viability of eosinophils upon treatment with 4F-P-4F DMPC sHDL nanodiscs (Fig 6D).

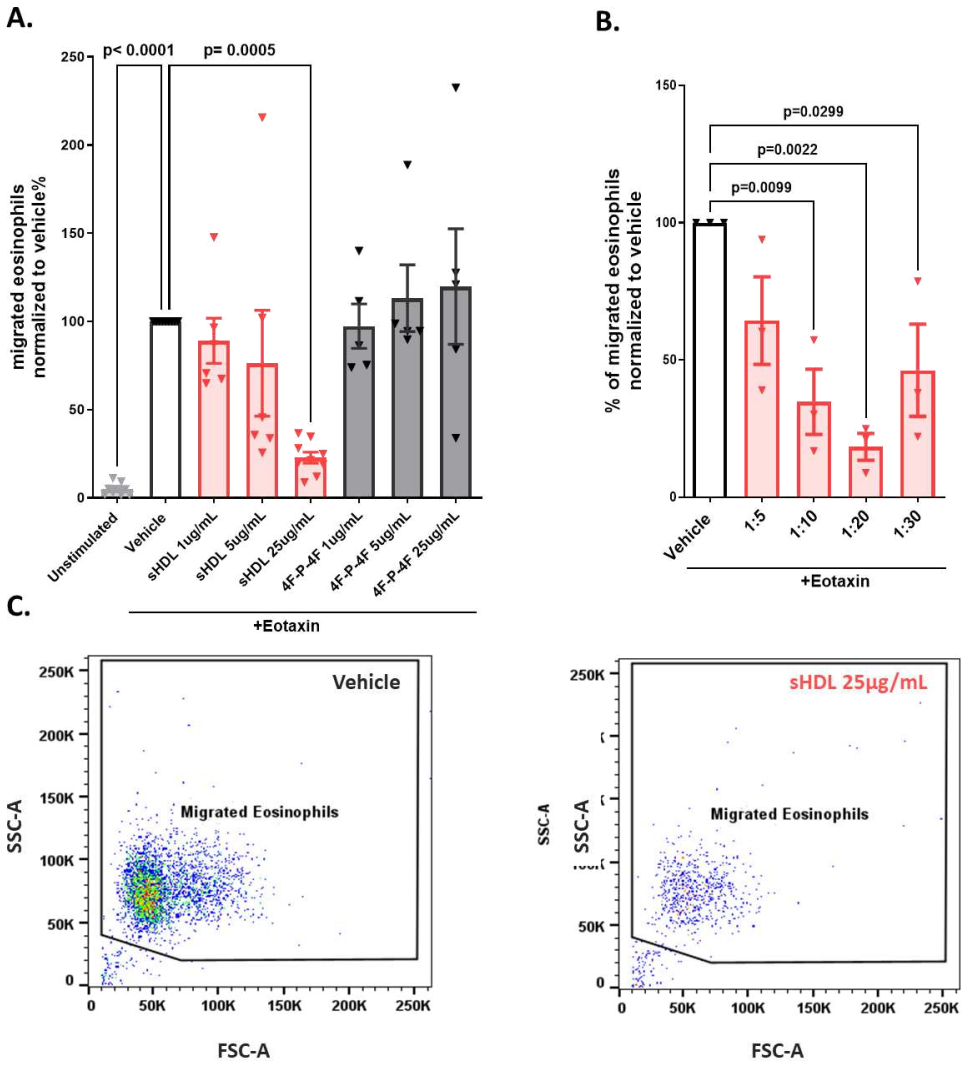

Figure 5. **sHDL Nanodiscs Inhibit Human Eosinophil Chemotaxis in a Concentration-Dependent Manner In Vitro. A**. Quantification of eotaxin-1-mediated chemotaxis for the particles in the 1:20 peptide to lipid ratios category **B**. Effect of the lipidation status of sHDL on eosinophil chemotaxis. **C.** Representative scatter plots illustrating gated eosinophils at the end of the assay. Data are expressed as percentages normalized to the vehicle control, presented as mean

± SEM from 5 to 9 independent experiments. Statistical significance was determined using one-way ANOVA with Dunnett's multiple comparison test B. and Turkey's multiple comparison test in A and Dunnett's in B, with p-values as reported and $p < 0.05$ considered significant. Adapted from (144) under the terms and conditions of the Creative Commons Attribution (CC BY) license (https://creativecommons.org/licenses/by/4.0/) which permits unrestricted use, distribution, and reproduction in any medium, provided the original authors and the source are credited.

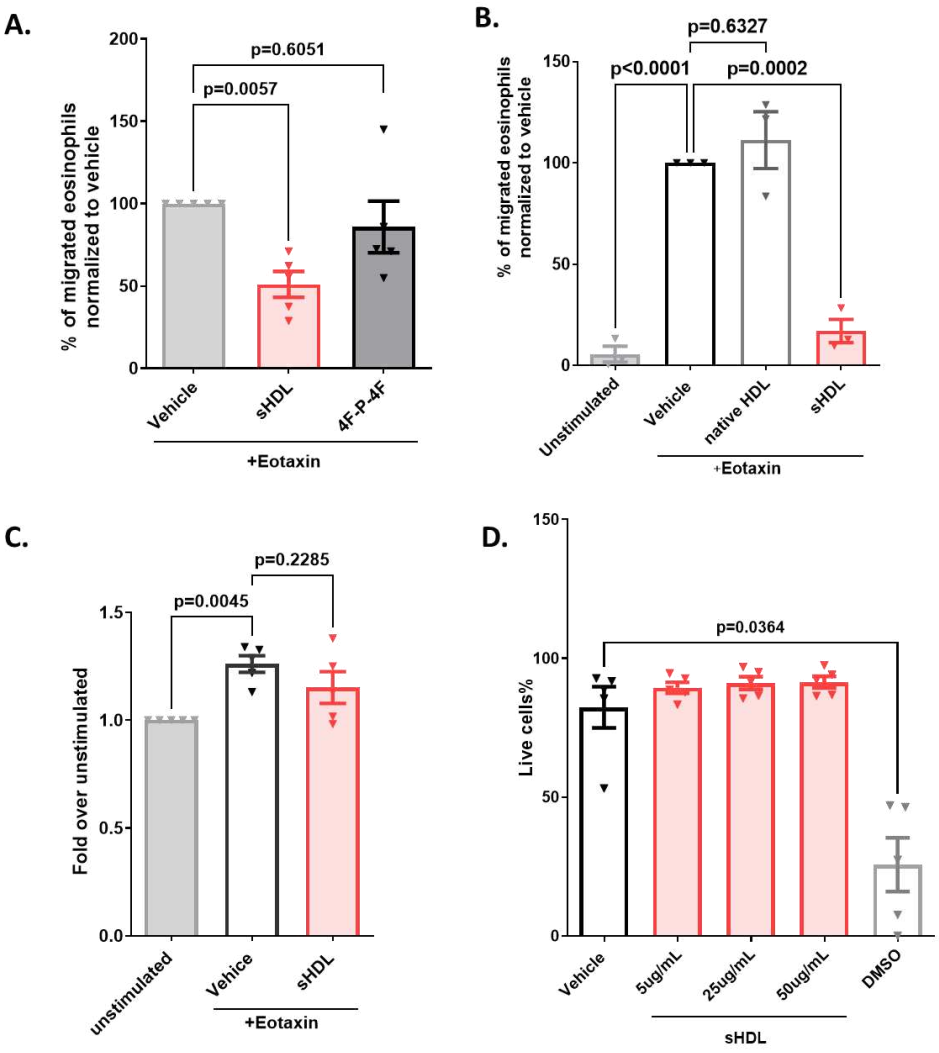

Figure 6. sHDL nanodiscs inhibit eosinophil chemotaxis in serum, without affecting the shape change and viability. A. Eosinophil chemotaxis assay performed in RPMI+10%FBS B.

Comparison of native HDL and sHDL (25ug/mL) on eosinophil chemotaxis. **C.** Shape change assay with eosinophils upon treatment with sHDL nanodiscs. **D**. Percentage of live cells quantified with Annexin V PI staining upon treatment with sHDL nanodiscs at mentioned concentrations for 4 hours. Values represent mean ± SEM. Statistical significance was determined using one-way ANOVA followed by Dunnett's multiple comparisons test; $p < 0.05$ was considered significant. Adapted from (144) under the terms and conditions of the Creative Commons Attribution (CC BY) license (https://creativecommons.org/licenses/by/4.0/) which permits unrestricted use, distribution, and reproduction in any medium, provided the original authors and the source are credited.

Eosinophils were confirmed to express the HDL-associated receptors scavenger receptor class B type I (SR-BI) and are known to express ATP-binding cassette transporter A1 (ABCA1) (Fig. 7A), (145). These receptors play distinct but complementary roles in cholesterol handling, with ABCA1 promoting cholesterol efflux to lipid-poor apolipoproteins and SR-BI facilitating cholesterol transfer to mature HDL particles, both of which are integral components of reverse cholesterol transport (146,147). To determine whether these receptors contributed to the inhibitory action of sHDL nanodiscs on eosinophil migration, cells were pretreated with blocking antibodies targeting SR-BI and ABCA1. Under these conditions, the suppressive effect of sHDL nanodiscs on eosinophil chemotaxis was completely abrogated (Fig.7B), indicating that engagement of these receptors is required for sHDL-mediated inhibition of eosinophil chemotaxis.

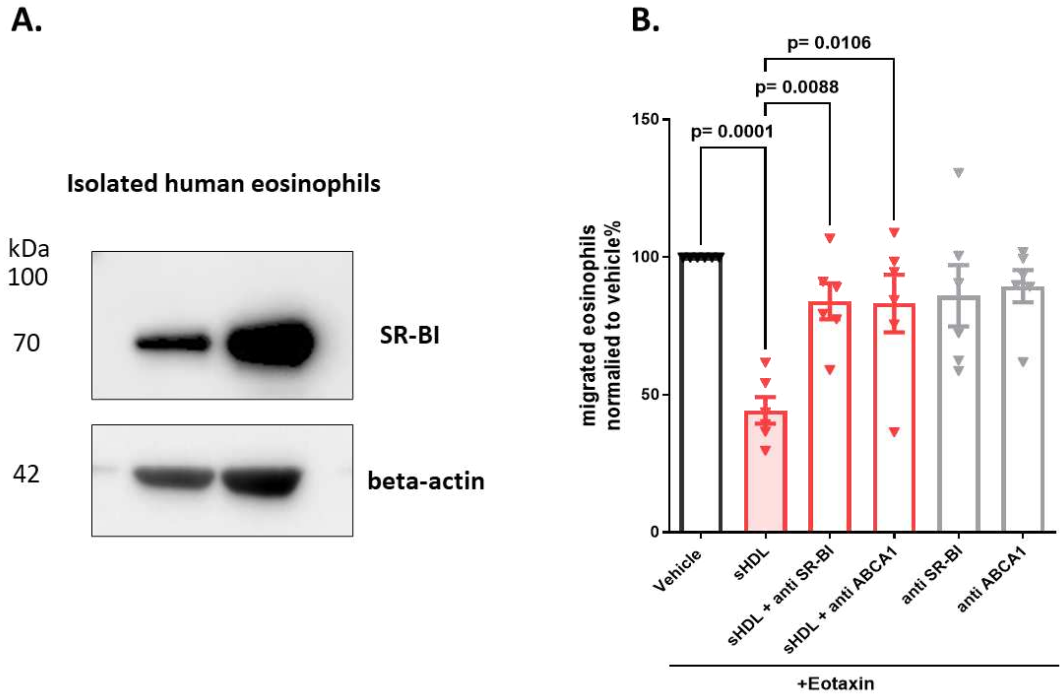

Figure 7. Inhibition of human eosinophil chemotaxis with sHDL is ABCA1 and SR-BI dependent. A. Western blots showing the presence of SR-BI in human eosinophils (n=2). **B.** Eosinophil chemotaxis assay in the presence and absence of blocking antibodies against ABCA1 and SR-BI showing the dependence of sHDL on these receptors**.** Values represent mean ± SEM. Statistical significance was determined using one-way ANOVA followed by Dunnett's multiple comparisons test; $p < 0.05$ was considered significant. Adapted from (144) under the terms and conditions of the Creative Commons Attribution (CC BY) license (https://creativecommons.org/licenses/by/4.0/) which permits unrestricted use, distribution, and reproduction in any medium, provided the original authors and the source are credited.

5.1.3 4F-P-4F DMPC sHDL nanodiscs efflux cholesterol from eosinophils

At the level of cellular lipid homeostasis, sHDL nanodiscs induced a pronounced reduction in eosinophil cholesterol content. This decrease was markedly greater than that achieved with the non-lipidated 4F-P-4F peptide, which exhibited only minimal cholesterol efflux activity (Fig. 8A). To further dissect the mechanisms underlying cholesterol removal, efflux assays were performed

in the presence or absence of blocking antibodies against ABCA1 and SR-BI. Surprisingly, inhibition of these receptors did not significantly diminish cholesterol efflux mediated by either native HDL or sHDL nanodiscs (Fig. 8B). Together, these findings indicate that while ABCA1 and SR-BI are essential for the ability of sHDL to suppress eosinophil chemotactic responses, the cholesterol efflux induced by sHDL proceeds through receptor-independent pathways.

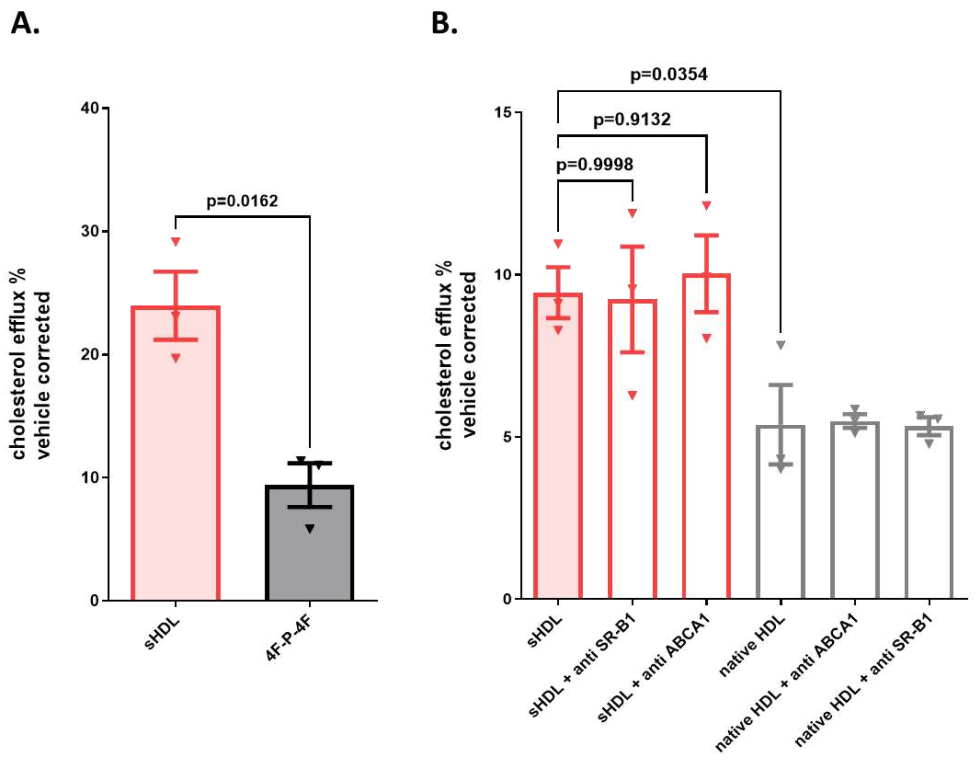

Figure 8. 4F-P-4F DMPC sHDL nanodiscs efflux cholesterol from eosinophils independent of ABCA1 and SR-B1. **A.** Cholesterol efflux from purified human eosinophils was assessed by measuring the proportion of radiolabeled [^{3}H]-cholesterol released following exposure to sHDL or the 4F-P-4F peptide (25 µg/mL). Background efflux from vehicle-treated cells, which remained below 1%, was subtracted from all samples to correct for nonspecific release. Results are presented as mean ± SEM from three independent experiments. Statistical differences were evaluated using Student's t-test. **B.** Eosinophils were pre-incubated with blocking antibodies targeting ABCA1 or SR-BI (2.5 µg/mL, 30 min) prior to treatment with sHDL or native HDL (25 µg/mL). Cholesterol efflux under these conditions is shown as mean ± SEM from three independent experiments.

Statistical analysis was performed using one-way ANOVA followed by Dunnett's multiple comparison test, with reported p values and a significance threshold of $p < 0.05$. Adapted from (144) under the terms and conditions of the Creative Commons Attribution (CC BY) license (https://creativecommons.org/licenses/by/4.0/) which permits unrestricted use, distribution, and reproduction in any medium, provided the original authors and the source are credited.

5.1.4 4F-P-4F DMPC sHDL nanodiscs modulate CCR3 internalization and downstream signaling

Eotaxin-1 serves as a principal chemoattractant for eosinophils by engaging the CCR3 receptor, thereby promoting eosinophil migration, adhesion, and activation in allergic inflammatory settings (148). Ligand-induced internalization of CCR3 constitutes a tightly regulated process that governs the intensity, persistence, and spatial orientation of eosinophil chemotaxis (59). This regulatory mechanism functions as a critical control point in eosinophil trafficking and has been implicated as a potential therapeutic target in eosinophil-driven diseases.

In this context, sHDL treatment significantly attenuated eotaxin-1-induced CCR3 internalization, indicating a disruption of receptor trafficking dynamics (Fig. 9A, B). The magnitude of this effect was comparable to that observed following treatment with phenylarsine oxide (PAO), a well-established inhibitor of CCR3 internalization (88,139). Notably, rescue of CCR3 surface expression by sHDL closely mirrored 8 μM PAO treatment-effects (Fig. 9C) suggesting that impaired CCR3 internalization contributes, at least in part, to the inhibition of CCR3-dependent eosinophil chemotaxis observed in the presence of sHDL.

Cholesterol-rich membrane microdomains, commonly referred to as lipid rafts, are essential for the spatial organization of receptors and intracellular signaling complexes at the plasma membrane (149) . Through its capacity to promote cholesterol efflux, sHDL may disrupt lipid raft architecture, thereby altering CCR3 localization and internalization. In contrast, neither isolated native HDL nor the non-lipidated 4F-P-4F peptide produced significant changes in eotaxin-1-induced CCR3 internalization (Fig, 9C), underscoring the requirement for lipidation and cholesterol-modulating activity in mediating this effect.

Collectively, these data indicate that sHDL selectively interferes with eotaxin-driven CCR3 internalization through modulation of membrane cholesterol organization, providing a mechanistic explanation for its inhibitory effects on eosinophil chemotaxis without broadly disrupting receptor signaling. To define downstream signaling events associated with sHDL-induced modulation of CCR3 internalization and cholesterol efflux, we analyzed intracellular phosphorylation patterns using a human phospho-proteome profiler array. Relative to vehicle controls, sHDL treatment produced pronounced alterations in the phosphorylation of multiple signaling mediators.

Specifically, sHDL significantly reduced phosphorylation of STAT3 at Tyr705 and Ser727, STAT1 at Tyr701, and ERK1/2 at Thr202/Tyr204 and Thr185/Tyr187 (Fig. 10 A, B). Given the central roles of STAT1/3 in inflammatory signaling (150) and ERK1/2 in eosinophil migration, proliferation, and survival (58,150), these changes are consistent with suppression of pro-inflammatory and pro-migratory pathways. Additional kinase phosphorylation changes were observed and are summarized in Supplementary Fig. 3A. In contrast, phosphorylation of Akt1/2/3 was markedly increased following sHDL treatment (Supplementary Fig. 3B), indicating activation of signaling programs associated with cell survival and metabolic regulation (151).

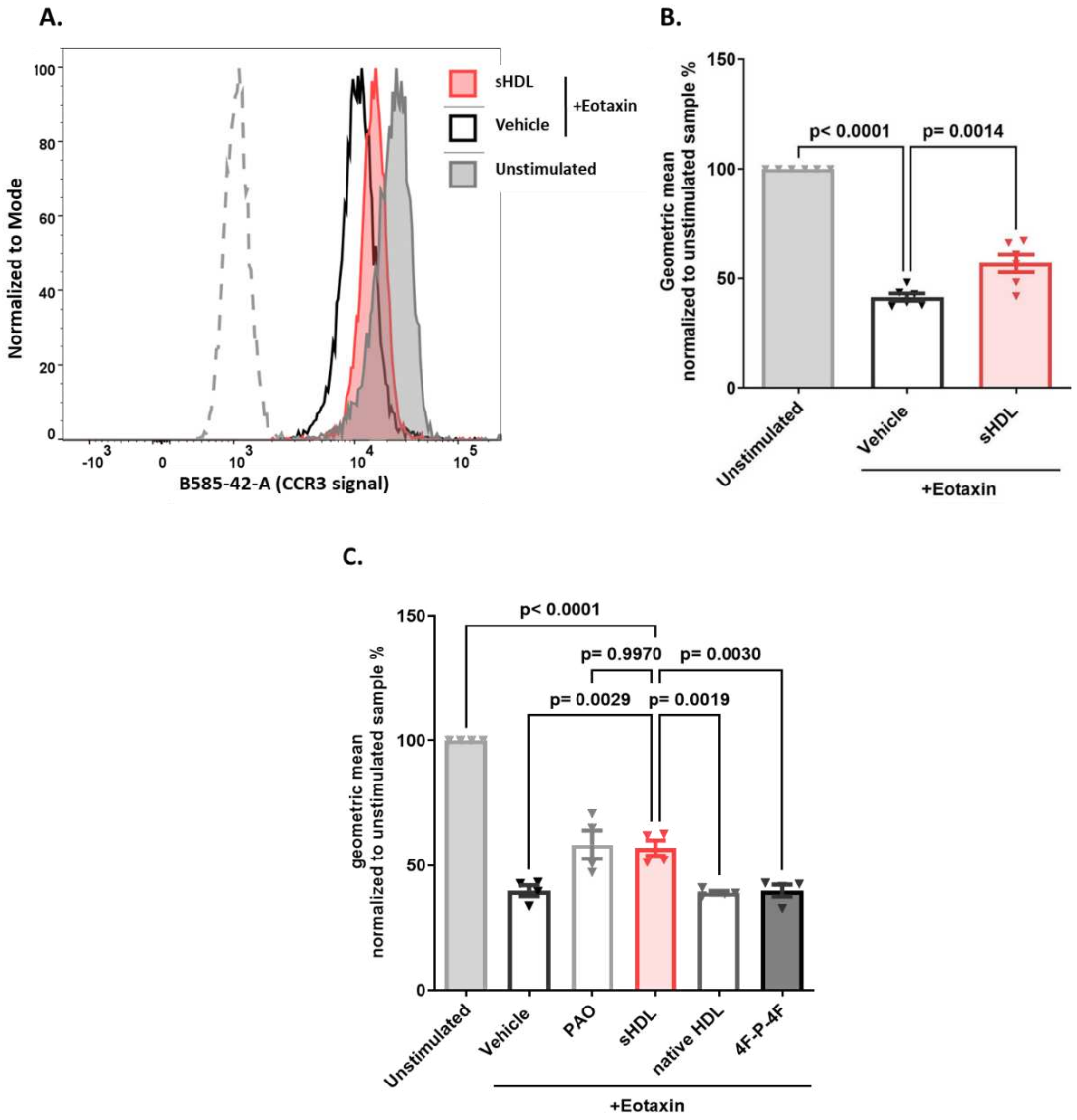

Figure 9. **sHDL Treatment Modulates CCR3 Internalization. A**. Overlay histograms showing CCR3 surface levels. Cells were exposed to vehicle or 25 µg/mL sHDL for 30 min and then stimulated with 10 nM eotaxin-1 for an additional 30 min. A no-eotaxin condition is included to define basal CCR3 expression and the dotted lines represent unstained population. **B.** Quantitative analysis of panel A, depicting the geometric mean CCR3 signal normalized to the corresponding unstimulated controls, expressed as mean ± SEM from six independent experiments. **C**. Eosinophils were preincubated with sHDL, native HDL, or the 4F-P-4F peptide (each at 25 µg/mL), or with phenylarsine oxide (PAO; 8 µM), followed by stimulation with eotaxin-1 (10 nM).

Results are expressed as mean ± SEM from four independent experiments. Differences among groups were analyzed using one-way ANOVA with Dunnett's post hoc multiple comparisons test, and statistical significance was defined as $p < 0.05$. Adapted from (144) under the terms and conditions of the Creative Commons Attribution (CC BY) license (https://creativecommons.org/licenses/by/4.0/) which permits unrestricted use, distribution, and reproduction in any medium, provided the original authors and the source are credited.

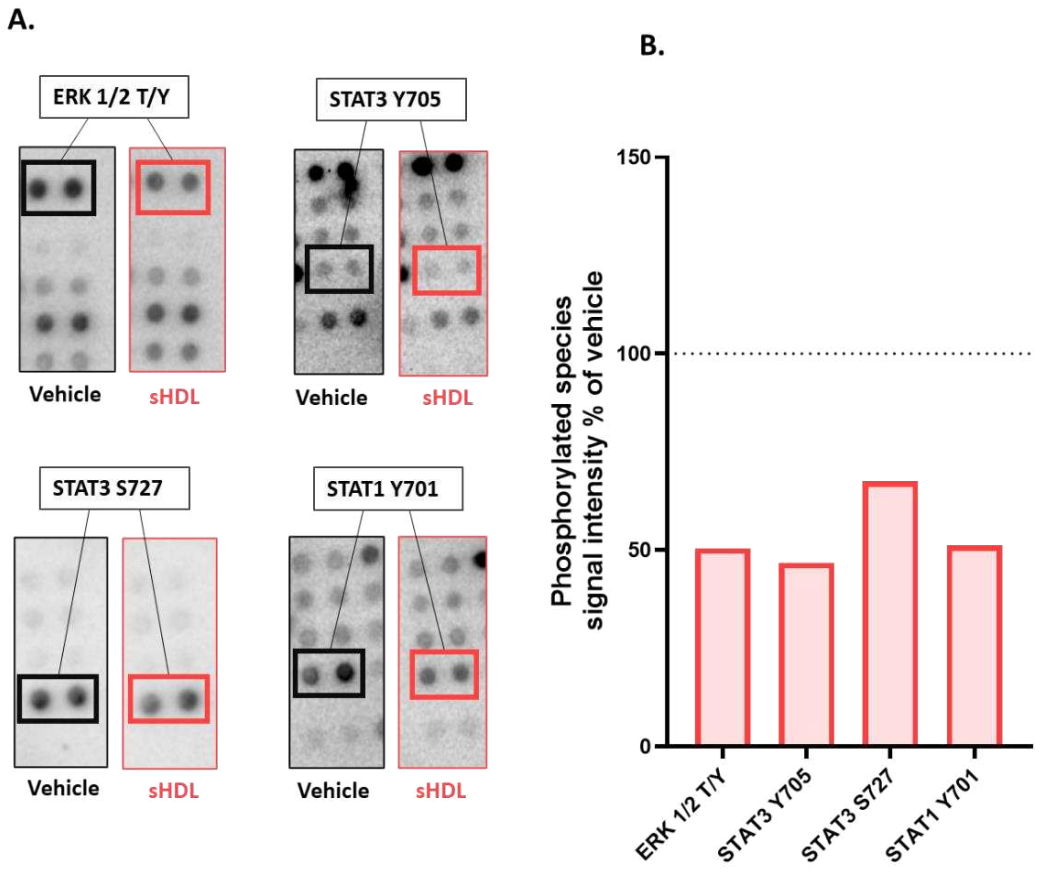

Figure 10. sHDL Treatment Modulates intracellular signaling. A. Phosphokinase array membrane images generated from pooled eosinophils of three individual donors, revealing changes at distinct phosphorylation sites. **B**. Densitometric analysis of the signals shown in panel A, reported as a percentage relative to vehicle-treated controls. Adapted from (144) under the terms

5.1.5 4F-P-4F DMPC sHDL nanodiscs modulate eosinophil migration in vivo

Treatment with sHDL nanodiscs markedly attenuated airway inflammatory cell recruitment in response to eotaxin challenge (Fig. 11). In three independent experiments, mice were administered a single intravenous injection of sHDL nanodiscs (75 mg/kg) or vehicle control, followed by intranasal delivery of eotaxin-2 (4 µg). Bronchoalveolar lavage samples were collected 4 h after eotaxin challenge and analyzed by flow cytometry (Fig. 11A). Eosinophils were identified using the gating strategy shown in Fig. 11B, enabling quantitative assessment of leukocyte recruitment to the airway compartment.

Mice receiving a single intravenous dose of sHDL (75 mg/kg) exhibited significantly reduced eosinophil and neutrophil counts in bronchoalveolar lavage (BAL) fluid compared with vehicle-treated controls (Fig. 11C, D). While eotaxins are primarily associated with eosinophil chemotaxis, previous studies have shown that eosinophil activation can indirectly promote neutrophil infiltration, which may account for the parallel reduction in both granulocyte populations observed following sHDL administration (87,152) A decrease in total immune cell counts was also noted in sHDL-treated animals; however, this trend did not reach statistical significance (Fig. 9E). In contrast, sHDL treatment did not significantly alter pan-lymphocyte or alveolar macrophage numbers in the BAL (Fig. 11F, G). These effects were evaluated using an established eotaxin-mediated eosinophil migration model in IL-5 transgenic mice, as previously reported (87,140,141). The sHDL dose was selected based on prior in vivo studies employing a comparable dosing (43). Together, these findings demonstrate that sHDL nanodisc treatment selectively suppresses eotaxin-induced granulocyte recruitment in vivo without broadly affecting other immune cell populations, supporting the translational relevance of the in vitro data.

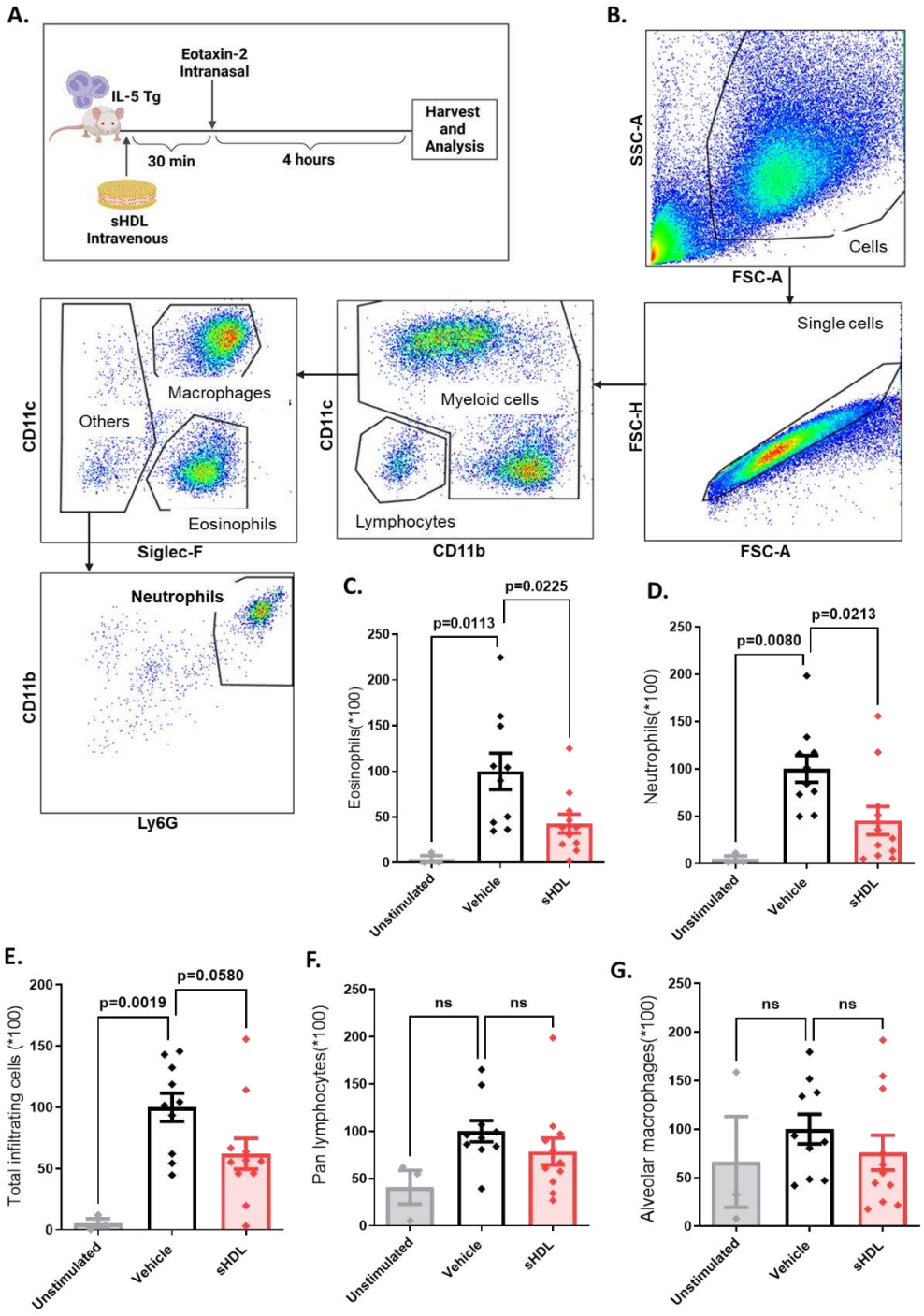

Figure 11. sHDL Treatment Modulates Eosinophil migration in vivo. A. Summary of the in vivo migration assay performed in IL-5 transgenic mice. **B.** Flow cytometry gating scheme used to analyze immune cells recovered from bronchoalveolar lavage, with eosinophils defined as Siglec-

F^+ $CD11c^-$ cells within the myeloid compartment. Immune cell infiltration was quantified for **C.** eosinophils, **D.** neutrophils, E. total infiltrating leukocytes, **F**. pan-lymphocytes, and **G.** alveolar macrophages. Results are derived from three independent experiments (n = 10–11 per treatment group), normalized to the vehicle control mean, and shown as mean ± SEM. Statistical analysis was performed using one-way ANOVA followed by Dunnett's post hoc test; reported p-values indicate significance, with $p < 0.05$ considered significant and ns denoting not significant. Adapted from (144) under the terms and conditions of the Creative Commons Attribution (CC BY) license (https://creativecommons.org/licenses/by/4.0/) which permits unrestricted use, distribution, and reproduction in any medium, provided the original authors and the source are credited.

5.2 Lysophosphatidylcholine-Enriched sHDL

5.2.1 Synthesis and characterization of LPC enriched sHDL nanoparticles

We successfully synthesized LPC enriched sHDL nanoformulations using an optimized freeze-drying method (25). This approach produced consistently formed particles suitable for downstream biological studies. To ensure that the lipid to peptide ratios remain the same, DMPC was substituted with 20% LPCs and each LPC was used at same molar concentration. We used molar ratios and the % of enrichment is the % of enrichment over DMPC.

Initial characterization with DLS confirmed successful sHDL synthesis, demonstrating uniform particle sizes and excellent colloidal stability with minimal large aggregates that could affect biological performance or safety (Table 2, Fig. 12). All formulations exhibited polydispersity index (PDI) values below 0.3, indicating a highly monodisperse particle population with low size variability, maximally around 10nm. The average values of PDI and size from three technical replicates for each formulation are listed in Table 2.

Population characteristics were further validated using gel permeation chromatography (GPC) (Fig 13). Across all LPC enrichment levels, GPC profiles closely matched the DLS data, confirming consistent size distributions. Notably, the retention times for LPC-enriched sHDL particles were

comparable to those of blank sHDL controls (Fig 13), indicating similar hydrodynamic sizes and no detectable aggregation or degradation during the enrichment process.

To confirm LPC incorporation into the sHDL nanodiscs, targeted liquid chromatography–mass spectrometry (LC-MS) was used. Size-exclusion cleanup using 7 kDa molecular weight cutoff columns to remove freely soluble lipid prior to lipid extraction. Subsequently, the column filtered sHDL formulations were analyzed. As shown in Table 3 presence of all the LPCs in the respective sHDL formulation were detected. These results demonstrate that LPCs are highly compatible with the sHDL self-assembly process, enabling their efficient incorporation and retention

Table 2. Particle size and polydispersity index of 22A DMPC based formulations with DLS.

Formulation	Size (nm)	PDI
Blank sHDL	10.3	0.18
LPC 14:0	10.8	0.22
LPC 16:0	10.2	0.18
LPC 18:0	10.4	0.18

Abbreviations: Dynamic Light Scattering (DLS), 1,2-Dimyristoyl-sn-glycero-3-phosphocholin, (DMPC) Polydispersity index (PDI), lysophosphatidylcholine (LPC), nm: nanometer (nm).

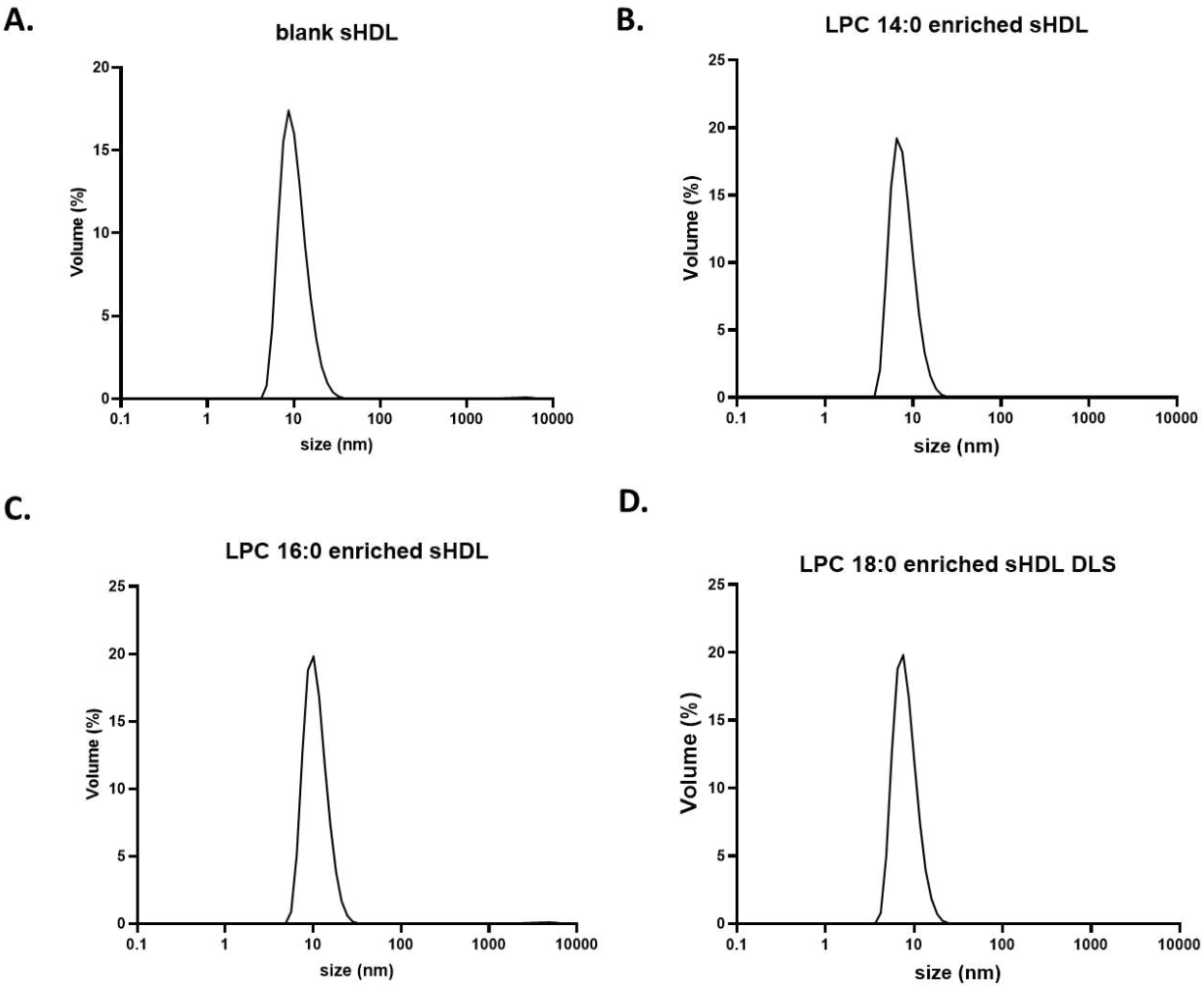

Figure 12. **Dynamic Light Scattering plots for different sHDL nanodiscs clearly depicting size overlap around 10nm for all the formulations A**. blank sHDL, **B**. 14:0 LPC enriched sHDL, **C**. 16:0 LPC enriched sHDL and **D**. 18:0 LPC enriched sHDL. A single clear peak for each formulation can be seen depicting low polydispersity. Each measurement was repeated 3 times and representative plots have been shown.

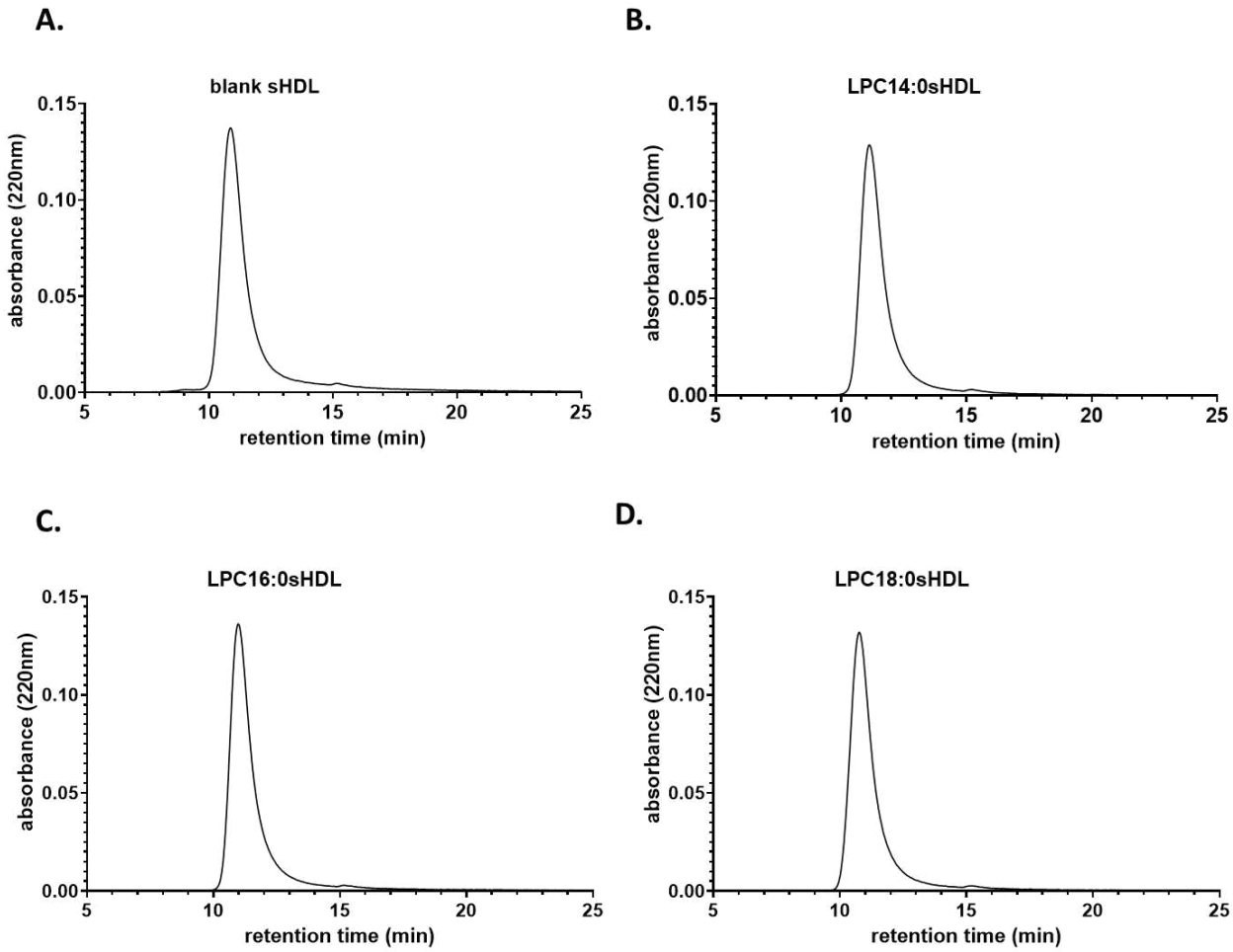

Figure 13. **Gel Permeation Chromatography histograms representing the retention time for the different sHDL nanodiscs A**. blank sHDL, **B**. 14:0 LPC enriched sHDL, **C**. 16:0 LPC enriched sHDL and **D**. 18:0 LPC enriched sHDL. The retention times for each of the blank as well as enriched sHDL are comparable, confirming near identical size distribution and no structural disruption due to enrichment.

Table 3. Semi-quantitative quantification of LPCs in enriched sHDL after size exclusion clean-up Concentrations reflect values measured directly in MS extracts using external calibration curves.

LPC species in respective sHDL	Peak area (a.u.)	Measured concentration in MS extract (µg/mL)
LPC 14:0	2,806,326	0.94
LPC 16:0	3,316,435	0.81
LPC 18:0	3,700,535	1.86

5.2.2 LPC enriched sHDL modulate neutrophil shape change without affecting viability

To evaluate the cytotoxicity of LPC-enriched sHDL nanodiscs, primary human polymorphonuclear leukocytes were incubated with increasing concentrations of sHDL nanodiscs, as shown in Figure 12. A 20% DMSO treatment was used as a positive control to induce cell death. All the treatments with the nanodiscs are based on protein concentrations. Following a 30-min incubation, cells were stained with Annexin V and propidium iodide (PI). The percentage of viable cells, defined as the double-negative population for Annexin V and PI staining, demonstrated no significant cytotoxicity associated with LPC enrichment compared to control sHDL formulations (Figure 14).

To assess the potential anti-inflammatory benefit of LPC enrichment, the effects of LPC-enriched sHDL nanodiscs were further examined in primary human PMNLs, which predominantly consist of neutrophils. Cells were pretreated with sHDL for 15 min, followed by stimulation with 3 nM IL-8 for 5 min at 37 °C. Cells were then fixed on ice using Cell Fix prior to data acquisition. Neutrophil activation was assessed by measuring changes in forward scatter area (FSC-A), indicative of cell shape change. Notably, LPC 18:0–enriched sHDL nanodiscs significantly attenuated IL-8–induced neutrophil shape change, whereas this effect was not statistically significant for blank sHDL nanodiscs (Figure 15).

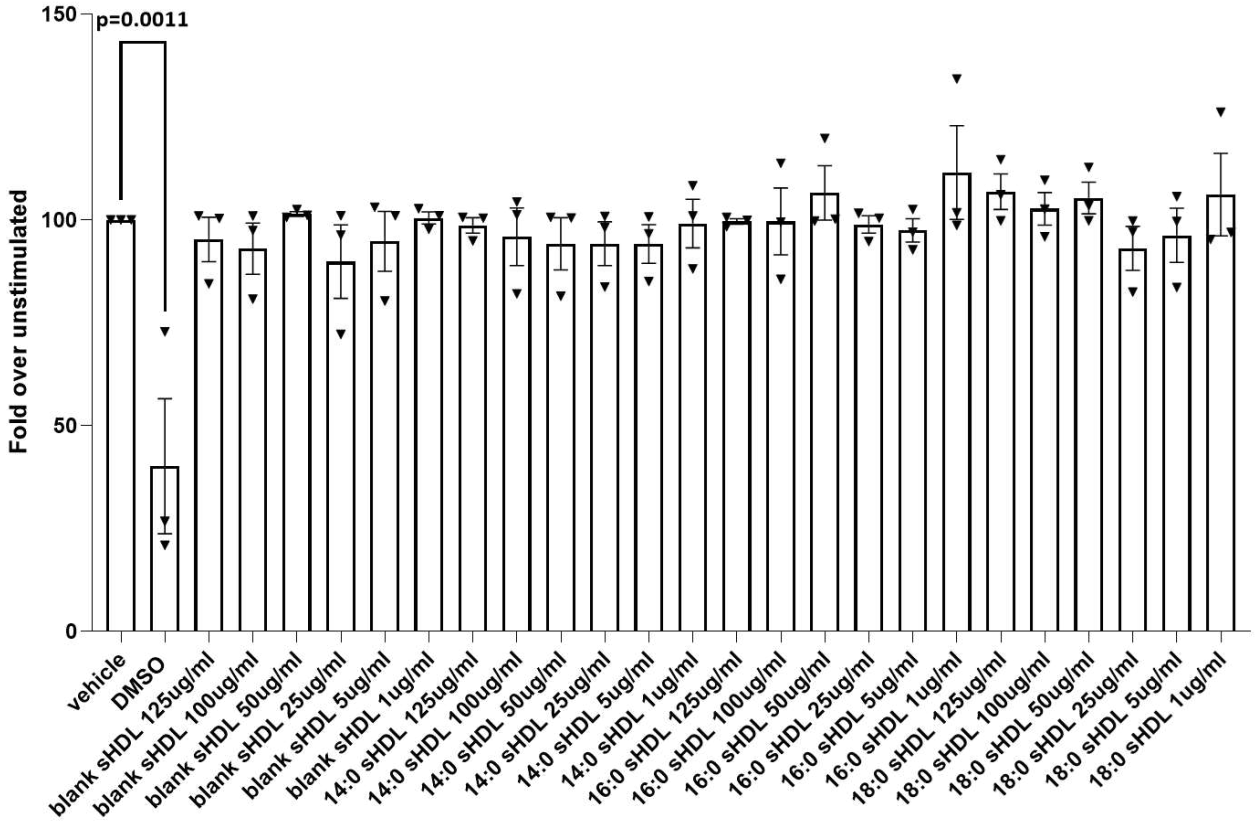

Figure 14. LPC enriched sHDL does not affect neutrophil viability. % Of live cells normalized to vehicle for LPC 14:0, 16:0 and 18:0 22A DMPC nanodiscs. Data shown as mean ± SEM for three individual experiments, as percentage of vehicle. Statistical analysis was performed using one-way ANOVA followed by Dunnett's post hoc test; reported p-values indicate significance, with $p < 0.05$ considered significant

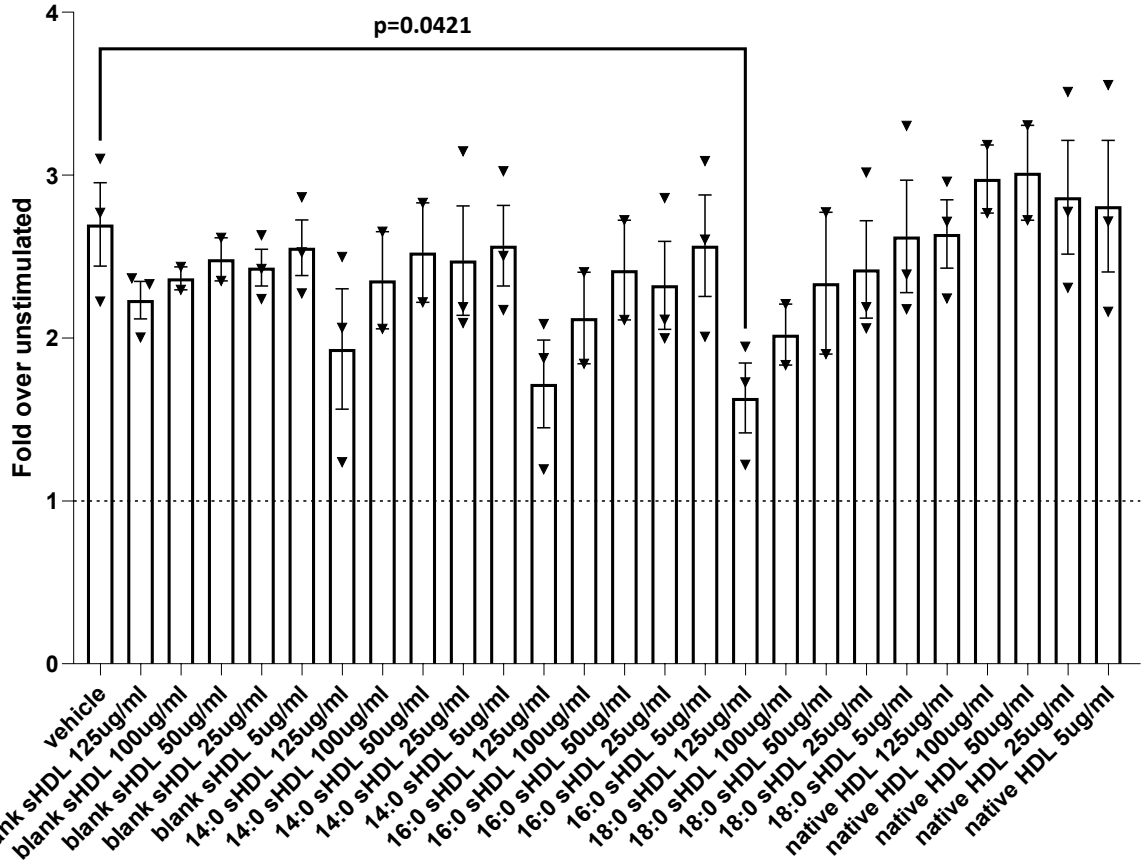

Figure 15. Selective modulation of neutrophil activation by LPC 18:0–enriched sHDL LPC18:0 enriched sHDL inhibits neutrophil shape change in response to IL-8. Data shown as mean ± SEM for three individual experiments, with 2-3 conditions in all experiments and normalized to unstimulated sample (no IL-8). Statistical analysis was performed using one-way ANOVA comparing all the 125ug/ml treatment conditions with vehicle, followed by Dunnett's post hoc test; reported p-values indicate significance, with $p < 0.05$ considered significant.

6. DISCUSSION

6.1 Peptide-based lipid nanodiscs and eosinophil recruitment and chemotaxis

6.1.1 Major findings

In this study we combined 4F-P-4F mimetic peptide with DMPC to generate stable sHDL nanodiscs. Computational (in silico) analyses were used to elucidate the structure–function relationships of sHDL nanodiscs and in enabling the systematic evaluation of their immunomodulatory properties. Integrated evidence from both experimental measurements and molecular simulations demonstrates that the peptides retain robust structural integrity when incorporated into their lipidated configurations, as reflected by consistent helicity profiles (Fig 3). A direct comparison of the CD spectra of 4F-P-4F and sHDL indicates that the conformational characteristics of HDL mimetic peptides is not universally conserved across different designs. Specifically, in contrast to the 18A mimetic peptide, lipidation of 4F-P-4F did not result in a measurable enhancement of α-helical content, underscoring peptide-specific structural responses to lipid association (36). These findings highlight the limitations of assuming generalized trends among different ApoA-I mimetic peptides and emphasize the need for individual structural evaluation for different mimetic peptides. Importantly, the development and application of reliable molecular dynamics simulation frameworks, such as the model employed here, provide a powerful platform for the early-stage screening of diverse design parameters, including variations in peptide sequence, lipid composition, and ligand incorporation. By enabling detailed structural evaluation and possible functional predictions prior to experimental validation, such computational approaches can substantially streamline the development pipeline and minimize reliance on extensive preliminary in vitro testing. Such an approach can enable the screening of several peptide-to-lipid combinations prior to attempting each combination experimentally, providing an efficient computational filter. Additionally, our experimental CD spectroscopy data further supports successful sHDL assembly by confirming that the peptide components adopt a predominantly α-helical conformation upon lipid association. These measurements provide direct experimental validation of peptide secondary structure, complementing both the computational predictions and the observed nanoscale particle formation (Fig 3).

DLS measurements confirmed the formation of nanoscale assemblies with hydrodynamic diameters consistent with HDL mimetics published before (7), supporting successful peptide–lipid self-assembly.

Transmission electron microscopy (TEM) was employed as a complementary technique for structural characterization of the sHDL nanoparticles described in this study. While ensemble-based methods such as dynamic light scattering provide information on average hydrodynamic size and polydispersity in solution, they do not directly resolve particle morphology. TEM addresses this limitation by enabling direct visualization of individual nanoparticles at nanometer resolution (Fig 4), thereby enabling clear evaluation of particle morphology and structural integrity, validating the synthesis approach.

Additionally, we e observed a single, well-defined elution peak in FPLC that indicates the presence of a uniform particle population and supports the conclusion that the formulation is largely free of aggregates or unassembled components. This result is particularly relevant when interpreted alongside DLS data, as both techniques independently report on particle homogeneity in solution. While DLS reflects the hydrodynamic size distribution, FPLC resolves species based on effective size and confirms that the particles behave as a single dominant assembly under chromatographic conditions. Together with TEM imaging, which verifies particle morphology, the FPLC profile strengthens the observation that the sHDL particles are structurally well-formed, monodisperse, and suitable for downstream biological evaluation.

The accumulation of eosinophils within tissues is a key contributor to disease progression, as their recruitment to sites of inflammation perpetuates chronic inflammatory signaling. Of particular importance, our results show that sHDL nanodiscs substantially inhibit chemotactic migration of human eosinophils towards eotaxin (Fig 5). These effects also remained consistent in the presence of serum (Fig 6), confirming the activity in more physiological states. sHDL nanodiscs demonstrate these anti-chemotactic effects while preserving cellular viability (Fig 6).

In contrast, the non-lipidated 4F-P-4F peptide did not significantly alter eosinophil migratory responses, underscoring the importance of lipidation for sHDL activity. Together, these findings suggest that incorporation of DMPC is a key determinant in improving the functional efficacy of

ApoA-I mimetic peptides and enabling their anti-inflammatory effects. An optimal peptide-to-lipid molar ratio of 1:20 was identified for its inhibitory effect on eosinophil chemotaxis (Fig 5). We also did not see an inhibitory effect of the endogenous HDL treatment on eosinophil migration towards eotaxin, at the same concentrations as the sHDL (Fig 6). Endogenous HDL mediated effects are reported at much higher concentrations (86) and are susceptible to donor-donor variation as well as sensitive to isolation techniques (121).

Cholesterol efflux has emerged as a central regulatory mechanism linking lipid metabolism to immune cell function and inflammation. Beyond its classical role in maintaining cellular cholesterol homeostasis, efflux to HDL or HDL-like particles profoundly influences membrane organization, particularly cholesterol-rich lipid rafts that serve as platforms for immune receptor clustering and signal transduction (7,10,153,154). Lipid rafts are dynamic, cholesterol- and sphingolipid-rich membrane nanodomains that organize receptors and signaling molecules to shape the strength and quality of immune responses. By promoting the clustering of antigen and pattern-recognition receptors into kinase-enriched platforms and altering the distribution of inhibitory phosphatases, raft dynamics critically regulate T cell receptors, B cell receptors, FcεRI, and TLR signaling, thereby tuning cytokine production, activation thresholds, and inflammatory output in innate and adaptive immune response (155). G-protein-coupled receptors are often concentrated within lipid rafts and the receptor conformation, spatial arrangement, and interaction with downstream signaling partners is directly influenced by changes in lipid rafts (156). Alterations in lipid raft architecture can disrupt receptor trafficking, impair internalization, and dampen the activation of inflammatory signaling pathways (157). Because membrane cholesterol is a key determinant of membrane fluidity, it plays a central role in maintaining lipid raft integrity and the functional organization of raft-associated proteins (158).

We observed that sHDL nanodiscs promote cholesterol efflux in eosinophils, suggesting a possible functional link between cholesterol content of the cells and chemotaxis. Accumulating evidence across multiple immune cell types including macrophages, neutrophils, and eosinophils supports the concept that efficient cholesterol efflux skews cells toward a less inflammatory state. For example, in sepsis, treatment with HDL mimetic ETC-642 lead to a decrease in TLR4 abundance in the lipid rafts in macrophages, which can be correlated to the efflux capacity of the mimetics in the same setting (25). In the same study, researchers have also shown a clear inverse correlation

between HDL-cholesterol content and survival rates in sepsis patients (25). In human neutrophils, our team has previously reported a link between cholesterol efflux and anti-inflammatory properties of HDL that rely on cholesterol depletion in the lipid rafts (101). Collectively, these findings position cholesterol efflux as a key immunomodulatory process and underscore the therapeutic potential of targeting cholesterol content of the cells for the management of inflammatory diseases.

Beyond lipid transport, ABCA1 and SR-BI receptors are increasingly recognized for their broader immunomodulatory functions. Prior studies have shown that SR-BI limits neutrophil recruitment and dampens pulmonary inflammation, with loss of SR-BI exacerbating asthma-like pathology in preclinical models (159). Similarly, ABCA1 has been implicated in the regulation of inflammatory signaling pathways, pointing to its potential relevance in pulmonary inflammatory diseases (160). Importantly, ABCA1-dependent signaling has been documented across multiple cell types, including macrophages, fibroblasts, and engineered renal cell systems, reinforcing the concept that ABCA1 functions as a multifunctional signaling receptor rather than solely a cholesterol transporter (161,162). In parallel, SR-BI is known to initiate intracellular signaling through activation of multiple kinase cascades, providing a plausible link between receptor engagement and downstream modulation of cell migration and inflammatory responses (163). Collectively, these findings suggest that sHDL nanodiscs may exert their anti-chemotactic effects on eosinophils through receptor-mediated signaling mechanisms that are at least partially independent of classical cholesterol efflux pathways (Fig 6). From a mechanistic standpoint, the use of blocking antibodies against the HDL receptors SR-BI and ABCA1 fully abolished the ability of sHDL nanodiscs to suppress eosinophil migration, highlighting the central involvement of these receptors in mediating the observed biological effects (Fig 5). ABCA1 is classically associated with cholesterol efflux to lipid-poor apolipoproteins, while SR-BI primarily facilitates lipid transfer to fully formed, lipid rich HDL particles (146,147).

Despite their apparent involvement in controlling eosinophil migration, pharmacological blockade of SR-BI and ABCA1 did not markedly reduce cholesterol efflux from eosinophils in response to either sHDL or native HDL (Fig 8). This finding indicates that cholesterol removal in eosinophils may rely predominantly on alternative mechanisms, such as passive membrane diffusion or

transport mediated by ABCG1, rather than on SR-BI or ABCA1. Although ABCG1 transcript expression has been reported in eosinophils (164), its predominantly intracellular localization presents a major technical limitation. Because antibody-based inhibitors primarily target cell surface proteins, they are poorly suited to interrogate the function of intracellular ABCG1, and its contribution was therefore not examined in the present study.

CCR3 is a chemokine receptor highly expressed on eosinophils and is a central driver of eosinophilic inflammation (165). It binds multiple eosinophil-active chemokines, most notably eotaxins, triggering eosinophil recruitment, activation, shape change, and tissue infiltration at sites of inflammation (165). Sustained CCR3 signaling amplifies inflammatory responses by promoting eosinophil survival and effector functions, making it a key contributor to chronic inflammation as well as tissue injury in the lung and gastrointestinal tract (165–167). While there is limited direct biochemical evidence showing that CCR3 is specifically enriched in lipid raft fractions, as a subclass of G protein-coupled receptors, it can be speculated that they likely reside in the lipid rafts (168). Furthermore, CCR3 contains predicted cholesterol interaction motifs, suggesting potential association with lipid rafts (169).

Previous studies have shown that eotaxin activates ERK signaling by engaging CCR3 (58) Consistent with this, our findings demonstrate that pretreatment with sHDL reduces eotaxin-1-driven phosphorylation of ERK1/2, STAT1 and STAT3 in eosinophils (Fig 9, 10). ERK1/2 signaling controls cell proliferation, differentiation and survival, while the JAK–STAT pathway mediates cytokine-dependent inflammatory responses. Both pathways play well-defined roles in eosinophilic inflammation and allergic disease pathology (58,150). In contrast, sHDL enhances the phosphorylation of Akt1/2/3, suggesting the activation of survival-associated or anti-apoptotic signaling that may preserve eosinophil viability during inflammatory conditions (151).

Our data showed that native HDL failed to prevent CCR3 internalization triggered by eotaxin. This outcome is likely related to the reduced ability of native HDL to promote cholesterol efflux when compared with sHDL, as illustrated in fig 9. Earlier studies have established that the capacity of isolated HDL to inhibit eosinophil shape change and chemotactic responses depends strongly on its lipid and apolipoprotein makeup, particularly the relative abundance of apolipoprotein A-II, apolipoprotein C-III, lysophosphatidylcholine, and triglycerides (84). This donor-dependent

heterogeneity in HDL composition likely explains the lack of a uniform response observed with native HDL in our experiments.

The in vivo efficacy of sHDL nanodiscs was validated in IL-5 transgenic mice, a well-established model of chronic eosinophilia, in which administration of sHDL nanodiscs led to a marked decrease in eosinophil and neutrophil numbers in bronchoalveolar lavage (Fig 11). Within this context, treatment with sHDL nanodiscs produced a clear anti-inflammatory effect, evidenced by a significant reduction in both eosinophil and neutrophil numbers in bronchoalveolar lavage fluid. The observed decrease in inflammatory cell burden indicates a meaningful attenuation of airway inflammation. The concomitant reduction in neutrophils further suggests that sHDL nanodiscs may exert broader immunomodulatory effects beyond eosinophil-specific pathways, potentially influencing leukocyte recruitment or survival within inflamed tissues (Fig 11).

Compared with antibody-based therapies that aim to systemically deplete eosinophils, sHDL-based interventions offer several conceptual and practical advantages that align more closely with the emerging view of eosinophils as multifunctional immune cells. Although eosinophils are well recognized for their pathogenic role in allergic airway inflammation and tissue damage when overactivated, accumulating evidence indicates that they also contribute to essential physiological processes, including maintenance of tissue homeostasis, immune regulation, and host defense against parasitic and certain bacterial infections (170). More recent studies further suggest beneficial roles for eosinophils in tumor surveillance and anti-tumor immunity, underscoring their context-dependent and potentially protective functions (171).

Current biologic therapies targeting IL-5, IL-5Rα, IL-4, or IL-13 effectively reduce circulating and tissue eosinophils and have demonstrated clinical benefit in severe eosinophilic asthma. However, these approaches achieve their efficacy largely through sustained eosinophil depletion, which has been associated with adverse effects and raises concerns regarding long-term immune competence (170,172,173). As the broader physiological importance of eosinophils becomes increasingly apparent, complete or prolonged ablation of this cell population may carry risks, including impaired host defense and secondary immune complications (174–176). These limitations highlight a key

drawback of antibody therapies that indiscriminately eliminate eosinophils rather than selectively modulating their pathogenic activities.

In this context, sHDL nanodiscs represent a more nuanced therapeutic strategy. By targeting eosinophil migration and chemotactic signaling rather than cell survival, sHDL therapy has the potential to limit pathological eosinophil accumulation at sites of allergic inflammation while preserving their systemic and homeostatic functions. Such an approach aligns with the dual nature of eosinophils, allowing attenuation of disease-driving recruitment without complete cellular eradication (177). Moreover, the defined size, structural stability, and compositional flexibility of sHDL nanodiscs further strengthen their translational appeal. sHDLs can be rationally engineered to enhance specific anti-inflammatory properties, for example through enrichment with bioactive lipids such as miltefosine (87) or lysophosphatidylcholine (88), potentially enabling tailored modulation of immune responses. Collectively, these features position sHDL therapy as a candidate for limiting eosinophil recruitment rather than eliminating eosinophils altogether represents a more balanced strategy. Targeting eosinophil migration using sHDL nanodiscs may therefore provide an effective means of modulating eosinophil recruitment while preserving beneficial functions.

6.1.2 Limitations

It is imperative to acknowledge the limitations of these findings. Firstly, it should be noted that the conclusions drawn are limited to the specific peptide-lipid formulation that was the subject of investigation in this study. Other ApoA-I mimetic peptides or phospholipid compositions were not examined and it is possible that these may differ in their biological activity. Secondly, the in vivo experiments were conducted over a relatively brief experimental period, which constrained the capacity to evaluate sustained inflammatory responses and progressive functional impairment of the lung that are hallmarks of chronic inflammatory airway diseases. Consequently, the potential effects of sHDL on disease evolution, as opposed to acute inflammatory cell recruitment, remain unresolved. Furthermore, sHDL treatment did not induce detectable changes in IL-6 or TNF-α concentrations in bronchoalveolar lavage fluid (Supplementary fig. 4), suggesting that, within the timeframe analyzed, the therapeutic effects of sHDL were not mediated through broad suppression

of these pro-inflammatory cytokines. Instead, these results may reflect more targeted modulation of eosinophil trafficking and signaling pathways. The field has evolved beyond the use of HDL mimetics solely as cholesterol acceptors toward their development as flexible platforms for targeted drug delivery. Recent work highlights the advantages of chemically conjugating therapeutic agents to HDL-based carriers, allowing improved tissue targeting (34,105). In addition to the existing findings, it is also worth exploring the enhanced targetability of sHDL nanodiscs towards eosinophils (178). Studies on improved endothelial cell targetability have been published with ApoA-I mimetic peptide based sHDL by conjugating with VCAM-1 specific peptides (104). Moreover, anti-platelet drugs have also been successfully loaded onto HDL mimetics, showcasing their structural flexibility (105). Building on this strategy, it may be possible to achieve eosinophil-directed targeting by exploiting both eosinophil chemotactic pathways and activation-state-specific surface markers. As eosinophils preferentially migrate to inflamed, Th2-skewed microenvironments in response to CCR3-binding chemokines such as eotaxin, the incorporation of CCR3 ligands onto sHDL nanodiscs could enhance the selective recruitment of eosinophils to inflammatory sites. Furthermore, targeting ligands that recognize activation-dependent eosinophil surface receptors could improve specificity towards pathogenic eosinophil subsets, minimizing off-target effects. This dual-targeting approach could improve the spatial precision and therapeutic efficacy of sHDL-based nanocarriers in treating eosinophil-associated inflammatory diseases.

6.2 Studies on neutrophils involving lysophosphatidylcholine-enriched sHDL

6.2.1 Major findings

While saturated lysophosphatidylcholines (LPCs) are known to exert acute anti-inflammatory effects on human granulocytes and significantly reduce pulmonary immune cell infiltration (179) their therapeutic delivery remains a challenge. In this study, we investigated the synthesis, physicochemical stability, and biological impact of LPC-enriched sHDL nanoparticles. These particles were engineered using a 22A peptide scaffold and DMPC lipid matrix to evaluate their potential as a stable delivery platform. Our central objective was to determine whether the partial substitution of DMPC with structurally distinct LPC species could be achieved without compromising nanoparticle integrity, while simultaneously conferring functional

immunomodulatory advantages. The results demonstrate that LPC enrichment is technically robust, yielding structurally stable nanoparticles that remain biologically active. Specifically, we show that certain LPC species exert selective anti-inflammatory effects by modulating neutrophil activation without inducing cytotoxicity, highlighting the potential for tailored lipid signaling in sHDL platforms.

A major concern when modifying lipid composition in discoidal HDL mimetics is the potential disruption of particle self-assembly, size homogeneity, or colloidal stability. LPCs possess only a single acyl chain and a larger effective headgroup area compared to phosphatidylcholines such as DMPC, that could theoretically destabilize discoidal nanostructures or promote micelle formation. The present results directly refute this concern for the enrichment levels tested.

Using an optimized freeze-drying protocol, all LPC-enriched sHDL formulations self-assembled reproducibly and exhibited physicochemical properties indistinguishable from sHDL controls. DLS showed highly uniform particle populations with mean diameters clustered around ~10 nm and PDI values consistently ≤ 0.22 (Table 2). This level of monodispersity is critical, as even modest increases in size heterogeneity or aggregation can confound biological interpretation, alter biodistribution, and increase nonspecific cellular interactions. The absence of secondary peaks or high-PDI tails indicates that LPC incorporation does not induce particle fusion, fragmentation, or large aggregate formation (Fig. 12).

Gel permeation chromatography independently validated these findings. Retention times for LPC-enriched particles overlapped almost perfectly with the control sHDL, confirming that hydrodynamic size and overall particle architecture were preserved. Importantly, no evidence of lipid dissociation or peptide degradation was detected, suggesting that the freeze-drying and rehydration process maintains structural integrity even when the lipid composition is altered. Together, the DLS and GPC data establish that up to 20% molar substitution of DMPC with LPC is structurally tolerated within the sHDL platform (Fig. 13).

The LC–MS data demonstrate that LPCs are retained within the sHDL nanodiscs after size-exclusion clean-up (Table 3). These findings underscore the compatibility of LPC species with the 22A peptide-driven self-assembly process. Furthermore, they demonstrate that LPCs can serve as

a versatile tool for systematically tuning lipid composition without compromising the structural integrity or physicochemical quality of the resulting sHDL nanoparticle.

Before functional immunological effects can be interpreted, it is essential to rule out cytotoxicity, particularly for LPCs, which have been historically associated with membrane disruption and inflammatory signaling at high concentrations (180,181). Importantly, all LPC-enriched sHDL formulations were well tolerated by primary human PMNLs over the concentration range tested.

Annexin V/PI staining revealed no significant increase in early or late apoptosis following 30-minute exposure to LPC-enriched nanodiscs. Viability remained comparable to vehicle-treated cells across LPC species (14:0, 16:0, and 18:0), indicating that the nanoparticle-bound presentation of LPC fundamentally alters its biological behavior relative to free lipid (Fig.14).

Free LPC can intercalate directly into plasma membranes, disrupt lipid packing, and trigger calcium flux or membrane lysis (180,181). In contrast, LPC presented within a stabilized sHDL nanodisc is spatially constrained, buffered by surrounding phospholipids, and shielded by the peptide scaffold. These data therefore reinforce the concept that context matters: LPCs that are pro-inflammatory or cytotoxic in isolation can become biologically neutral or even protective when incorporated into structured lipid nanoparticles (179).

Neutrophil shape change, as measured by forward scatter, is an early and sensitive indicator of activation, cytoskeletal rearrangement, and chemotactic readiness. It precedes adhesion, degranulation, and reactive oxygen species production, making it a highly relevant functional readout (182,183). While control sHDL showed only modest, non-significant effects, enrichment with LPC 18:0 produced a clear and statistically significant reduction in IL-8–induced neutrophil shape change when each of the 125 ug/ml sample were compared (Fig 15). This indicates that lipid composition alone is sufficient to modify neutrophil responsiveness to chemokine stimulation.

The chain-length specificity of this effect is particularly important. LPC 14:0 and LPC 16:0 did not produce comparable inhibition, suggesting that the anti-inflammatory activity is not a generic property of LPC enrichment but rather depends on acyl chain length. Longer saturated acyl chains such as stearoyl (18:0) increase lipid packing density and decrease membrane fluidity by enhancing

van der Waals interactions and reducing area per lipid (184), which may influence how sHDL interacts with cell surface receptors or lipid rafts.

These findings have broader implications for the design of HDL-based nanotherapeutics. Traditional sHDL formulations have focused primarily on cholesterol efflux capacity and macrophage biology. The present study expands this paradigm by showing that sHDL can be engineered to directly modulate neutrophil activation, a key driver of acute and chronic inflammation such as cardiovascular disease (185) and sepsis (186).

Importantly, the anti-inflammatory effect observed here occurs without altering cell viability, suggesting a regulatory rather than immunosuppressive mode of action. This distinction is crucial for clinical translation, as broad neutrophil suppression increases susceptibility to infection (187).

6.2.2 Limitations

Despite these strengths, several limitations exist. First, molecular dynamic simulations and transmission electron microscopy are needed to understand the structural aspects that lead to the stability of this enrichment. Additionally, the current study is in its preliminary stage and focuses on short-term neutrophil responses and early activation markers. Whether LPC-enriched sHDL also affects downstream functions such as chemotaxis, degranulation, phagocytosis, extracellular trap formation and oxidative burst, remains to be determined. The mechanistic studies dissecting receptor involvement and intracellular signaling pathways are needed to define how LPC 18:0 exerts its inhibitory effect. These effects also need to be compared with free LPC and albumin bound LPCs to clearly establish the need for an sHDL based platform. Future in vivo studies are required to translate these findings to complex physiological environments where systemic components may influence nanoparticle behavior. Given that bihelical scaffolds (e.g., 4F-P-4F) provide enhanced structural stability compared to single-helix peptides like 22A, evaluating LPC integration into these advanced systems is of great interest. If achieved, this dual-scaffold approach could offer a versatile therapeutic strategy for broader inflammatory pathologies, including both neutrophilic and eosinophilic subtypes

7. CONCLUSIONS

As interest in HDL-based infusion therapies continues to grow in clinical settings, it is increasingly important to clarify how sHDL formulations interact with circulating immune cells. Extensive evidence demonstrates that HDL mimetics can suppress cytokine production, limit oxidative stress, and modulate G-protein-coupled receptor signaling in human immune cells (9,115,120), reinforcing their potential utility in the treatment of chronic inflammatory diseases.

The present investigation demonstrates that sHDL nanodiscs formulated with the ApoA-I mimetic peptide 4F-P-4F potently suppress human eosinophil migration via a defined receptor- and signaling-dependent mechanism. In vitro, these nanodiscs have been shown to inhibit eotaxin-induced eosinophil chemotaxis, a process that can be reversed by blockade of the HDL receptors SR-BI and ABCA1, suggesting that targeted receptor engagement is necessary for activity. Mechanistically, sHDL enhances cholesterol efflux from eosinophil membranes, which disrupts ligand-induced CCR3 internalization and alters downstream signaling. This is accompanied by modulation of key intracellular pathways, including decreased phosphorylation of ERK1/2 and altered STAT1 and STAT3 activation, linking changes in membrane cholesterol homeostasis to impaired chemotactic signaling (144). In vivo administration of sHDL has been demonstrated to reduce eosinophil recruitment to the bronchoalveolar lavage in IL-5 transgenic mice, thereby confirming its functional relevance in an inflammatory setting. These findings position sHDL nanodiscs as a compelling add-on therapeutic strategy for modulating eosinophil chemotaxis in chronic inflammatory conditions, such as asthma and eosinophilic esophagitis, where dysregulated trafficking drives disease pathology.

Simultaneously, we establish that lysophosphatidylcholine can be efficiently incorporated into sHDL nanodiscs without compromising structural integrity or cell viability. Utilizing a 22A peptide-DMPC model system, we identified that LPC 18:0 uniquely attenuates IL-8-induced neutrophil shape change, emphasizing the role of specific lipid species in dictating the platform's bioactivity. Together, these results define LPC-enriched sHDL as a modular and tunable platform for targeted immunomodulation. While previous studies have focused on the LPS-sequestration capacity of HDL mimetics in monocytes and neutrophils, our work extends this paradigm by

demonstrating a broader functional scope: the modulation of diverse agonist-driven responses across multiple granulocyte populations

9. BIBLIOGRAPHY

1. Feingold KR, Grunfeld C. Introduction to lipids and lipoproteins. In: Feingold KR, Anawalt B, Boyce A, Chrousos G, Dungan K, Grossman A, et al., South Dartmouth (MA): MDText.com, Inc.; 2000 Available from: https://www.ncbi.nlm.nih.gov/books/NBK305896

2. Kuijpers PMJC. History in medicine: the story of cholesterol, lipids and cardiology [Internet]. European Society of Cardiology; c2021 Available from: https://www.escardio.org/Journals/E-Journal-of-Cardiology-Practice/Volume-19/history-in-medicine-the-story-of-cholesterol-lipids-and-cardiology

3. Olson RE. Discovery of the Lipoproteins, Their Role in Fat Transport and Their Significance as Risk Factors1. J Nutr. 1998 Feb 1;128(2):439S-443S.

4. Kontush A, Lindahl M, Lhomme M, Calabresi L, Chapman MJ, Davidson WS. Structure of HDL: particle subclasses and molecular components. Handb Exp Pharmacol. 2015;224:3–51.

5. Gordon T, Castelli WP, Hjortland MC, Kannel WB, Dawber TR. High density lipoprotein as a protective factor against coronary heart disease: The Framingham study. Am J Med. 1977 May 1;62(5):707–14.

6. Tran-Dinh A, Diallo D, Delbosc S, Varela-Perez LM, Dang Q, Lapergue B, et al. HDL and endothelial protection. Br J Pharmacol. 2013 June;169(3):493–511.

7. Rani A, Marsche G. A Current Update on the Role of HDL-Based Nanomedicine in Targeting Macrophages in Cardiovascular Disease. Pharmaceutics. 2023 May;15(5):1504.

8. Trakaki A, Marsche G. High-density lipoprotein (HDL) in allergy and skin diseases: focus on immunomodulating functions. Biomedicines. 2020 Dec 1;8(12):558.

9. Trakaki A, Marsche G. Current Understanding of the Immunomodulatory Activities of High-Density Lipoproteins. Biomedicines. 2021 June;9(6):587.

10. Grao-Cruces E, Lopez-Enriquez S, Martin ME, Montserrat-de la Paz S. High-density lipoproteins and immune response: A review. Int J Biol Macromol. 2022 Jan 15;195:117–23.

11. von Eckardstein A, Nordestgaard BG, Remaley AT, Catapano AL. High-density lipoprotein revisited: biological functions and clinical relevance. Eur Heart J. 2023 Apr 21;44(16):1394–407.

12. Böttcher A, Heeren J, Koliwad S, et al. Modulation of the cellular microRNA landscape: contribution to the protective effects of high-density lipoproteins (HDL). Biology (Basel). 2023 Sep;12(9):1232

13. Michell DL, Vickers KC. HDL and microRNA therapeutics in cardiovascular disease. Pharmacol Ther. 2016 Dec 1;168:43–52.

14. Davidson WS, Shah AS, Sexmith H, Gordon SM. The HDL Proteome Watch: Compilation of studies leads to new insights on HDL function. Biochim Biophys Acta BBA - Mol Cell Biol Lipids. 2022 Feb 1;1867(2):159072.

15. Kontush A, Lhomme M, Chapman MJ. Unraveling the complexities of the HDL lipidome1. J Lipid Res. 2013 Nov;54(11):2950–63.

16. Zannis VI, Fotakis P, Koukos G, Kardassis D, Ehnholm C, Jauhiainen M, et al. HDL Biogenesis, Remodeling, and Catabolism. In: von Eckardstein A, Kardassis D, editors. High Density Lipoproteins: From Biological Understanding to Clinical Exploitation [Internet]. Cham: Springer International Publishing; 2015 [cited 2026 Jan 5]. p. 53–111. Available from: https://doi.org/10.1007/978-3-319-09665-0_2

17. Xu S, Laccotripe M, Huang X, Rigotti A, Zannis VI, Krieger M. Apolipoproteins of HDL can directly mediate binding to the scavenger receptor SR-BI, an HDL receptor that mediates selective lipid uptake. J Lipid Res. 1997 July;38(7):1289–98.

18. de Beer MC, Durbin DM, Cai L, Jonas A, de Beer FC, van der Westhuyzen DR. Apolipoprotein A-I conformation markedly influences HDL interaction with scavenger receptor BI. J Lipid Res. 2001 Feb;42(2):309–13.

19. Barter PJ, Nicholls S, Rye KA, Anantharamaiah GM, Navab M, Fogelman AM. Antiinflammatory Properties of HDL. Circ Res. 2004 Oct 15;95(8):764–72.

20. Denimal D. Antioxidant and Anti-Inflammatory Functions of High-Density Lipoprotein in Type 1 and Type 2 Diabetes. Antioxidants. 2023 Dec 28;13(1):57.

21. Calabresi L, Gomaraschi M, Franceschini G. Endothelial Protection by High-Density Lipoproteins. Arterioscler Thromb Vasc Biol. 2003 Oct;23(10):1724–31.

22. Tao X, Tao R, Wang K, Wu L. Anti-inflammatory mechanism of Apolipoprotein A-I. Front Immunol. 2024 July 8;15:1417270.

23. Busnelli M, Manzini S, Chiara M, Colombo A, Fontana F, Oleari R, et al. Aortic Gene Expression Profiles Show How ApoA-I Levels Modulate Inflammation, Lysosomal Activity, and Sphingolipid Metabolism in Murine Atherosclerosis. Arterioscler Thromb Vasc Biol. 2021 Feb;41(2):651–67.

24. Guo K, Hu C, Li L, Liu X, Liu Y, Zhang D, et al. ApoA1/HDL and sepsis-associated vascular endothelial injury: a narrative review. Crit Care. 2025 Oct 8;29:426.

25. Guo L, Morin EE, Yu M, Mei L, Fawaz MV, Wang Q, et al. Replenishing HDL with synthetic HDL has multiple protective effects against sepsis in mice. Sci Signal. 2022 Mar 15;15(725):eabl9322.

26. Rani A, Stadler JT, Marsche G. HDL-based therapeutics: A promising frontier in combating viral and bacterial infections. Pharmacol Ther. 2024 Aug 1;260:108684.

27. Huang Y, Zhang J, Zhao Q, Hu X, Zhao H, Wang S, et al. Impact of reduced apolipoprotein A-I levels on pulmonary arterial hypertension. Hellenic J Cardiol. 2024 Nov 1;80:31–46.

28. Brunham LR. The role of high-density lipoproteins in sepsis. J Lipid Res. 2025 Jan 1;66(1):100728.

29. Vaisar T, Tang C, Babenko I, Hutchins P, Wimberger J, Suffredini AF, et al. Inflammatory remodeling of the HDL proteome impairs cholesterol efflux capacity[S]. J Lipid Res. 2015 Aug 1;56(8):1519–30.

30. Zheng L, Nukuna B, Brennan ML, Sun M, Goormastic M, Settle M, et al. Apolipoprotein A-I is a selective target for myeloperoxidase-catalyzed oxidation and functional impairment in subjects with cardiovascular disease. J Clin Invest. 2004 Aug 16;114(4):529–41.

31. Ronsein GE, Vaisar T. Inflammation, Remodeling and Other Factors Affecting HDL Cholesterol Efflux. Curr Opin Lipidol. 2017 Feb;28(1):52–9.

32. Vyletelová V, Nováková M, Pašková Ľ. Alterations of HDL's to piHDL's Proteome in Patients with Chronic Inflammatory Diseases, and HDL-Targeted Therapies. Pharmaceuticals. 2022 Oct;15(10):1278.

33. Navab M, Reddy ST, Van Lenten BJ, Fogelman AM. HDL and cardiovascular disease: atherogenic and atheroprotective mechanisms. Nat Rev Cardiol. 2011 Apr;8(4):222–32.

34. Kuai R, Li D, Chen YE, Moon JJ, Schwendeman A. High-Density Lipoproteins: Nature's Multifunctional Nanoparticles. ACS Nano. 2016 Mar 22;10(3):3015–41.

35. Wang G, Sparrow JT, Cushley RJ. The Helix-Hinge-Helix Structural Motif in Human Apolipoprotein A-I Determined by NMR Spectroscopy,. Biochemistry. 1997 Nov 1;36(44):13657–66.

36. Anantharamaiah GM, Jones JL, Brouillette CG, Schmidt CF, Chung BH, Hughes TA, et al. Studies of synthetic peptide analogs of the amphipathic helix. Structure of complexes with dimyristoyl phosphatidylcholine. J Biol Chem. 1985 Aug 25;260(18):10248–55.

37. Zhao Y, Imura T, Leman LJ, Curtiss LK, Maryanoff BE, Ghadiri MR. Mimicry of high-density lipoprotein: functional peptide-lipid nanoparticles based on multivalent peptide constructs. J Am Chem Soc. 2013 Sept 11;135(36):13414–24.

38. Bielicki JK, Zhang H, Cortez Y, Zheng Y, Narayanaswami V, Patel A, et al. A new HDL mimetic peptide that stimulates cellular cholesterol efflux with high efficiency greatly reduces atherosclerosis in mice. J Lipid Res. 2010 June;51(6):1496–503.

39. Patel H, Ding B, Ernst K, Shen L, Yuan W, Tang J, et al. Characterization of apolipoprotein A-I peptide–phospholipid interaction and its effect on HDL nanodisc assembly. Int J Nanomedicine. 2019 Apr 30;14:3069–3086.

40. Amar MJA, D'Souza W, Turner S, Demosky S, Sviridov D, Stonik J, et al. 5A Apolipoprotein Mimetic Peptide Promotes Cholesterol Efflux and Reduces Atherosclerosis in Mice. J Pharmacol Exp Ther. 2010 Aug;334(2):634–41.

41. Xu R, Li S, Shi M, Li Z, Wang Y, Li J, et al. Peptide-based high-density lipoprotein promotes adipose tissue browning and restrains development of atherosclerosis and type 2 diabetes. Nano Today. 2021 Feb 1;36:101054.

42. Bricarello DA, Smilowitz JT, Zivkovic AM, German JB, Parikh AN. Reconstituted Lipoprotein: A Versatile Class of Biologically-Inspired Nanostructures. ACS Nano. 2011 Jan 25;5(1):42–57.

43. Tang J, Li D, Drake L, Yuan W, Deschaine S, Morin EE, et al. Influence of route of administration and lipidation of apolipoprotein A-I peptide on pharmacokinetics and cholesterol mobilization. J Lipid Res. 2017 Jan;58(1):124–36.

44. D'Souza W, Stonik JA, Murphy A, Demosky SJ, Sethi AA, Moore XL, et al. Structure-function relationships of apolipoprotein A-I mimetic peptides: implications for anti-atherogenic activities of high density lipoprotein. Circ Res. 2010 July 23;107(2):217–27.

45. Schwendeman A, Sviridov DO, Yuan W, Guo Y, Morin EE, Yuan Y, et al. The effect of phospholipid composition of reconstituted HDL on its cholesterol efflux and anti-inflammatory properties. J Lipid Res. 2015 Sept;56(9):1727–37.

46. Kim SY, Kang J, Fawaz MV, Yu M, Xia Z, Morin EE, et al. Phospholipids impact the protective effects of HDL-mimetic nanodiscs against lipopolysaccharide-induced inflammation. Nanomed. 18(29):2127–42.

47. Fawaz MV, Kim SY, Li D, Ming R, Xia Z, Olsen K, et al. Phospholipid Component Defines Pharmacokinetic and Pharmacodynamic Properties of Synthetic High-Density Lipoproteins. J Pharmacol Exp Ther. 2020 Feb 1;372(2):193–204.

48. Darabi M, Lhomme M, Dahik VD, Guillas I, Frisdal E, Tubeuf E, et al. Phosphatidylserine enhances anti-inflammatory effects of reconstituted HDL in macrophages via distinct intracellular pathways. FASEB J. 2022;36(5):e22274.

49. Yu M, Dorsey KH, Halseth T, Schwendeman A. Enhancement of Anti-Inflammatory Effects of Synthetic High-Density Lipoproteins by Incorporation of Anionic Lipids. Mol Pharm. 2023 Nov 6;20(11):5454–62.

50. George-Gay B, Parker K. Understanding the complete blood count with differential. J Perianesth Nurs. 2003 Apr 1;18(2):96–117.

51. Sinning J, Berliner N. Granulocytes in health and disease. In: Hatton C, Hay D, Firth J, Conlon C, Cox T, editors. Oxford Textbook of Medicine [Internet]. Oxford University Press; 2020 [cited 2026 Jan 6]. p. 0. Available from: https://doi.org/10.1093/med/9780198746690.003.0513

52. Wechsler ME, Munitz A, Ackerman SJ, Drake MG, Jackson DJ, Wardlaw AJ, et al. Eosinophils in Health and Disease: A State-of-the-Art Review. Mayo Clin Proc. 2021 Oct 1;96(10):2694–707.

53. Arnold IC, Munitz A. Spatial adaptation of eosinophils and their emerging roles in homeostasis, infection and disease. Nat Rev Immunol. 2024 Dec;24(12):858–77.

54. Holgate ST. Targeting eosinophil biology in asthma therapy. Am J Respir Cell Mol Biol. 2011 Oct ; 45(4):667-74.

55. Muir A, Falk GW. Eosinophilic Esophagitis: A Review. JAMA. 2021 Oct 5;326(13):1310–8.

56. Fujieda S, Imoto Y, Kato Y, Ninomiya T, Tokunaga T, Tsutsumiuchi T, et al. Eosinophilic chronic rhinosinusitis. Allergol Int. 2019 Oct 1;68(4):403–12.

57. Lee YL, Heriyanto DS, Yuliani FS, Laiman V, Choridah L, Lee KY, et al. Eosinophilic inflammation: a key player in COPD pathogenesis and progression. Ann Med. 2024 Dec;56(1):2408466.

58. Kampen GT, Stafford S, Adachi T, Jinquan T, Quan S, Grant JA, et al. Eotaxin induces degranulation and chemotaxis of eosinophils through the activation of ERK2 and p38 mitogen-activated protein kinases: Presented in part at the annual meetings of the American Academy of Allergy, Asthma, and Immunology in Washington, DC, March 13-18, 1998, and in Orlando, FL, February 26-March 3, 1999. Blood. 2000 Mar 15;95(6):1911–7.

59. Zimmermann N, Conkright JJ, Rothenberg ME. CC Chemokine Receptor-3 Undergoes Prolonged Ligand-induced Internalization*. J Biol Chem. 1999 Apr 30;274(18):12611–8.

60. Combadiere C, Ahuja SK, Murphy PM. Cloning and Functional Expression of a Human Eosinophil CC Chemokine Receptor *. J Biol Chem. 1995 July 14;270(28):16491–4.

61. Erin EM, Williams TJ, Barnes PJ, Hansel TT. Eotaxin Receptor (CCR3) Antagonism in Asthma and Allergic Disease. Curr Drug Targets - Inflamm Allergy. 1(2):201–14.

62. Rothenberg ME. Eotaxin. Am J Respir Cell Mol Biol. 1999 Sept;21(3):291–5.

63. Dent G, Hadjicharalambous C, Yoshikawa T, Handy RLC, Powell J, Anderson IK, et al. Contribution of Eotaxin-1 to Eosinophil Chemotactic Activity of Moderate and Severe Asthmatic Sputum. Am J Respir Crit Care Med. 2004 May 15;169(10):1110–7.

64. Blanchard C, Wang N, Stringer KF, Mishra A, Fulkerson PC, Abonia JP, et al. Eotaxin-3 and a uniquely conserved gene-expression profile in eosinophilic esophagitis. J Clin Invest. 2006 Feb 1;116(2):536–47.

65. Shamri R, Young KM, Weller PF. PI3K, ERK, p38 MAPK and integrins regulate CCR3-mediated secretion of mouse and human eosinophil-associated RNases. Allergy. 2013 July;68(7):880–9.

66. Schratl P, Sturm EM, Royer JF, Sturm GJ, Lippe IT, Peskar BA, et al. Hierarchy of eosinophil chemoattractants: role of p38 mitogen-activated protein kinase. Eur J Immunol. 2006;36(9):2401–9.

67. Ma W, Bryce PJ, Humbles AA, Laouini D, Yalcindag A, Alenius H, et al. CCR3 is essential for skin eosinophilia and airway hyperresponsiveness in a murine model of allergic skin inflammation. J Clin Invest. 2002 Mar;109(5):621–8.

68. Wegmann M, Göggel R, Sel S, Sel S, Erb KJ, Kalkbrenner F, et al. Effects of a Low-Molecular-Weight CCR-3 Antagonist on Chronic Experimental Asthma. Am J Respir Cell Mol Biol. 2007 Jan;36(1):61–7.

69. Wang J, Man K, Ng KTP. Emerging roles of C-C motif ligand 11 (CCL11) in cancers and liver diseases: mechanisms and therapeutic implications. Int J Mol Sci. 2025 May 13;26(10):4662

70. Filippone RT, Dargahi N, Eri R, Uranga JA, Bornstein JC, Apostolopoulos V, et al. Potent CCR3 receptor antagonist SB328437 suppresses colonic eosinophil chemotaxis and inflammation in the Winnie murine model of spontaneous chronic colitis. Int J Mol Sci. 2022 Jul 14;23(14):7780.

71. Liew PX, Kubes P. The Neutrophil's Role During Health and Disease. Physiol Rev. 2019 Apr;99(2):1223–48.

72. Rosales C, Demaurex N, Lowell CA, Uribe-Querol E. Neutrophils: Their Role in Innate and Adaptive Immunity. J Immunol Res. 2016;2016:1469780.

73. Houk AR, Jilkine A, Mejean CO, Boltyanskiy R, Dufresne ER, Angenent SB, et al. Membrane tension maintains cell polarity by confining signals to the leading edge during neutrophil migration. Cell. 2012 Jan 20;148(1–2):175–88.

74. Matsushima K, Yang D, Oppenheim JJ. Interleukin-8: An evolving chemokine. Cytokine. 2022 May 1;153:155828.

75. Guo RF, Ward PA. Role of C5a in inflammatory responses. Annu Rev Immunol. 2005;23:821–52.

76. Dorward DA, Lucas CD, Chapman GB, Haslett C, Dhaliwal K, Rossi AG. The Role of Formylated Peptides and Formyl Peptide Receptor 1 in Governing Neutrophil Function during Acute Inflammation. Am J Pathol. 2015 May;185(5):1172–84.

77. Nathan C. Neutrophils and immunity: challenges and opportunities. Nat Rev Immunol. 2006 Mar;6(3):173–82.

78. Shen X, Cao K, Jiang J, Guan W, Du J. Neutrophil dysregulation during sepsis: an overview and update. J Cell Mol Med. 2017 Sept;21(9):1687–97.

79. Sreejit G, Johnson J, Jaggers RM, Dahdah A, Murphy AJ, Hanssen NMJ, et al. Neutrophils in cardiovascular disease: warmongers, peacemakers, or both? Cardiovasc Res. 2021 Sept 17;118(12):2596–609.

80. Wigerblad G, Kaplan MJ. Neutrophil extracellular traps in systemic autoimmune and autoinflammatory diseases. Nat Rev Immunol. 2023;23(5):274–88.

81. Soehnlein O. Multiple Roles for Neutrophils in Atherosclerosis. Circ Res. 2012 Mar 16;110(6):875–88.

82. Atehortua L, Davidson WS, Chougnet CA. Interactions Between HDL and CD4+ T Cells: A Novel Understanding of HDL Anti-Inflammatory Properties. Arterioscler Thromb Vasc Biol. 2024 June;44(6):1191–201.

83. Wen J, Zhuang R, He C, Giri M, Guo S. High-density lipoprotein cholesterol is inversely associated with blood eosinophil counts among asthmatic adults in the USA: NHANES 2011–2018. Front Immunol. 2023 Apr 24;14:1166406

84. Trakaki A, Sturm GJ, Pregartner G, Scharnagl H, Eichmann TO, Trieb M, et al. Allergic rhinitis is associated with complex alterations in high-density lipoprotein composition and function. Biochim Biophys Acta BBA - Mol Cell Biol Lipids. 2019 Oct 1;1864(10):1280–92.

85. Trieb M, Wolf P, Knuplez E, Weger W, Schuster C, Peinhaupt M, et al. Abnormal composition and function of high-density lipoproteins in atopic dermatitis patients. Allergy. 2019 Feb;74(2):398–402.

86. Roula D, Theiler A, Luschnig P, Sturm GJ, Tomazic PV, Marsche G, et al. Apolipoprotein A-IV acts as an endogenous anti-inflammatory protein and is reduced in treatment-naïve allergic patients and allergen-challenged mice. Allergy. 2020 Feb;75(2):392–402.

87. Knuplez E, Kienzl M, Trakaki A, Schicho R, Heinemann A, Sturm EM, et al. The anti-parasitic drug miltefosine suppresses activation of human eosinophils and ameliorates allergic inflammation in mice. Br J Pharmacol. 2021 Mar;178(5):1234–48.

88. Knuplez E, Curcic S, Theiler A, Bärnthaler T, Trakaki A, Trieb M, et al. Lysophosphatidylcholines inhibit human eosinophil activation and suppress eosinophil migration in vivo. Biochim Biophys Acta BBA - Mol Cell Biol Lipids. 2020 July 1;1865(7):158686.

89. Tucker B, Ephraums J, King TW, Abburi K, Rye KA, Cochran BJ. Impact of Impaired Cholesterol Homeostasis on Neutrophils in Atherosclerosis. Arterioscler Thromb Vasc Biol. 2023 May;43(5):618–27.

90. Hunjadi M, Lamina C, Kahler P, Bernscherer T, Viikari J, Lehtimäki T, et al. HDL cholesterol efflux capacity is inversely associated with subclinical cardiovascular risk markers in young adults: The cardiovascular risk in Young Finns study. Sci Rep. 2020 Nov 5;10(1):19223.

91. Jiang M, Sun J, Zou H, Li M, Su Z, Sun W, et al. Prognostic Role of Neutrophil to High-Density Lipoprotein Cholesterol Ratio for All-Cause and Cardiovascular Mortality in the General Population. Front Cardiovasc Med. 2022 Feb 8;9:807339.

92. Hang LH, Zhou J, Luo Z, Zhang L. Association between neutrophil to high-density lipoprotein cholesterol ratio and 28-day mortality in sepsis patients: Analysis from the MIMIC-IV database. Medicine (Baltimore). 2025 Dec 12;104(50):e46397.

93. Chen DL, Lin YK, Wang GJ, Chang KC. Neutrophil to high-density lipoprotein cholesterol ratio as a potential inflammatory marker for predicting all-cause mortality in out-of-hospital cardiac arrest survivors. Sci Rep. 2025 May 17;15(1):17181.

94. Feingold KR, Grunfeld C. The role of HDL in innate immunity. J Lipid Res. 2011 Jan;52(1):1–3.

95. Meilhac O, Tanaka S, Couret D. High-Density Lipoproteins Are Bug Scavengers. Biomolecules. 2020 Apr 12;10(4):598.

96. Lotz S, Aga E, Wilde I, van Zandbergen G, Hartung T, Solbach W, et al. Highly purified lipoteichoic acid activates neutrophil granulocytes and delays their spontaneous apoptosis via CD14 and TLR2. J Leukoc Biol. 2004 Mar;75(3):467–77.

97. Brzezinska AA, Johnson JL, Munafo DB, Ellis BA, Catz SD. Signalling mechanisms for Toll-like receptor-activated neutrophil exocytosis: key roles for interleukin-1-receptor-

associated kinase-4 and phosphatidylinositol 3-kinase but not Toll/IL-1 receptor (TIR) domain-containing adaptor inducing IFN-β (TRIF). Immunology. 2009 July;127(3):386–97.

98. Raupachova J, Kopecky C, Cohen G. High-density lipoprotein from chronic kidney disease patients modulates polymorphonuclear leukocytes. Toxins (Basel). 2019 Feb 1;11(2):73

99. Theilmeier G, Schmidt C, Herrmann J, Keul P, Schäfers M, Herrgott I, et al. High-Density Lipoproteins and Their Constituent, Sphingosine-1-Phosphate, Directly Protect the Heart Against Ischemia/Reperfusion Injury In Vivo via the S1P3 Lysophospholipid Receptor. Circulation. 2006 Sept 26;114(13):1403–9.

100. Murphy AJ, Woollard KJ, Suhartoyo A, Stirzaker RA, Shaw J, Sviridov D, et al. Neutrophil Activation Is Attenuated by High-Density Lipoprotein and Apolipoprotein A-I in In Vitro and In Vivo Models of Inflammation. Arterioscler Thromb Vasc Biol. 2011 June;31(6):1333–41.

101. Curcic S, Holzer M, Frei R, Pasterk L, Schicho R, Heinemann A, et al. Neutrophil effector responses are suppressed by secretory phospholipase A2 modified HDL. Biochim Biophys Acta BBA - Mol Cell Biol Lipids. 2015 Feb 1;1851(2):184–93.

102. Jeong S, Kim B, Byun DJ, Jin S, Seo BS, Shin MH, et al. Lysophosphatidylcholine alleviates acute lung injury by regulating neutrophil motility and neutrophil extracellular trap formation. Front Cell Dev Biol. 2022 Jul 4;10:941914.

103. Dal-Fabbro R, Yu M, Mei L, Sasaki H, Schwendeman A, Bottino MC. Synthetic high-density lipoprotein (sHDL): a bioinspired nanotherapeutics for managing periapical bone inflammation. Int J Oral Sci. 2024 July 2;16(1):50.

104. Yu M, Hong K, Adili R, Mei L, Liu L, He H, et al. Development of activated endothelial-targeted high-density lipoprotein nanoparticles. Front Pharmacol. 2022 Aug 29;13:902269.

105. He H, Adili R, Liu L, Hong K, Holinstat M, Schwendeman A. Synthetic high-density lipoproteins loaded with an antiplatelet drug for efficient inhibition of thrombosis in mice. Sci Adv. 2020 Dec 4;6(49):eabd0130.

106. Zhen J, Li X, Yu H, Du B. High-density lipoprotein mimetic nano-therapeutics targeting monocytes and macrophages for improved cardiovascular care: a comprehensive review. J Nanobiotechnology. 2024 May 17;22:263.

107. Tabet F, Remaley AT, Segaliny AI, Millet J, Yan L, Nakhla S, et al. The 5A Apolipoprotein A-I Mimetic Peptide Displays Antiinflammatory and Antioxidant Properties In Vivo and In Vitro. Arterioscler Thromb Vasc Biol. 2010 Feb;30(2):246–52.

108. Apalama ML, Givran L, Navarette B, Bringart M, Giraud P, Rondeau P, et al. Aerosolized ApoA1 nanoparticles synthesized by microfluidics cross the lung barrier and modulate inflammation. bioRxiv [Preprint]. 2025 Jul 9 Available from: https://www.biorxiv.org/content/10.1101/2025.07.09.663869v1

109. Yao X, Vitek MP, Remaley AT, Levine SJ. Apolipoprotein mimetic peptides: a new approach for the treatment of asthma. Front Pharmacol. 2012 Mar 9;3:37.

110. Yao X, Gordon EM, Barochia AV, Remaley AT, Levine SJ. The A's Have It: Developing Apolipoprotein A-I Mimetic Peptides Into a Novel Treatment for Asthma. Chest. 2016 Aug;150(2):283–8.

111. Yao X, Dai C, Fredriksson K, Dagur PK, McCoy JP, Qu X, et al. 5A, an Apolipoprotein A–I Mimetic Peptide, Attenuates the Induction of House Dust Mite-induced Asthma. J Immunol Baltim Md 1950. 2011 Jan 1;186(1):576–83.

112. Nandedkar SD, Weihrauch D, Xu H, Shi Y, Feroah T, Hutchins W, et al. D-4F, an apoA-1 mimetic, decreases airway hyperresponsiveness, inflammation, and oxidative stress in a murine model of asthma. J Lipid Res. 2011 Mar;52(3):499–508.

113. Moudry R, Spycher MO, Doran JE. Reconstituted high density lipoprotein modulates adherence of polymorphonuclear leukocytes to human endothelial cells. Shock. 1997 Mar;7(3):175.

114. Stasi A, Fiorentino M, Franzin R, Staffieri F, Carparelli S, Losapio R, et al. Beneficial effects of recombinant CER-001 high-density lipoprotein infusion in sepsis: results from a bench to bedside translational research project. BMC Med. 2023 Nov 2;21:392.

115. Sharifov OF, Xu X, Gaggar A, Grizzle WE, Mishra VK, Honavar J, et al. Anti-Inflammatory Mechanisms of Apolipoprotein A-I Mimetic Peptide in Acute Respiratory Distress Syndrome Secondary to Sepsis. PLOS ONE. 2013 May 14;8(5):e64486.

116. Radtke D, Voehringer D. Granulocyte development, tissue recruitment, and function during allergic inflammation. Eur J Immunol. 2023;53(8):2249977.

117. Margraf A, Lowell CA, Zarbock A. Neutrophils in acute inflammation: current concepts and translational implications. Blood. 2022 Apr 7;139(14):2130–44.

118. Fox CB, Baldwin SL, Duthie MS, Reed SG, Vedvick TS. Immunomodulatory and Physical Effects of Phospholipid Composition in Vaccine Adjuvant Emulsions. AAPS PharmSciTech. 2012 June 1;13(2):498–506.

119. Rodriguez A, Yu M, Gan J, Phoo MT, Rani A, Marsche G, et al. Phospholipase A2 Products Influence the Antiplatelet Functions of Synthetic High-Density Lipoproteins. J Lipid Res. 2025 Dec 29;100972.

120. Rodriguez A, Yu M, Phoo MT, Holinstat M, Schwendeman A. Antiplatelet effects of DMPC-based synthetic high-density lipoproteins: exploring particle structure and non-cholesterol efflux mechanisms. Mol Pharm. 2025 Jan 31. Epub ahead of print. doi:10.1021/acs.molpharmaceut.4c01000

121. Holzer M, Ljubojevic-Holzer S, Souza Junior DR, Stadler JT, Rani A, Scharnagl H, et al. HDL Isolated by Immunoaffinity, Ultracentrifugation, or Precipitation is Compositionally and Functionally Distinct. J Lipid Res. 2022 Dec 1;63(12):100307.

122. Rey J, Murail S, de Vries S, Derreumaux P, Tuffery P. PEP-FOLD4: a pH-dependent force field for peptide structure prediction in aqueous solution. Nucleic Acids Res. 2023 July 5;51(W1):W432–7.

123. Qi Y, Lee J, Klauda JB, Im W. CHARMM-GUI Nanodisc Builder for modeling and simulation of various nanodisc systems. J Comput Chem. 2019 Mar 15;40(7):893–9.

124. Salnikov ES, Anantharamaiah GM, Bechinger B. Supramolecular Organization of Apolipoprotein-A-I-Derived Peptides within Disc-like Arrangements. Biophys J. 2018 Aug 7;115(3):467–77.

125. Mishra VK, Palgunachari MN, Krishna NR, Glushka J, Segrest JP, Anantharamaiah GM. Effect of Leucine to Phenylalanine Substitution on the Nonpolar Face of a Class A Amphipathic Helical Peptide on Its Interaction with Lipid: HIGH RESOLUTION SOLUTION NMR STUDIES OF 4F-DIMYRISTOYLPHOSPHATIDYLCHOLINE DISCOIDAL COMPLEX*. J Biol Chem. 2008 Dec 5;283(49):34393–402.

126. Mishra VK, Anantharamaiah GM, Segrest JP, Palgunachari MN, Chaddha M, Sham SWS, et al. Association of a Model Class A (Apolipoprotein) Amphipathic α Helical Peptide with Lipid: HIGH RESOLUTION NMR STUDIES OF PEPTIDE·LIPID DISCOIDAL COMPLEXES*. J Biol Chem. 2006 Mar 10;281(10):6511–9.

127. Huang J, Rauscher S, Nawrocki G, Ran T, Feig M, de Groot BL, et al. CHARMM36m: an improved force field for folded and intrinsically disordered proteins. Nat Methods. 2017 Jan;14(1):71–3.

128. Pronk S, Páll S, Schulz R, Larsson P, Bjelkmar P, Apostolov R, et al. GROMACS 4.5: a high-throughput and highly parallel open source molecular simulation toolkit. Bioinformatics. 2013 Apr 1;29(7):845–54.

129. Hopkins CW, Le Grand S, Walker RC, Roitberg AE. Long-Time-Step Molecular Dynamics through Hydrogen Mass Repartitioning. J Chem Theory Comput. 2015 Apr 14;11(4):1864–74.

130. Parrinello M, Rahman A. Polymorphic transitions in single crystals: A new molecular dynamics method. J Appl Phys. 1981 Dec 1;52(12):7182–90.

131. Evans DJ, Holian BL. The Nose–Hoover thermostat. J Chem Phys. 1985 Oct 15;83(8):4069–74.

132. Darden T, York D, Pedersen L. Particle mesh Ewald: An N·log(N) method for Ewald sums in large systems. J Chem Phys. 1993 June 15;98(12):10089–92.

133. Drew ED, Janes RW. PDBMD2CD: providing predicted protein circular dichroism spectra from multiple molecular dynamics-generated protein structures. Nucleic Acids Res. 2020 July 2;48(W1):W17–24.

134. Miles AJ, Ramalli SG, Wallace BA. DichroWeb, a website for calculating protein secondary structure from circular dichroism spectroscopic data. Protein Sci Publ Protein Soc. 2022 Jan;31(1):37–46.

135. Sreerama N, Woody RW. A reference database for circular dichroism spectroscopy covering fold and secondary structure space. Bioinformatics. 2006 Aug 15;22(16):1955–1962.

136. Morrisett JD, David JSK, Pownall HJ, Gotto AMJr. Interaction of an apolipoprotein (apoLP-alanine) with phosphatidylcholine. Biochemistry. 1973 Mar 27;12(7):1290–9.

137. Murray J, Ward C, O'Flaherty JT, Dransfield I, Haslett C, Chilvers ER, et al. Role of leukotrienes in the regulation of human granulocyte behaviour: dissociation between agonist-induced activation and retardation of apoptosis. Br J Pharmacol. 2003;139(2):388–98.

138. Ochkur SI, Jacobsen EA, Lacy P. Eosinophil Shape Change and Secretion. In: Walsh GM, editor. Eosinophils: Methods and Protocols [Internet]. New York, NY: Springer US; 2021 [cited 2025 Dec 11]. p. 199–219. Available from: https://doi.org/10.1007/978-1-0716-1095-4_17

139. Dulkys Y, Kluthe C, Buschermöhle T, Barg I, Knöß S, Kapp A, et al. IL-3 Induces Down-Regulation of CCR3 Protein and mRNA in Human Eosinophils1. J Immunol. 2001 Sept 15;167(6):3443–53.

140. Theiler A, Bärnthaler T, Platzer W, Richtig G, Peinhaupt M, Rittchen S, et al. Butyrate ameliorates allergic airway inflammation by limiting eosinophil trafficking and survival. J Allergy Clin Immunol. 2019 Sept;144(3):764–76.

141. Ochkur SI, Jacobsen EA, Protheroe CA, Biechele TL, Pero RS, McGarry MP, et al. Coexpression of IL-5 and eotaxin-2 in mice creates an eosinophil-dependent model of respiratory inflammation with characteristics of severe asthma. J Immunol Baltim Md 1950. 2007 June 15;178(12):7879–89.

142. Islam RM, Pourmousa M, Sviridov D, Gordon SM, Neufeld EB, Freeman LA, et al. Structural properties of apolipoprotein A-I mimetic peptides that promote ABCA1-dependent cholesterol efflux. Sci Rep. 2018 Feb 13;8(1):2956.

143. Salnikov ES, Aisenbrey C, Anantharamaiah GM, Bechinger B. Solid-state NMR structural investigations of peptide-based nanodiscs and of transmembrane helices in bicellar arrangements. Chem Phys Lipids. 2019 Mar 1;219:58–71.

144. Rani A, Balandin D, Ravi R, Teppan J, Vidakovic I, Kienzl M, et al. Peptide-based lipid nanodiscs suppress eosinophil recruitment and chemotaxis. J Controlled Release. 2025 Sept 10;385:114060.

145. Immune cell - ABCA1 - The Human Protein Atlas [Internet]. [cited 2024 Aug 2]. Available from: https://www.proteinatlas.org/ENSG00000165029-ABCA1/immune+cell

146. Tall AR, Yvan-Charvet L, Terasaka N, Pagler T, Wang N. HDL, ABC Transporters, and Cholesterol Efflux: Implications for the Treatment of Atherosclerosis. Cell Metab. 2008 May 7;7(5):365–75.

147. Ji Y, Jian B, Wang N, Sun Y, Moya M de la L, Phillips MC, et al. Scavenger Receptor BI Promotes High Density Lipoprotein-mediated Cellular Cholesterol Efflux*. J Biol Chem. 1997 Aug 22;272(34):20982–5.

148. Zimmermann N, Rothenberg ME. Receptor internalization is required for eotaxin-induced responses in human eosinophils. J Allergy Clin Immunol. 2003 Jan 1;111(1):97–105.

149. Sviridov D, Mukhamedova N, Miller YI. Lipid rafts as a therapeutic target: Thematic Review Series: Biology of Lipid Rafts. J Lipid Res. 2020 May 1;61(5):687–95.

150. Hu X, Li J, Fu M, Zhao X, Wang W. The JAK/STAT signaling pathway: from bench to clinic. Signal Transduct Target Ther. 2021 Nov 26;6(1):1–33.

151. Zheng A, Dubuis G, Ferreira CSM, Pétremand J, Vanli G, Widmann C. The PI3K/Akt pathway is not a main driver in HDL-mediated cell protection. Cell Signal. 2019 Oct 1;62:109347.

152. Yousefi S, Hemmann S, Weber M, Hölzer C, Hartung K, Blaser K, et al. IL-8 is expressed by human peripheral blood eosinophils. Evidence for increased secretion in asthma. J Immunol. 1995 May 15;154(10):5481–90.

153. Sorci-Thomas MG, Thomas MJ. High Density Lipoprotein Biogenesis, Cholesterol Efflux, and Immune Cell Function. Arterioscler Thromb Vasc Biol. 2012 Nov;32(11):2561–5.

154. Catapano AL, Pirillo A, Bonacina F, Norata GD. HDL in innate and adaptive immunity. Cardiovasc Res. 2014 Aug 1;103(3):372–83.

155. Varshney P, Yadav V, Saini N. Lipid rafts in immune signalling: current progress and future perspective. Immunology. 2016 Sep ;149(1):13–24.

156. Villar VAM, Cuevas S, Zheng X, Jose PA. Localization and signaling of GPCRs in lipid rafts. In: Shukla AK, editor. Methods in Cell Biology. G protein-coupled receptors. Academic Press; 2016 Feb 132: 3–23.

157. Neel NF, Schutyser E, Sai J, Fan GH, Richmond A. Chemokine receptor internalization and intracellular trafficking. Cytokine Growth Factor Rev. 2005 Dec;16(6):637–58.

158. Simons K, Ehehalt R. Cholesterol, lipid rafts, and disease. J Clin Invest. 2002 Sept 1;110(5):597–603.

159. Reece SW, Varikuti S, Kilburg-Basnyat B, Dunigan-Russell K, Hodge MX, Luo B, et al. Scavenger Receptor BI Attenuates IL-17A–Dependent Neutrophilic Inflammation in Asthma. Am J Respir Cell Mol Biol. 2021 June;64(6):698–708.

160. He P, Gelissen IC, Ammit AJ. Regulation of ATP binding cassette transporter A1 (ABCA1) expression: cholesterol-dependent and – independent signaling pathways with relevance to inflammatory lung disease. Respir Res. 2020 Sept 25;21(1):250.

161. Zhao GJ, Yin K, Fu Y chang, Tang CK. The Interaction of ApoA-I and ABCA1 Triggers Signal Transduction Pathways to Mediate Efflux of Cellular Lipids. Mol Med. 2012 Feb;18(2):149–58.

162. Liu Y, Tang C. Regulation of ABCA1 functions by signaling pathways. Biochim Biophys Acta BBA - Mol Cell Biol Lipids. 2012 Mar 1;1821(3):522–9.

163. Saddar S, Mineo C, Shaul PW. Signaling by the High-Affinity HDL Receptor Scavenger Receptor B Type I. Arterioscler Thromb Vasc Biol. 2010 Feb;30(2):144–50.

164. Tarling EJ, Edwards PA. ATP binding cassette transporter G1 (ABCG1) is an intracellular sterol transporter. Proc Natl Acad Sci. 2011 Dec 6;108(49):19719–24.

165. Fulkerson PC, Fischetti CA, McBride ML, Hassman LM, Hogan SP, Rothenberg ME. A central regulatory role for eosinophils and the eotaxin/CCR3 axis in chronic experimental allergic airway inflammation. Proc Natl Acad Sci U S A. 2006 Oct 31;103(44):16418–23.

166. Huaux F, Gharaee-Kermani M, Liu T, Morel V, McGarry B, Ullenbruch M, et al. Role of Eotaxin-1 (CCL11) and CC Chemokine Receptor 3 (CCR3) in Bleomycin-Induced Lung Injury and Fibrosis. Am J Pathol. 2005 Dec 1;167(6):1485–96.

167. Manousou P, Kolios G, Valatas V, Drygiannakis I, Bourikas L, Pyrovolaki K, et al. Increased expression of chemokine receptor CCR3 and its ligands in ulcerative colitis: the role of colonic epithelial cells in in vitro studies. Clin Exp Immunol. 2010 Nov;162(2):337–47.

168. Mañes S, Lacalle RA, Gómez-Moutón C, Real G del, Mira E, Martínez-A C. Membrane raft microdomains in chemokine receptor function. Semin Immunol. 2001 Apr 1;13(2):147–57.

169. van Aalst E, Koneri J, Wylie BJ. In silico identification of cholesterol binding motifs in the chemokine receptor CCR3. Membranes (Basel). 2021 Jul;11(8):570.

170. Lombardi C, Berti A, Cottini M. The emerging roles of eosinophils: Implications for the targeted treatment of eosinophilic-associated inflammatory conditions. Curr Res Immunol. 2022 Mar 21;3:42–53.

171. Munitz A, Hogan SP. Alarming eosinophils to combat tumors. Nat Immunol. 2019 Mar;20(3):250–2.

172. Roufosse F. Targeting the interleukin-5 pathway for treatment of eosinophilic conditions other than asthma. Front Med (Lausanne). 2018 Apr 6;5:49.

173. Busse WW, Bleecker ER, FitzGerald JM, Ferguson GT, Barker P, Sproule S, et al. Long-term safety and efficacy of benralizumab in patients with severe, uncontrolled asthma: 1-year results from the BORA phase 3 extension trial. Lancet Respir Med. 2019 Jan;7(1):46–59.

174. Lee JJ, Jacobsen EA, McGarry MP, Schleimer RP, Lee NA. Eosinophils In Health and Disease: The LIAR Hypothesis. Clin Exp Allergy J Br Soc Allergy Clin Immunol. 2010 Apr;40(4):563–75.

175. Ortega H, Llanos JP, Lafeuille MH, Duh MS, Germain G, Lejeune D, et al. Effects of systemic corticosteroids on blood eosinophil counts in asthma: real-world data. J Asthma. 2019 Aug 3;56(8):808–15.

176. Geri G, Rabbat A, Mayaux J, Zafrani L, Chalumeau-Lemoine L, Guidet B, et al. Strongyloides stercoralis hyperinfection syndrome: a case series and a review of the literature. Infection. 2015 Dec 1;43(6):691–8.

177. Fulkerson PC, Rothenberg ME. Targeting eosinophils in allergy, inflammation and beyond. Nat Rev Drug Discov. 2013 Feb;12(2):117–29.

178. Sharma P, Dhanjal DS, Chopra C, Tambuwala MM, Sohal SS, van der Spek PJ, et al. Targeting eosinophils in chronic respiratory diseases using nanotechnology-based drug delivery. Chem Biol Interact. 2022 Sept 25;365:110050.

179. Knuplez E, Marsche G. An Updated Review of Pro- and Anti-Inflammatory Properties of Plasma Lysophosphatidylcholines in the Vascular System. Int J Mol Sci. 2020 Jan;21(12):4501.

180. Chaudhuri P, Colles SM, Damron DS, Graham LM. Lysophosphatidylcholine Inhibits Endothelial Cell Migration by Increasing Intracellular Calcium and Activating Calpain. Arterioscler Thromb Vasc Biol. 2003 Feb;23(2):218–23.

181. Yadav P, Beura SK, Panigrahi AR, Kulkarni PP, Yadav MK, Munshi A, et al. Lysophosphatidylcholine induces oxidative stress and calcium-mediated cell death in human blood platelets. Cell Biol Int. 2024;48(9):1266–84.

182. McNeil PL, Kennedy AL, Waggoner AS, Lansing Taylor D, Murphy RF. Light-scattering changes during chemotactic stimulation of human neutrophils: Kinetics followed by flow cytometry. Cytometry. 1985;6(1):7–12.

183. Denk S, Taylor RP, Wiegner R, Cook EM, Lindorfer MA, Pfeiffer K, et al. Complement C5a-induced changes in neutrophil morphology during inflammation. Scand J Immunol. 2017 Sept;86(3):143–55.

184. Hianik T, Haburcák M, Lohner K, Prenner E, Paltauf F, Hermetter A. Compressibility and density of lipid bilayers composed of polyunsaturated phospholipids and cholesterol. Colloids Surf Physicochem Eng Asp. 1998 Aug 10;139(2):189–97.

185. Gaul DS, Stein S, Matter CM. Neutrophils in cardiovascular disease. Eur Heart J. 2017 June 7;38(22):1702–4.

186. Zhang J, Shao Y, Wu J, Zhang J, Xiong X, Mao J, et al. Dysregulation of neutrophil in sepsis: recent insights and advances. Cell Commun Signal. 2025 Feb 14;23(1):87.

187. Zhang F, Xia Y, Su J, Quan F, Zhou H, Li Q, et al. Neutrophil diversity and function in health and disease. Signal Transduct Target Ther. 2024 Dec 6;9(1):343.

8. APPENDIX

Supplementary Table 1: Simulation Details of the Three Systems Considered for Molecular Dynamics Simulations

Number of peptides	Number of DMPC molecules	Number of water molecules	Number of counter ions		Simulation box size (nm^3)	Simulation time (ns)
			Na^+	Cl^-		
10	250	168 775	475	475	17x17x17	1 000
18	734	549 145	1 551	1 551	26x26x26	300
28	1 434	1 165 966	3 392	3 392	33x33x33	200
2	0	18115	51	51	8x8x8	500

Supplementary Table 2: Secondary structure details from Circular Dichroism comparing experimental (exp) and theoretical (sim) values.

Supplementary Table 2A: Secondary structure analysis of various MD models of 4F-P-4F and sHDL: the secondary structure elements were directly calculated from the MD trajectories

Samples	**Helix (%)**	Strand (%)	Turns (%)	Unordered (%)
4F-P-4F sim.	81	0	4	15
sHDL sim. (11.7 nm)	77	0	7	17
sHDL sim. (18.0 nm)	76	0	7	17
sHDL sim. (25.6 nm)	72	0	9	19

Supplementary Table 2B: All derived CD spectra (experimentally and simulation-based) were analyzed for their secondary structure composition with DichroWeb

The CDSSTR method was applied, using reference data set SP175

	DichroWeb, CDSSTR, Reference set SP175t			
	Helix (%)	Strand (%)	Turns (%)	Unordered (%)
4F-P-4F exp.	70	7	11	12
sHDL exp.	56	9	10	24
4F-P-4F sim.	80	1	9	10
sHDL sim. (11.7 nm)	78	1	9	12
sHDL sim. (18.0 nm)	75	2	9	13
sHDL sim. (25.6 nm)	67	5	10	18

Method for the calculation of fractional helicity (*f*H) adapted from (136)

The Mean Residue Ellipticity values (MRE [θ] in deg cm^2 $dmol^{-1}$ $residue^{-1}$) at 222 nm were extracted from the CD spectra and the fractional helicity was calculated, based on the following equation:

$$fH = \frac{[\theta]_{222nm} - 3000}{-36000 - 3000}$$

*f*H*100 yields the per cent α-helicity. The following equations were used to convert the raw CD spectra from Theta Machine Units θ in millidegrees (mdeg) to either Delta Epsilons (Δε, in mdeg M^{-1} cm^{-1}) or Mean Residue Ellipticity (MRE [θ] in deg cm^2 $dmol^{-1}$ $residue^{-1}$). The output format of MD-simulation-derived CD spectra was Δε.

$$\Delta\varepsilon = \frac{\theta * 0.1 * MRW}{P * conc * 3298}$$

with θ machine units in mdeg

MRW = mean residue weight

$$MRW = \frac{Peptide\ molecular\ weight}{No.of\ residues - 1}$$

path length P in cm (here 0.1 cm), concentration in mg/ml (here 0.2 mg/ml).

To calculate back to [θ] MRE we used the following correlation:

$$\Delta\varepsilon = [\theta]/3298$$

Supplementary Table 2C: Fractional helicity (*f*H) based on the method described by (136)

Samples	**$[\theta]_{222nm}$**	**Helicity (%)**
4F-P-4F exp.	-25174	**72**
sHDL exp.	-21643	**63**
4F-P-4F sim. (A)	-27051	**77**
sHDL sim. (11.7 nm)	-25777	**74**
sHDL sim. (18.0 nm)	-25081	**72**
sHDL sim. (25.6 nm)	-23480	**68**

Supplementary Table 2D: Summary of comparisons between simulated, calculated and experimental values of the secondary structure (helical content) analysis:

Samples	MD simulations, helical content (%)	Calculated helicity based on $[\theta]_{222nm}$ (%)	DichroWeb exp, helical content (%)
4F-P-4F exp.	-	72	70
sHDL exp.	-	63	56
4F-P-4F sim.	81	77	80
sHDL sim. (11.7 nm)	77	74	78
sHDL sim. (18.0 nm)	76	72	75
sHDL sim. (25.6 nm)	72	68	67

Adapted from (144) under the terms and conditions of the Creative Commons Attribution (CC BY) license (https://creativecommons.org/licenses/by/4.0/) which permits unrestricted use, distribution, and reproduction in any medium, provided the original authors and the source are credited.

Supplementary Figure 1:

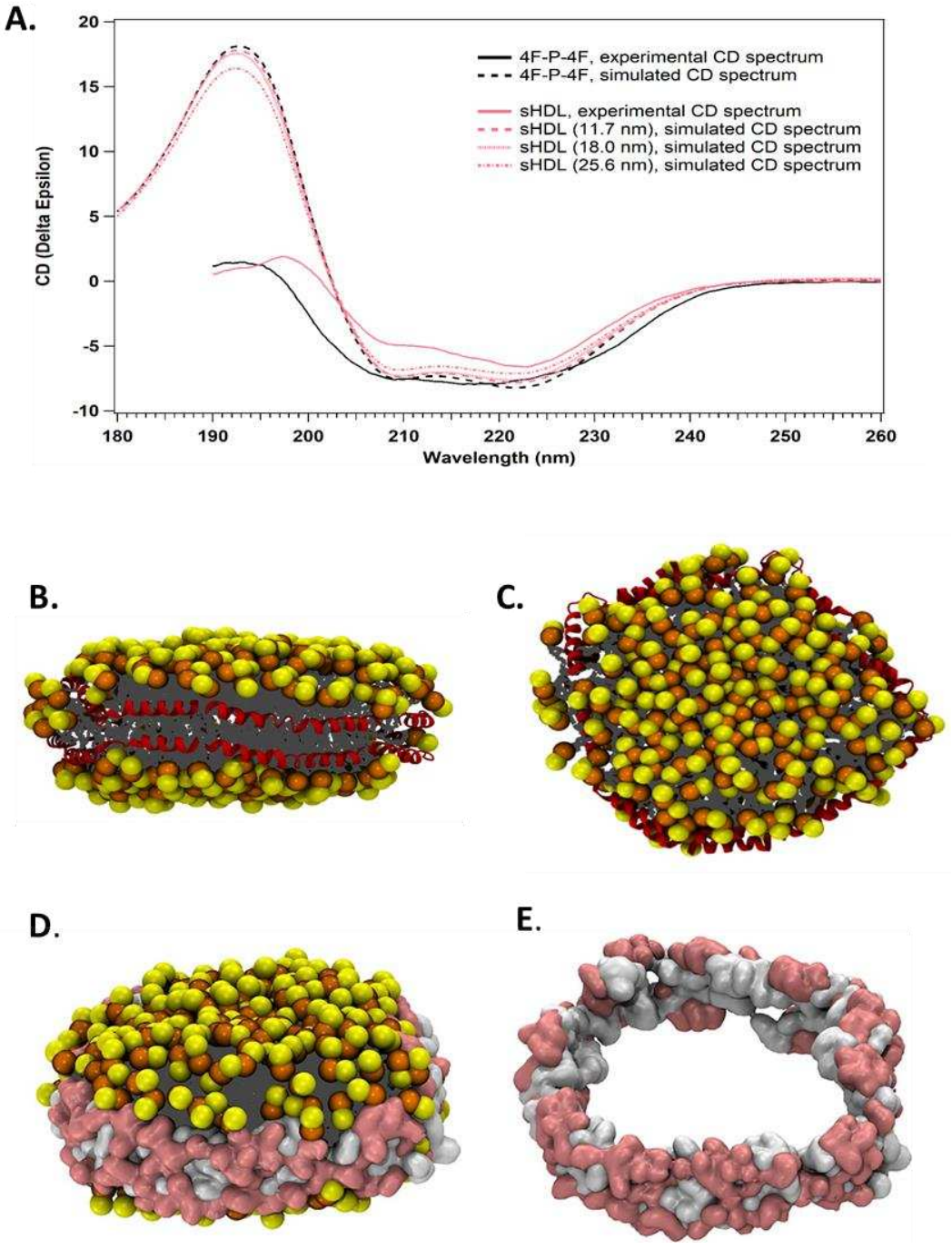

Supplementary Figure 1: A. Circular dichroism (CD) spectra comparing Molecular Dynamic simulation as well as experimental values for the sHDL formulations of various sizes and the non-

lipidated 4F-P-4F peptide using DichroWeb. Representation of a configuration of the 11.7 nm diameter 4F-P-4F DMPC nanodisc sampled during the MD simulation. **B**. Side and **C**. Top view showing the circular arrangement of 4F-P-4F peptides at the nanodisc rim as a belt. The DMPC lipid acyl chains are represented in grey, while the phosphate group and choline moieties of the lipid head groups are displayed respectively as orange and yellow balls. **D**. and **E**. Alternative views emphasizing the hydrophobic (white) and hydrophilic (pink) residues of the 4F-P-4F dimers to highlight the amphipathic arrangement of the peptide side chains and their orientation with respect to the lipid core and the solvent. Adapted from (144) under the terms and conditions of the Creative Commons Attribution (CC BY) license (https://creativecommons.org/licenses/by/4.0/) which permits unrestricted use, distribution, and reproduction in any medium, provided the original authors and the source are credited.

Supplementary Table 3: Average number of salt bridges formed between the amino groups of the lysine residues (K4, K9, K13, K15, K23, K28, K32, K34) of the 4F-P-4F peptides and the phosphorus of the phosphate groups in the DMPC lipids, or between the carbon of the carboxyl groups of the glutamate residues (E12, E16, E31, E35) of the 4F-P-4F peptides and the nitrogen of the choline groups in the DMPC molecules. Salt bridges were considered when the distances between the interacting groups were 4.6 Å or 6 Å. The averages were calculated over the last 50 ns of each simulation for the three systems, normalized by the number of 4F-P-4F peptides. Adapted from (144) under the terms and conditions of the Creative Commons Attribution (CC BY) license (https://creativecommons.org/licenses/by/4.0/) which permits unrestricted use, distribution, and reproduction in any medium, provided the original authors and the source are credited.

4F-P-4F:DMPC ratio	**Average number of salt bridges per peptide**	
	Lys-Phos	**Glu-Choline**
1:25	2.69	0.60
1:40	2.98	0.75
1:51	2.85	0.82

Supplementary Figure 2

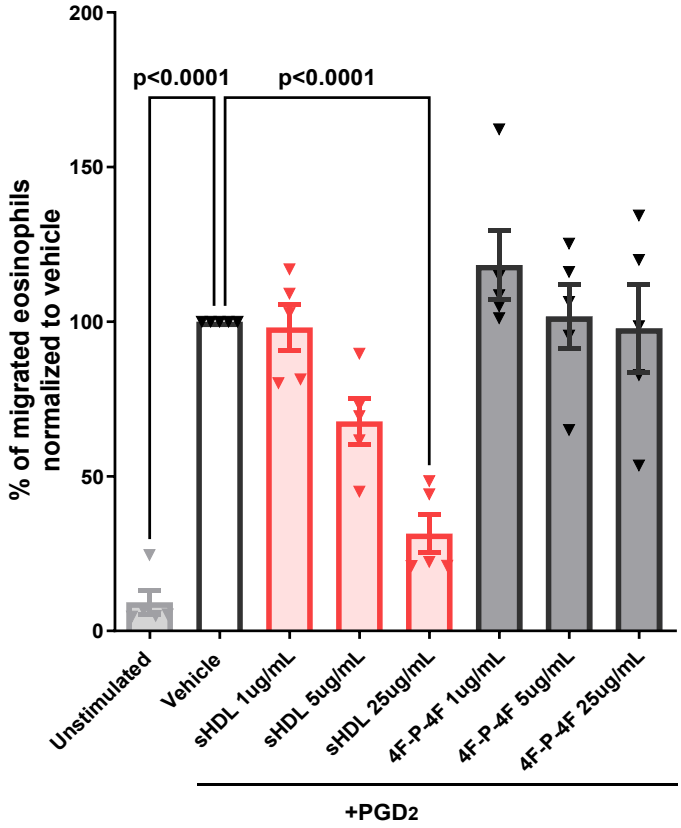

Supplementary Figure 2: sHDL Nanodiscs Modulate Human Eosinophil Chemotaxis sHDL nanodiscs effectively inhibit human eosinophil chemotaxis towards prostaglandin D_2 in a concentration-dependent manner (n=5). Notably, the non-lipidated peptide alone does not exhibit this inhibitory effect. Values represent mean ± SEM. Statistical significance was determined using one-way ANOVA followed by Dunnett's multiple comparisons test; $p < 0.05$ was considered significant. Adapted from (144) under the terms and conditions of the Creative Commons Attribution (CC BY) license (https://creativecommons.org/licenses/by/4.0/) which permits unrestricted use, distribution, and reproduction in any medium, provided the original authors and the source are credited.

Supplementary Figure 3:

A.

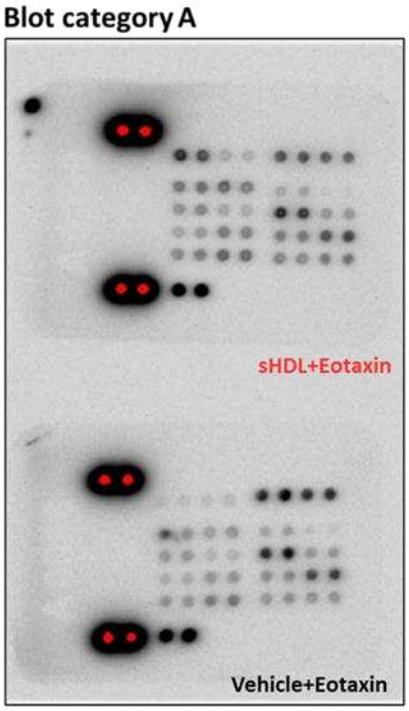

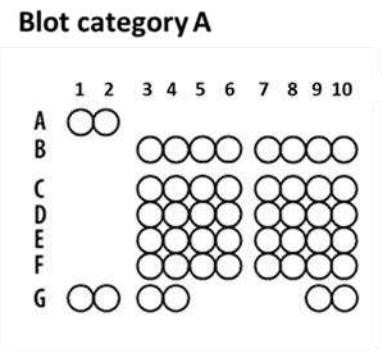

Refer to the table below for the Human Phospho-Kinase Array coordinates.

Membrane/ Coordinate	Target/Control	Phosphorylation Site
A-A1, A2	Reference Spot	—
B-A11, A12	Akt 1/2/3	T308
B-A13, A14	Akt 1/2/3	S473
B-A17, A18	Reference Spot	—
A-B3, B4	CREB	S133
A-B5, B6	EGF R	Y1086
A-B7, B8	eNOS	S1177
A-B9, B10	ERK1/2	T202/Y204, T185/Y187
B-B11, B12	Chk-2	T68
B-B13, B14	c-Jun	S63
A-C3, C4	Fgr	Y412
A-C5, C6	GSK-3α/β	S21/S9
A-C7, C8	GSK-3β	S9
A-C9, C10	HSP27	S78/S82
B-C11, C12	p53	S15
B-C13, C14	p53	S46
B-C15, C16	p53	S392
A-D3, D4	JNK 1/2/3	T183/Y185, T221/Y223
A-D5, D6	Lck	Y394
A-D7, D8	Lyn	Y397
A-D9, D10	MSK1/2	S376/S360
B-D11, D12	p70 S6 Kinase	T389
B-D13, D14	p70 S6 Kinase	T421/S424
B-D15, D16	PRAS40	T246

Membrane/ Coordinate	Target/Control	Phosphorylation Site
A-E3, E4	p38α	T180/Y182
A-E5, E6	PDGF Rβ	Y751
A-E7, E8	PLC-γ1	Y783
A-E9, E10	Src	Y419
B-E11, E12	PYK2	Y402
B-E13, E14	RSK1/2	S221/S227
B-E15, E16	RSK1/2/3	S380/S386/S377
A-F3, F4	STAT2	(pY690)
A-F5, F6	STAT5a/b	Y694/Y699
A-F7, F8	WNK1	T60
A-F9, F10	Yes	Y426
B-F11, F12	STAT1	Y701
B-F13, F14	STAT3	Y705
B-F15, F16	STAT3	S727
A-G1, G2	Reference Spot	—
A-G3, G4	β-Catenin	—
A-G9, G10	PBS (Negative Control)	—
B-G11, G12	STAT6	Y641
B-G13, G14	HSP60	—
B-G17, G18	PBS (Negative Control)	—

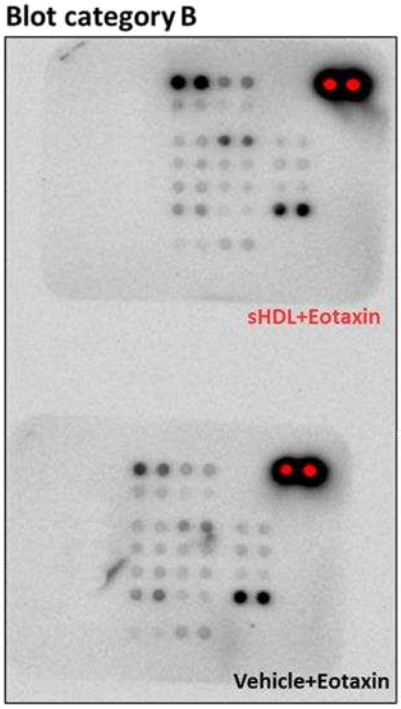

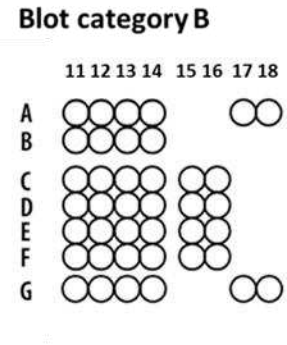

B.

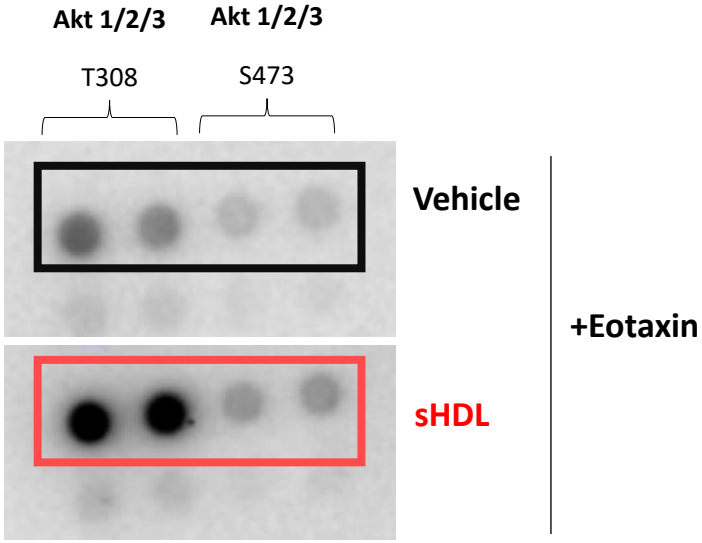

Supplementary Figure 3: Phosphorylation Profiles and Viability of Eosinophils Treated with sHDL. A. Phosphokinase array results from pooled human eosinophil donors (n=3). The panel shows a labeling guide alongside representative complete blots, illustrating phosphorylation sites in vehicle- and sHDL-treated eosinophils stimulated with eotaxin-1. Vehicle and sHDL blots were exposed simultaneously for chemiluminescent detection. Note that different exposure times were utilized for individual targets due to varying phosphokinase abundance. **B.** Magnified phosphokinase array blots from pooled human eosinophil donors (n=3) for vehicle- and sHDL-treated cells stimulated with eotaxin-1, specifically highlighting changes in Akt phosphorylation. Adapted from (144) under the terms and conditions of the Creative Commons Attribution (CC BY) license (https://creativecommons.org/licenses/by/4.0/) which permits unrestricted use, distribution, and reproduction in any medium, provided the original authors and the source are credited.

Supplementary Figure 4

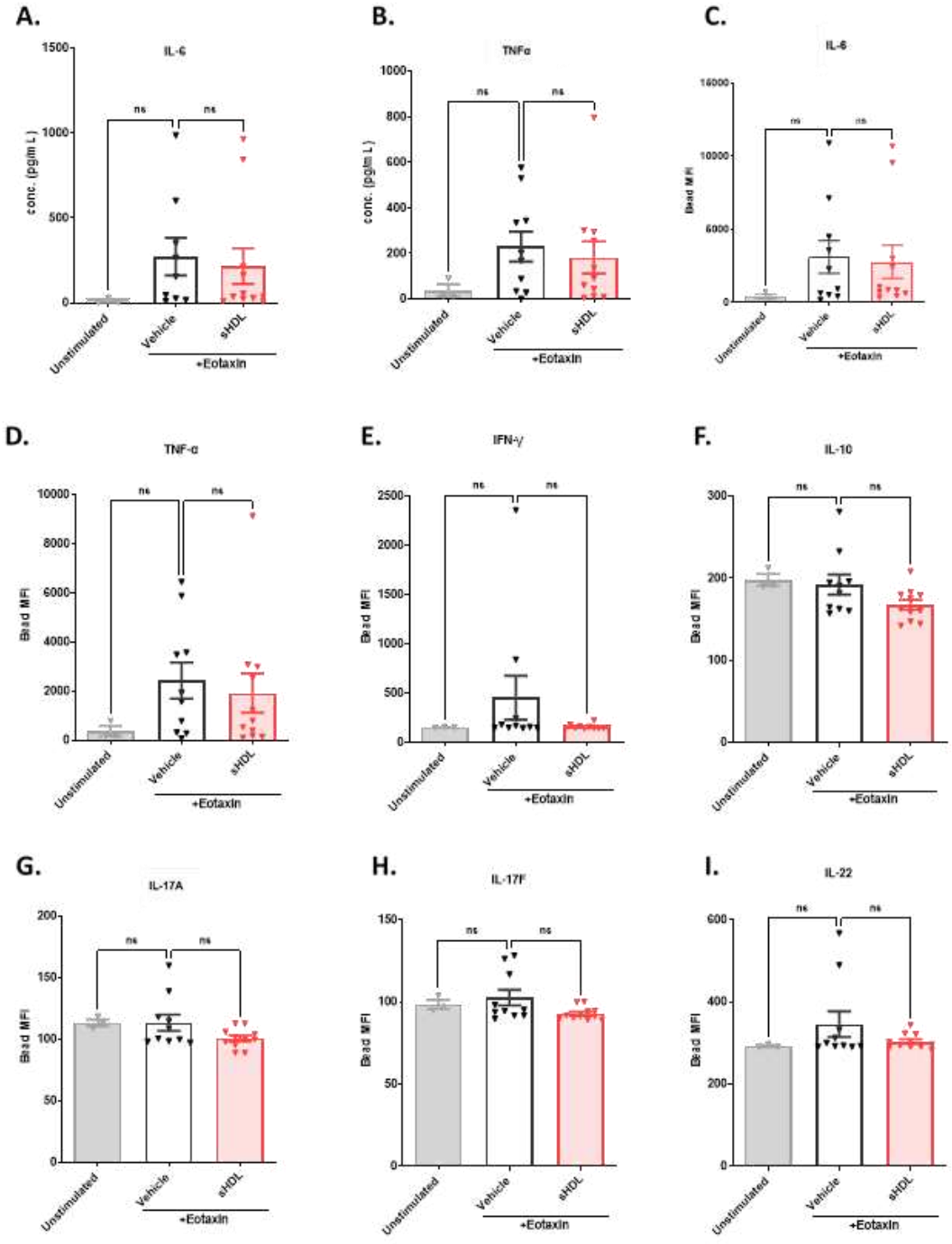

Supplementary Figure 4: Cytokine analysis from BAL samples A. IL-6 and **B.** TNF-α concentrations in the bronchioalveolar lavage of IL-5 transgenic mice treated with vehicle or sHDL and stimulated with eotaxin-2 (n = 9 - 11). **C-I.** Median Fluorescent Intensity (MFI) of the beads

for indicated target analytes IL-6, TNF-α, IFN-γ, IL-10, IL-17A, IL-17F and IL-22 respectively, in the bronchioalveolar lavage of IL-5 transgenic mice treated with vehicle or sHDL and stimulated with eotaxin-2. Data presented as mean ± SEM (n=10-11 in the treatment groups) using the LEGENDplex cytokine quantification kit as described in Supplementary Methods 1.2. Samples with cytokine levels below the standard curve detection range were excluded in the treatment groups, data presented as mean ± SEM. Statistical significance was determined using one-way ANOVA followed by Dunnett's multiple comparisons test, with $p < 0.05$ considered significant. Adapted from (144) under the terms and conditions of the Creative Commons Attribution (CC BY) license (https://creativecommons.org/licenses/by/4.0/) which permits unrestricted use, distribution, and reproduction in any medium, provided the original authors and the source are credited.

LEGENDplex Cytokine Quantification method: Bronchoalveolar lavage (BAL) samples were analyzed using the LEGENDplex™ Mouse Th17 Panel (7-plex) with V-bottom plates (BioLegend, San Diego, California, USA). This panel simultaneously detects IL-6, IL-10, IFN-γ, TNF-α, IL-17A, IL-17F, and IL-22. Following the manufacturer's protocol, BAL fluid was incubated with fluorescent capture beads. After washing, beads were acquired on a BD FACS Canto II flow cytometer for PE and APC detection. Cytokine concentrations were quantified using LEGENDplex™ Data Analysis Software with five-parameter logistic curve fitting. For these BAL samples, only IL-6 and TNF-α concentrations fell within the assay's detection range. All reagents were used as per the manufacturer's kit protocol, and samples were run in duplicate. Adapted from (144) under the terms and conditions of the Creative Commons Attribution (CC BY) license (https://creativecommons.org/licenses/by/4.0/) which permits unrestricted use, distribution, and reproduction in any medium, provided the original authors and the source are credited.

The following tool was used to optimize the language of the text:

• Name and version of the tool: ChatGPT (GPT-5.2 Go)

• Publisher/Provider (company, organization or person that offers or programmed the tool): OpenAI

• Date the content was generated: January 2026

• Uniform resource locator: https://chat.openai.com
